AD_____

Award Number: W81XWH-09-1-0042

TITLE: Non-invasive detection of lactate as a biomarker of response using spectral-selective multiple quantum editing sequence (SS-SelMQC)

PRINCIPAL INVESTIGATOR: Sunitha B. Thakur, Ph.D.

CONTRACTING ORGANIZATION: Memorial Sloan-Kettering Cancer Center
New York, NY-10065

REPORT DATE: November 2013

TYPE OF REPORT: Final

PREPARED FOR: U.S. Army Medical Research and Materiel Command
Fort Detrick, Maryland 21702-5012

REPORT DOCUMENTATION PAGE

Form Approved
OMB No. 0704-0188

1. REPORT DATE	2. REPORT TYPE	3. DATES COVERED
Novemvber 2013	Final	1 May 2009 – 31 October 2013

4. TITLE AND SUBTITLE

Non-invasive detection of lactate as a biomarker of response using spectral-selective multiple quantum editing sequence (SS-SelMQC)

5a. CONTRACT NUMBER

5b. GRANT NUMBER
W81XWH-09-1-0042

5c. PROGRAM ELEMENT NUMBER

6. AUTHOR(S)

Sunitha B. Thakur, Ph.D.

E-Mail: thakurs@mskcc.org

5d. PROJECT NUMBER

5e. TASK NUMBER

5f. WORK UNIT NUMBER

7. PERFORMING ORGANIZATION NAME(S) AND ADDRESS(ES)

Memorial Sloan-Kettering Cancer Center
New York, NY-10065

8. PERFORMING ORGANIZATION REPORT NUMBER

9. SPONSORING / MONITORING AGENCY NAME(S) AND ADDRESS(ES)
U.S. Army Medical Research and Materiel Command
Fort Detrick, Maryland 21702-5012

10. SPONSOR/MONITOR'S ACRONYM(S)

11. SPONSOR/MONITOR'S REPORT NUMBER(S)

12. DISTRIBUTION / AVAILABILITY STATEMENT
Approved for Public Release; Distribution Unlimited

13. SUPPLEMENTARY NOTES

14. ABSTRACT

This application focuses on enhancing cancer care by developing non-invasive techniques to determine better biomarkers to improve diagnostic specificity and decrease the number of negative biopsies, and also as markers of response with novel targeted agents such as Trastuzumab and Bevacizumab. We developed SS1-SelMQC sequence for lactate detection and T1- and T2-versions for T1 and T2 measurements to facilitate the absolute lactate quantifications. We completed data collection and analysis of lactate MR spectroscopy data of in vivo breast tumors with different expression levels of ER, PR, HER-2 as a function their growth. Lactate concentrations are high at low tumor volumes and decreases as increasing tumor volumes in all tumor models. The classification of two groups (triple-negative vs non-triple negative) showed great predictive power using LDA and logistic regression. When these tumors were treated with targeted drugs, [Lac] was shown to be an early marker and predicted the treatment response within 48 hours following the treatment. These results may help in understanding the tumor aggressiveness and its relation to LDH-A expression levels in these tumors. Additionally, monotherapy treatment results in our mammary tumors will help to explore the treatment response using combinational therapy in breast cancer patients.

15. SUBJECT TERMS
None provided.

16. SECURITY CLASSIFICATION OF:			17. LIMITATION OF ABSTRACT	18. NUMBER OF PAGES	19a. NAME OF RESPONSIBLE PERSON
a. REPORT	b. ABSTRACT	c. THIS PAGE			USAMRMC
U	U	U	UU	46	19b. TELEPHONE NUMBER *(include area code)*

Table of Contents

Introduction

Early detection of breast cancer and novel treatments further improves the survival rates of patients and will require novel strategies. Enhancing diagnostic specificity leads to a decreased need for biopsy and would be a major advance in breast cancer care. This application focuses on using lactate as a marker in breast cancer. The main objective of the proposal is developing and evaluating a more effective method of detecting lactate (Lac) non-invasively by magnetic resonance spectroscopy (MRS) techniques. Lac is present in very small quantities (milli moles) compared to lipid (Lip) (moles) and water and the signal of Lac occurs in the same position as Lip, thereby making it very difficult to be detected. Treatment of breast cancers with novel targeted agents such as Trastuzumab and Bevacizumab have led to significant gains, although the drugs can be toxic. Breast tumors are usually sensitive to many drugs but subsequently develop resistance. There is strong interest in applying drugs that interfere with angiogenesis and signaling pathways related to breast cancer growth and metastasis. Low extracellular pH and high Lac levels were shown to be indicators of metastatic risk in breast cancer xenografts. Elevated Lac in biopsy samples was shown to correlate with increased risk of metastasis and poor patient survival in different aggressive cancers, while a decrease Lac levels observed in tumor response to radiation and chemotherapy. Therefore, non-invasive measurement of Lac concentrations ([Lac]) may be an additional characteristic marker for breast cancer; it may improve diagnostic specificity, serve as an early marker of tumor response, and provide functional information about prognosis.

Body

During this award period, (I) we initially evaluated the SS-SelMQC (SELective Multiple Quantum coherence for signal enhancement using Spectral-Selective binomial radiofrequency pulses) [1] in breast tumors to ensure that it is superior with regards to signal to noise (SNR), uniformity of signal detection within the coil, and quality of suppression of the lipid and water signals. The Lac SNR obtained from this sequence was compared with the conventional SelMQC [2] and PRESS methods. We have developed SS-SelMQC sequence using higher order binomial pulses (SS1-SelMQC) [3] and T1-and T2-versions [4] of this sequence for T1 and T2 relaxation measurements to facilitate the lactate quantification. To detect lactate from mammary tumors with varying tumor volumes, various radiofrequency (RF) coils with high quality factors were designed and the homogeneity of these coils were tested using phantoms with known concentrations (Lac with without Gd-DTPA doping, and Lac/Lip solutions). Once the RF coils are optimized, signal to noise (SNR) between SelMQC and SS1-SelMQC sequence for detecting Lac signal was measured. (II) Subsequently we have completed MRS data collection for non-localized, 1D and 2D localized chemical shift images (CSI) and quantified the lactate concentrations in breast tumor models to evaluate the utility of [Lac] to predict tumor aggressiveness. A method was developed to extract texture features from MR images to evaluate incremental predictive nature of separating tumors with different aggressiveness. (III) Finally as part of our research design, we treated all

tumors to determine if Lac is a marker of sensitivity to novel targeted drugs and compared breast mammary tumors that are sensitive and resistant to Herceptin and Bevacizumab and changes that occur early in the course of treatment. For tumor treatment, we used tumors at volumes between 140-200 mm^3 where highest lactate concentrations were observed. The texture features from T_2-MR images were also evaluated pre and post treatment.

Methods and Materials

All MR imaging and spectroscopy experiments were performed on a 4.7 T Bruker horizontal bore system (Bruker BioSpin; Bruker, Billerica, MA) running ParaVision 4.0 software.

Phantoms: Prior to actual animal MR imaging and spectroscopy scans, the sensitivity of pulse sequence and coil homogeneity were tested using cylindrical phantoms (10mm and 15mm diameter) with 5, 15 and 30 mM lactate/ saline doped with and without 25 µM Gd-DPTA solutions. For Lac/Lip phantoms, 10% intralipid, (Baxter Healthcare Corporation) was mixed with three different concentration solution viz, 5, 15 and 30 mM separately to facilitate the single compartment for both lipid and lactate to demonstrate the non-localized Lac detection with water and lipid suppression. The data from these scans were used as a standard reference for quantification of lactate concentrations in animals.

Animal studies: These studies were conducted in compliance with protocols approved by the animal care protocols in Memorial Sloan-Kettering Cancer Center. Cancer cells (MCF-7, BT-474, MDA-MB-231 and MDA-MB-435) were purchased from American Type Culture Collection (ATCC, Manassas, VA, US). Five million cells were injected into the inguinal mammary fat pad (MFP) of anaesthetized mice. 4-6-week-old female athymic nu/nu mice (Animal Production Area of the NCI-Frederick Cancer Research Facility, Frederick, MD). Mice were allowed to acclimatize and mature for 2 weeks before implantation of tumor cells. Two days prior to implantation of MCF-7 and BT-474 tumors (estrogen positive), estrogen pellets containing 0.72 mg of estrogen (IRA, Toledo, OH) were inserted into

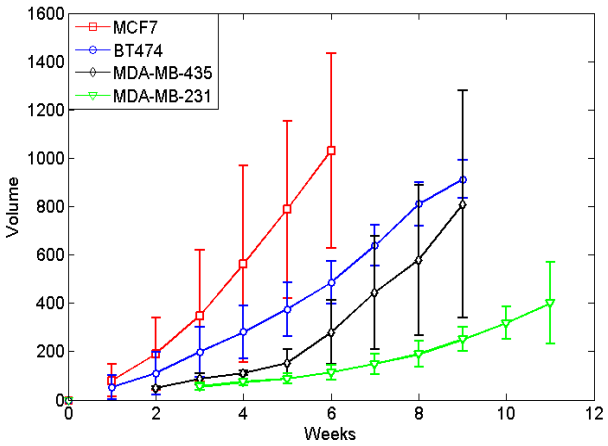

Figure 1. Growth curves of four human breast tumor cell lines injected into mammary fat pad (m.f.p) in nude mice. Tumor cells (5x106 cells) were injected into the m.f.p and tumor growth was measured upto 7-12 weeks. Tumor growth was significantly different in all four tumor models ($p < 0.001$).

the subcutaneous fat in the hips of animals that were about to receive these tumors. Mice were monitored twice weekly for tumor growth. Tumor growth became evident on visual inspection about 10 days after implantation into the MFP and its volume (whole) was measured using a digital caliper using a hemi-ellipsoid formula $V = (\pi/6) \times l \times b \times h$, where l, b and h are the length, width and depth of the tumor, respectively. Only one person measured all the tumors in the experiments to prevent observation differences, since measurements by more than one person can lead to different results. The tumor was measured once in three days. (**Figure 1**). Once the tumors reached the volume of approximately 100-150 mm^3, they were studied with MR imaging and spectroscopy.

MR Imaging and Lactate MR spectroscopy: Mice were anesthetized with a mixture of 50%:50% between isoflurane (1.5-2%) and oxygen and placed inside a home-built MR animal holder. The respiration and temperature were monitored using an MR compatible small animal monitoring and gating system (SA Instruments Inc, Stony Brook, NY). The tumor was placed inside a 2 turn home built 10-11 mm (upto 300 mm^3) and 15-16 mm (> 300 mm^3) diameter tuned RF coil. Temperature was maintained at 37°C by blowing warm air through the bore of the magnet. Tumor bearing mice were typically studied 3-4 times. The Bruker ParaVision Tripilot pulse sequence was used to create three perpendicular images (FOV = 20 mm) as scout images for positioning of the animal tumor within the coil to ensure that the tumor was in the center of the magnet. Using these Tripilot scout images, T_2-weighted MR sagittal images with a 5 mm thickness and five 1 mm slices, using a Multi Slice Multi Echo (MSME) sequence repetition time (TR) = 2250 ms; echo time (TE) = 52 ms; 256 × 256 matrix, echo train length (ETL) 8 number of excitations (NEX) = 1; field of view (FOV) = 20 mm were obtained from the tumor located at isocenter. Total MR image acquisition including shimming took about 12 minutes. T_2 MR image with 5 mm slice thickness was used as scout image for preparing the spectroscopy scan. The observed line width of lactate at FWHM for phantoms was between 20-25 Hz and for animal studies between 30-50Hz.

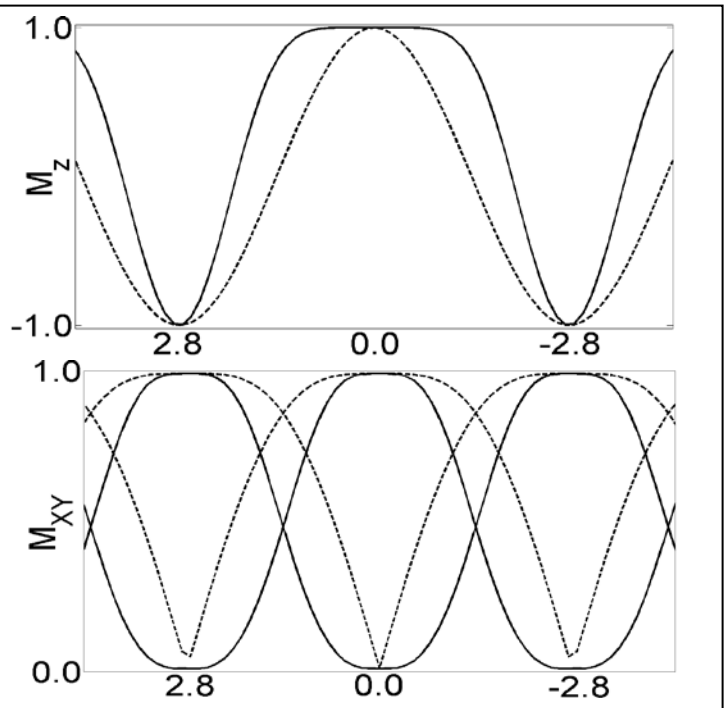

Figure 2**.** Theoretical inversion (top) and excitation (bottom) following 1331 (solid) and 11 pulse sequence for spectral selection for (B), as a function of chemical shift. Inversion profile shows the inversion of -2.8 ppm resonances with 0 ppm at equilibrium. In these simulations, the Lac CH peak was referenced to '0' ppm and hence Lac CH_3 will appear at '2.8' ppm on the chemical shift. RF pulse parameters and interpulse durations were chosen to match the experimental conditions given in the text.

Non-localized lactate signal was obtained using a modified SS-SelMQC sequence [1] with the higher order binomial bp1, bp2 and bp3 for spectral selection (SS1-SelMQC)[3] for inversion and excitation (**Figure 2**); bp1= $[(\pi/16)_{-x} - \Delta_1 - (3\pi/16)_x - \Delta_1 - (3\pi/16)_{-x}) - \Delta_1 - (\pi/16)_x]$, bp2=$[(\pi/16)_x - \Delta_1 - (3\pi/16)_x - \Delta_1 - (3\pi/16)_x) - \Delta_1 - (\pi/16)_x]$, and bp3= $[(\pi/8)_{-x} - \Delta_2 - (3\pi/8)_x - \Delta_2 - (3\pi/8)_{-x} - \Delta_2 - (\pi/8)_x]$. Width of each pulse within bp1 and bp2 is 200 us and bp3 is 400us three-lobe sinc shaped pulses with their phases set to 0 (x) or 180 (-x). Number of scans are 16 with a repetition time (TR) of 3 s and spectral width of 12.5 ppm. Due to RF finite pulse widths within the binomial pulse blocks, Δ_1 and Δ_2 values were adjusted to include the chemical shift evolution starting from the center of the first pulse to the center of the second pulse. In the binomial spectral-selective pulses, we chose to use broad band sinc shaped RF pulses. Multiple quantum selection gradients are with duration $\delta1 = \delta2 = \delta3 = 2$ ms. Transmitter is set at CH frequency of Lac and the ZQ $\rightarrow$DQ coherence transfer pathway is selected with the Gsel gradients in a ratio of 0:-1:2; Other MR acquisition parameters are similar to SS-SelMQC [1].

For absolute quantification of lactate in vivo tumors, we calculated the relaxation correction factors by modifying the SS1-SelMQC sequence using additional inversion pulses (2ms Mao4 shaped pulse for T1 measurement and 10ms single lobe Sinc for T2 measurement). Non localized lactate spectra were obtained with 16 transients for T_1 by varying the inversion time (TI) and 32 transients for T_2 measurements. For T2 measurements, repetition time (TR) = 10s used. *In vivo* measurements of T1 and T2 of Lac were performed on several mice from each tumor line. In 3-4 mice per group and few measurements were repeated on same mice at different tumor volumes to estimate the repeatability of the measurement and to track the changes in the T1 and T2 values with the tumor growth.

Data Processing

T1 and T2 Measurements: The relaxation times, T1 and T2, were measured using modified T1-SS1-SelMQC and T2-SS1-SelMQC sequences developed during this project [4]. The integral values of lacate peak were calculated using XWINNMR (BRUKER) were used for the T_1 and T_2 calculation. The T_1 was calculated using $S= S_0 (1-2 \exp^{(-TI/T_1)}) - S_0$, where S is Signal intensity at variable inversion delay (TI) and T_1 is spin-lattice relaxation time. The T_2-relaxation delay was calculated using $S= S_0 \exp^{(-TR/TE')}$, where TR is recycle delay and TE' is echo time. The Matlab was used to fit the curve.

Lactate data quantification:

Absolute concentrations of Lac metabolite from MR data using multiple quantum editing can be calculated using two methods. These include the external reference quantification method, which uses an external standard with the known concentration and internal reference method which uses water as a reference. We found similar concentrations in phantoms using both methods as expected. As the water CSI scan takes extra 10 minutes of scan time and involves careful adjustment of receiver gain in some tumors, we decided to use the external standard or substitution method. This method requires careful measurements of the relative power each time one acquires data and comparing the power required for different pulses when the subject

(experimental mice) is in place, vs that required when a phantom (whose quantitation is accurately known) is in place.

1D data: Time domain spin echo lactate 1D data were imported to the PC and were processed using home-built program written in Matlab. This data was Fourier transformed using 2 Hz exponential and 1.5 Hz Gaussian filtering. After calculating the power spectrum, lactate peaks were fitted with a Gaussian function. The area under the lactate peak was calculated and the lactate concentration was computed using phantom substitution method using an external standard with the known concentration. The accuracy of lactate quantification of was verified using one phantom (30 mM) as the object of interest and the other phantom (15 mM) as the reference. The mean measured lactate concentration was within 4% of the nominal concentration. In vivo lactate concentration was calculated similarly. The concentration of in vivo tumor lactate, C, can be calculated from the phantom solution of known lactate concentration C^{ref} as:

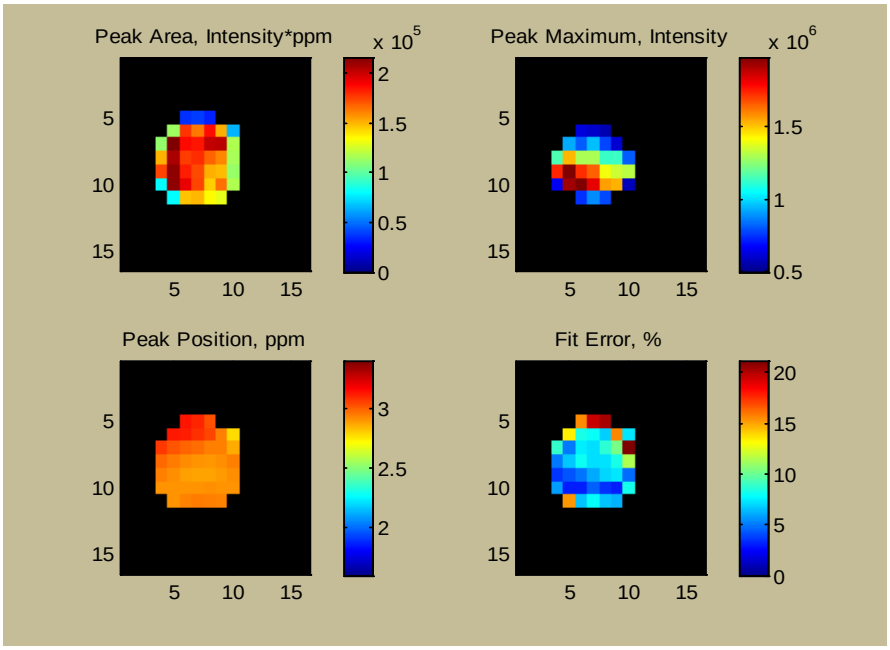

Figure. 3: Lactate peak fitting from 2D chemical shift image for quantification: peak area under peak (top left), peak maximum (top right), peak position (bottom left), and fit error (bottom right). Low fit error shows the estimate of quantification accuracy.

$$C = C^{ref} \times f_{T_1,T_2} \times \frac{A}{A^{ref}}$$

where A and A^{ref} are the measured areas under the fitted peaks in tumor and in the reference phantom, respectively. The correction factor for T1 and T2 differences between phantom and in vivo data is:

$$f_{T_1,T_2} = \exp\left[TE\left(\frac{1}{T_{2\ vivo}} - \frac{1}{T_{2\ phantom}}\right)\right] \times \frac{\left[1-\exp\left(-TR/T_{1\ phantom}\right)\right]}{\left[1-\exp\left(-TR/T_{1\ vivo}\right)\right]}$$

2D data: 2D CSI data were imported into 3DiCSI and superimposed onto T2 images. Voxel spectra were then exported in ASCII format and lactate peaks were fitted with a Gaussian function in Matlab. The area under the lactate peak was calculated and the lactate concentration was computed voxel-by-voxel using phantom substitution method (**Figure 3**).

Statistical analysis was performed using SPSS (SPSS 10.0, SPSS, Chicago, IL). A repeated-measures analysis of variance (ANOVA) was used to test difference in tumor growth between different mouse models. [Lac], T1 and T2 values were compared between groups of slow growing and fast growing, HER2 positive and HER2 negative, triple negative tumors and rest of tumors. The mean and standard deviations of lactate concentrations, T1, and T2 values for each tumor cell line were compared using t-test. Lactate concentrations were compared between pre and post treatment.

Image feature extraction from 2D T2 images:

Image software for segmentation: Prior to the extraction of features from T2-weighted images, for the segmentation of tumor, we used a useful software package called MIJ (http://bigwww.epfl.ch/sage/soft/mij/) that enables to link between ImageJ/Fiji and Matlab. From the segmented tumor image obtained using ImageJ, we extracted image features.

Image features: For analysis of mice model data, we extracted the lactate concentration for a tumor slice and whole tumor from MR spectroscopy data. Also, the volume of tumor slice and whole tumor volume were extracted. In addition, we extracted statistical features including kurtosis and skewness and image texture features including contrast, correlation, energy, homogeneity, and entropy. From a co-occurrence matrix created based on raw image intensity values, five texture features were computed, which are defined as follows:

1) Contrast: $\sum_{i,j}|i-j|^2 p(i,j)$
2) Correlation: $\sum_{i,j}\frac{ijp(i,j)-\mu_x\mu_y}{\sigma_x\sigma_y}$

   where μ_x, μ_y and $\sigma_{x,}\sigma_y$ denote the mean and standard deviations of the row and column sums of the matrix, respectively.
3) Energy: $\sum_{i,j} p(i,j)^2$
4) Homogeneity: $\sum_{i,j}\frac{p(i,j)}{1+|i-j|}$
5) Entropy: $-\sum_{i,j} p(i,j)\log_2[p(i,j)]$.

Classification of mice models: For classification of mice models, we employed linear discriminant analysis (LDA) and logistic regression approaches. Linear discriminant analysis (LDA) is a traditional statisitcal method based on feature reduction. We used LDA for multiclass classification of different mice models. The classifical LDA faces a problem known as singularity where the number of features is much larger than the number of samples. However, in our problem, since the number of samples is larger than the number of features, we simply employed the classfical LDA. Logistic regression is widely used for statistical analysis of binary data. In this study, we dichotomized the data into two groups: group 1 (MCF7+BT474) (fast growing, non-triple negative) versus group 2 (MDA213+MDA435) (slow growing, triple negative). The formula for logistic regression is

$$p = \frac{1}{1+\exp(-\mathrm{Y})}$$

where Y takes the form of linear regression. In this analysis, group 1 and group 2 were coded as 0 and 1, respectively.

Results:

Lac spectroscopic studies were carried out using MCF-7(0-800 mm^3), MDA-MB-231(0-600 mm^3), MDA-MB-435 (0-650 mm3), BT-474 (0-900 mm^3) mammary tumors with different molecular profiles (**Table 1**). We collected non-localized Lac signal from 1D and slice localized 1D and 2D chemical shift imaging data.

Table 1. Molecular classification of breast tumors

Cell line	Immunoprofile
MCF7	ER+,PR+,HER2-
BT-474	ER+,PR+,HER2+
MDA-MB-231	ER-,PR-,HER2-
MDA-MB-435	ER-,PR-,HER2-

ER, estrogen receptor; PR, progesterone receptor; HER2, human epidermal growth factor receptor 2; ER/PR/HER2 status were mentioned according to the histopathology reports with the published literature.

We implemented the SS-SelMQC using higher order binomial pulses (SS1-SelMQC) as described in methods for lactate detection with better Lip suppression and compared with SS-SelMQC [1] (**Figure 4**). The lactate signal enhancement was consistent wrt SelMQC [2] sequence. Subsequently, T1- and T2-versions of this sequence for T_1 and T_2 measurements to facilitate absolute Lac quantification.

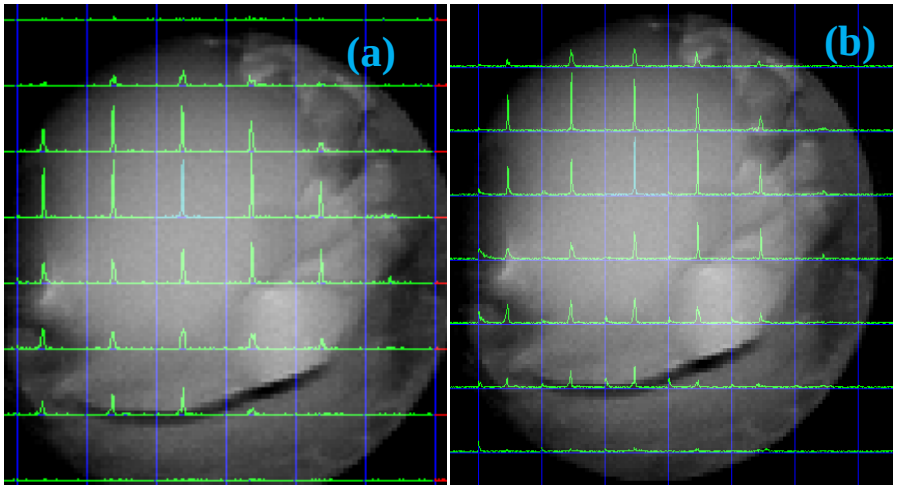

Figure 4: 2D CSI of 30mMol Lactate/lipid (a)SS-SelMQC (b) SS1-SelMQC sequence for in plane resolution of 1.25x1.25 mm2 at 4.7T using FOV=20mm slice thickness is 5mm, TR=2s Number of scans=8 and acquisition time= 76 minutes. Better lipid suppression at outer layer of tumor is noted.

Lactate detection in 4T1 mice tumors and its relation to LDH-A levels and metastatic potential: Lactate detection and quantification methods were also implemented for studying mice breast tumor cell lines such as 4T1 and 67NR. This work demonstrated lactate as a biomarker for tumor aggressiveness in fast growing 4T1 mice breast tumors compared to 67NR [5]. Lactate concentrations were related to LDH-A levels and they were increased when associated with metastasis [5]. We observed reduction in lactate levels by knocking down the LDH-A pathways in 4T1 breast tumors [6].

In our attempt to study the relation between Lac signal and the tumor aggressiveness, we calculated [Lac] in all four mammary tumor models (Table. 1). A representative stacked plot of slice-localized lactate signal in MCF7 tumors as a function of increasing tumor volumes (**Figure 5**) was shown.

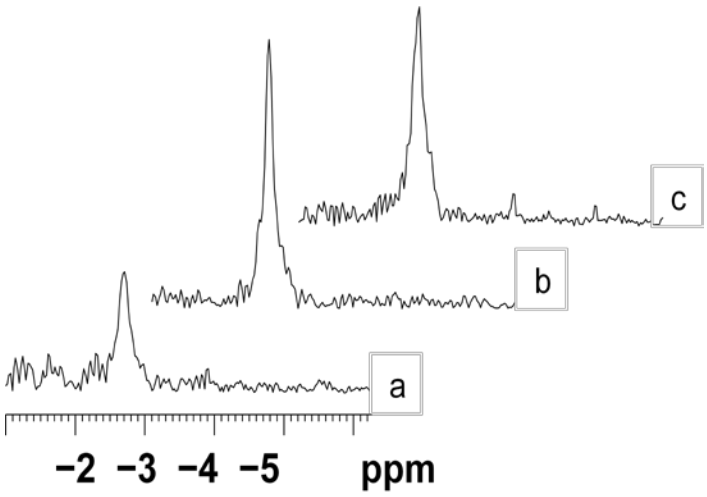

Figure 5. *In vivo* Lac spectra of MCF-7 tumor with slice thickness is 5mm at various tumor volume (a) 150 mm^3, (b) =330 mm^3 and (c) =750 mm^3; TR=3s; Number of scans=16 and acquisition time= 48 minutes.

Using T1- and T2- versions of SS1-SelMQC pulse sequence, T1 and T2 values were calculated for in vivo MCF, BT-474, MDA231 and MDA435 breast tumors. A representative stacked plot of T1 and T2 decay of lactate signal was shown (**Figure 6**). We found no significant correlation of T1 values in tumors with different expression levels of ER, PR and HER2 levels (**Figure 7**). T2 values are significantly lower in triple negative tumors compared with other tumors. These factors lead to correction factors in calculating lactate concentrations. For quantification of lactate 1D and 2D data sets, external spherical phantom with 15 mM lactate solution was used as a reference.

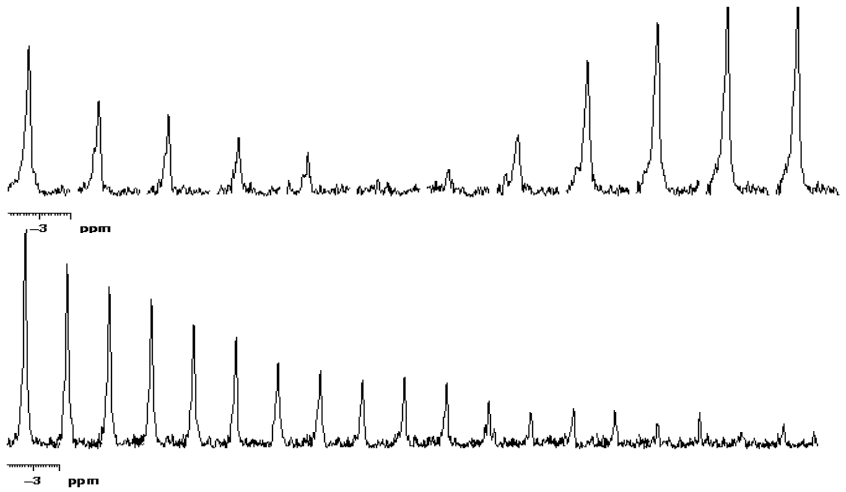

Figure 6. A representative MCF tumor with volume of 300 mm^3 in-vivo Lac spectra: In vivo (MCF-7 tumor) Lac signal recovery of T_1-SS-SelMQC with variable inversion time 0.1, 0.2, 0.4, 0.6, 0.8, 1.0, 1.5, 2, 4, 6, 8 and 10s. (Top). In vivo (MCF-7 tumor) Lac signal decay T_2-SS-SelMQC with 2*TE′(0.08 to 0.42s) with 0.02 s increments (Bottom). The calculated T_1 1.6 s and T_2 0.16 s.

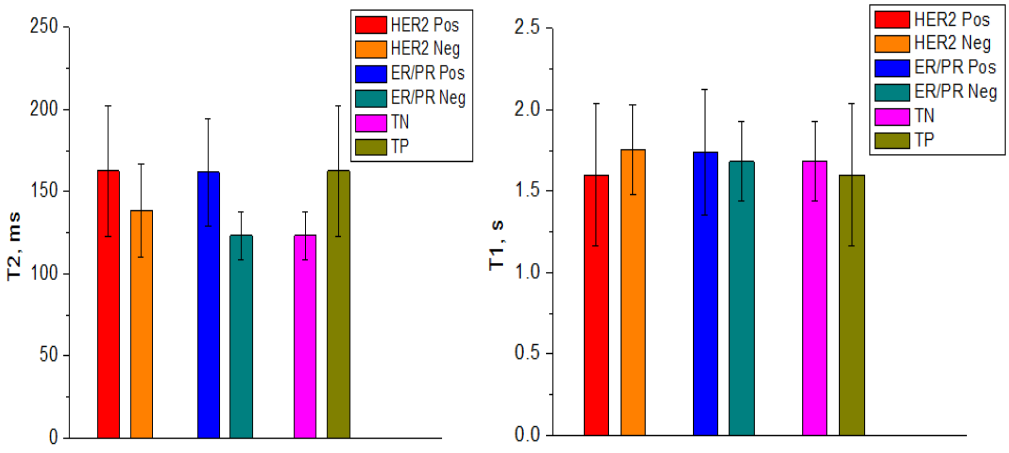

Figure 7. Comparison of T1 (A) and T2 (B) values in breast mammary tumors with different growth rates and protein expression levels. T1 and T2 values are defined as (mean ± standard deviation); MCF-7, BT-474, MDA-231 and MDA-435 tumors were classified into HER2 Pos, HER2 Neg, ER/PR Pos, ER/PR Neg, Triple negative (TN), and Triple positive (TP) groups. No significant differences were observed in T1 values between any two groups ($P < 0.05$). *Significant differences in T2 were observed between ER/PR pos versus ER/PR neg groups ($p = 0.02$), TN versus TP ($p = 0.0667$), and HER2 pos versus HER2 neg ($p = 0.2398$).

We calculated concentrations from 1D signal using external reference phantom of 15mM lactate. For 2D data sets, lactate concentrations were estimated, which are similar to 1D slice Lac concentrations and histology correlation was done. For all tumor models, lactate concentrations [Lac] were calculated using external reference method. The [Lac] in MCF-7, BT-474, MDA-MB-231 and MDA-MB-435 tumors were measured with respect to tumor volume (**Figure. 8**). This work is under submission to magnetic resonance in medicine.

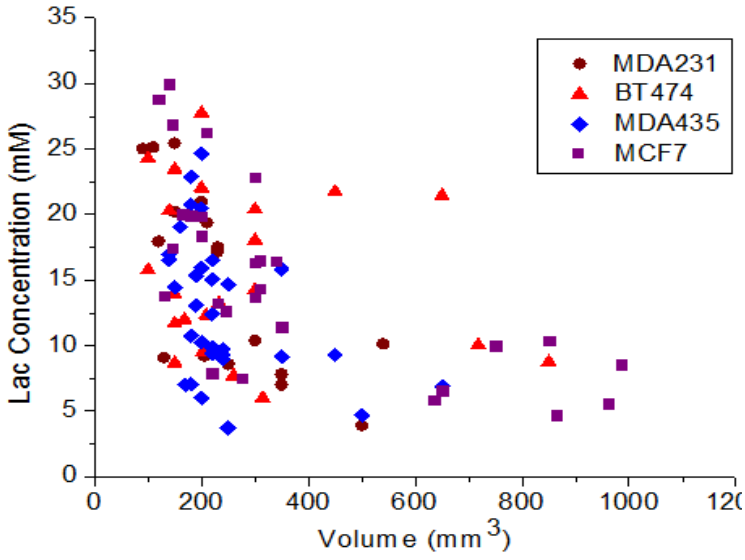

Figure 8: [Lac] with increasing tumor volumes.

Representative 2D lactate color maps overlaid on T2 images were generated for BT-474 tumor at three different tumor volumes (**Figure 9A**). Combined with the histology correlations (Figure. 9B) and texture features from T2 images (Table 2), results are finalized and in the process of submission.

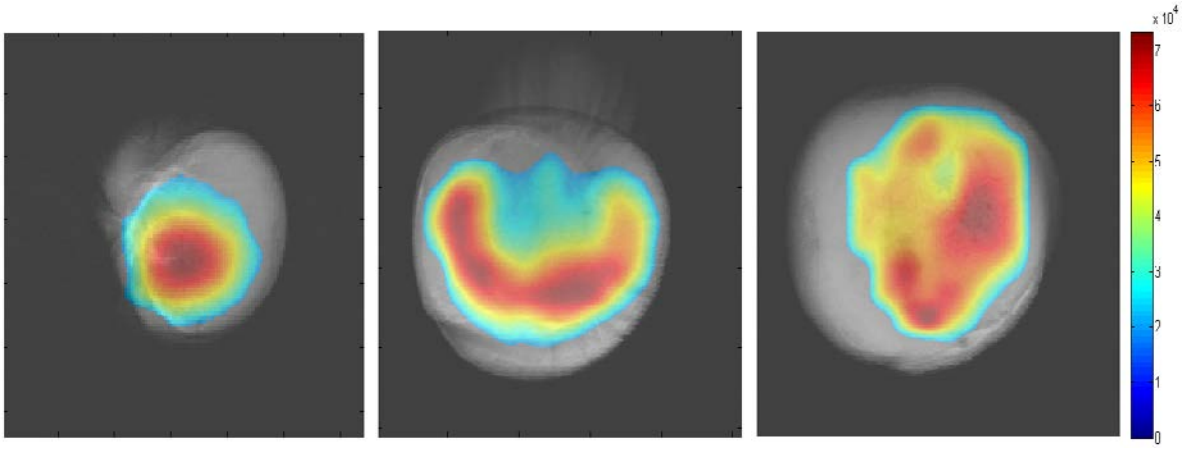

Figure 9A. Lactate area under the peak plotted as color map with increasing tumor volumes **in BT-474 tumors** shown by grey T2 images. Area under the peak will be converted into millimole concentrations using external reference data. Tumor volumes: (left) 200 mm3 (middle) 450 mm3 (right) 718mm3.

Tumor Slice Volume (mm3)	Tumor Slice [Lac]	Tumor Whole Volume (mm3)	Tumor Whole [Lac]	Contrast	Correlation	Energy	Homogeneity	Entropy	Kurtosis	Skewness
399.05	23.74	650	21.44	0.22	0.97	0.23	0.94	1.85	2.05	-0.83
167.16	33.29	200	22.02	0.77	0.94	0.14	0.88	2.49	1.35	-0.16
197.60	5.71	209	12.33	0.34	0.97	0.19	0.93	2.12	1.73	-0.65
554.73	8.48	850	8.75	0.23	0.98	0.21	0.95	1.93	1.68	-0.58
219.95	8.65	315	6.00	0.30	0.94	0.29	0.93	1.75	1.93	-0.52
247.58	18.01	300	20.38	0.45	0.94	0.15	0.90	2.39	1.78	-0.16
211.00	19.95	200	27.75	0.51	0.94	0.17	0.88	2.18	1.57	-0.53
131.00	8.69	150	11.71	0.33	0.96	0.19	0.91	2.10	1.57	-0.52
149.00	8.97	150	8.69	0.52	0.95	0.18	0.91	2.33	1.46	0.29
253.14	12.97	300	14.27	0.42	0.97	0.16	0.90	2.26	1.43	-0.42
195.78	6.46	260	7.68	0.23	0.96	0.21	0.93	1.93	1.62	-0.45
227.59	18.25	300	18.04	0.45	0.95	0.15	0.86	2.32	1.71	-0.60
91.75	23.75	140	20.30	0.60	0.95	0.16	0.88	2.37	1.27	0.09
191.87	16.86	150	23.46	0.39	0.97	0.18	0.93	2.14	1.33	-0.34
446.39	11.69	450	21.75	0.26	0.97	0.15	0.95	2.23	1.46	-0.11
214.89	12.06	233	13.26	0.27	0.97	0.26	0.94	1.85	1.21	-0.11
437.59	10.44	718	10.05	0.26	0.97	0.21	0.95	1.96	2.16	-0.92

Table 2. Texture features of BT-474 tumors as a function of tumor volume.

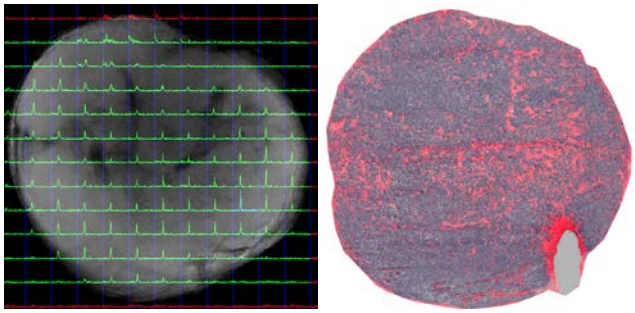

Figure 9B. *In vivo* T1-weighted/lactate MRS imaging (left) and *ex vivo* H&E histologic staining with superimposed LDH-A immunostaining (red) from the same xenograft tumor (right). Orientation of tumor sections was maintained with respect to MRI imaging using angiocatheters inserted post-imaging as fiduciary markers. LDH-A immunostaining and imaging was carried out using 10mm frozen tumor sections. Subsequent H&E staining was preformed using the same section. Regions of LDH-A expression show a general correspondence with regions of high lactate concentration (e.g. lower right quadrant), and is absent from regions of low tumor lactate (e.g upper left quadrant). An exact spatial correspondence is not expected due to large differences in the respective resolution of each method (5mm MRS vs 10mm IHC). However, the data shown is consistent with there being a spatial relationship between LDH-A expression and elevated levels of lactate within the tumor.

In LDA analysis, we tested three scenarios with the different number of groups using leave-one-out cross-validation (LOOCV): four groups (MCF7 vs BT474 vs MDA213 vs MDA435), three groups (MCF7 vs BT474 vs [MDA213+MDA435]), and two groups ([MCF7+BT474] vs [MDA213+MDA435]). Note that MDA213 and MDA435 are triple negative models. The following three tables show the results of classification for four, three, and two groups. In the case of classification with triple-negative and non-triple-negative, considerable accuracy was obtained with 77.3%.

Four groups

	MCF7	BT474	MDA231	MDA435
MCF7	6	11	0	8
BT474	5	6	0	6
MDA231	0	0	9	7
MDA435	1	3	4	22

Three groups

	MCF7	BT-474	MDA231+MDA435
MCF7	8	11	6
BT-474	5	6	6
MDA231+ MDA435	3	5	38

Two groups

	MCF7+BT474	MDA231+MDA435
MCF7+BT474	28	14
MDA231+MDA435	6	40

In analysis using logistic regression, we used the loocv approach to find the best model. The following graph shows Spearman's correlation coefficient (Rs) for different model orders (**Figure 10**). Here the model order represents the number of model features (degree of complexity of the model). The graph represents that the best model has three features.

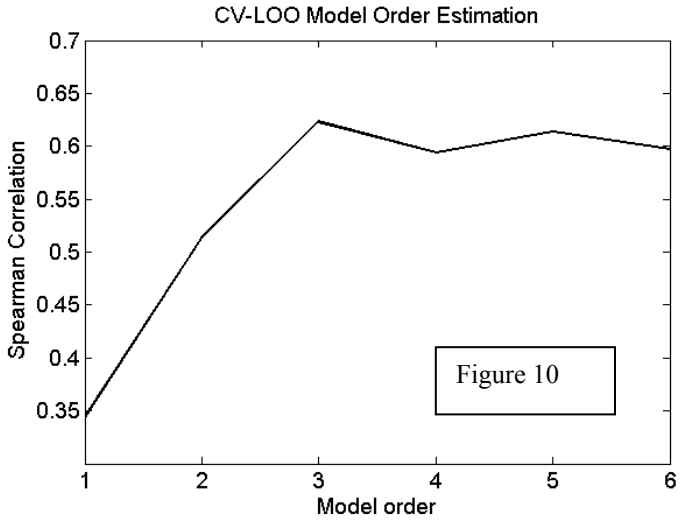

Figure 10

Once we found the best model, we applied it to our dataset. The following logistic regression model with three features including Tumor Slice [Lac], Tumor Whole Volume, and Homogeneity was found to be the best model:

Y=−0.243 × Tumor Slice [Lac] – 0.0104 × Tumor Whole Volume + 78 x Homogeneity – 66.4.

This model shows significant predictive power with Rs=0.67 ($p < 0.0001$) and area under the receiver operating characteristic (ROC) curve (AUC) = 0.89.
To investigate the predictive power without using texture features, we built another logistic regression model using only Tumor Slice [Lac] and Tumor Whole Volume. We achieved Rs=0.54 ($p < 0.0001$) and AUC = 0.812 with the following logistic regression model:

Y=−0.257 × Tumor Slice [Lac] – 0.0055 × Tumor Whole Volume + 4.61.

In comparison of two models found above, it is obvious that there was great performance improvement using the homogeneity feature, especially in Rs.

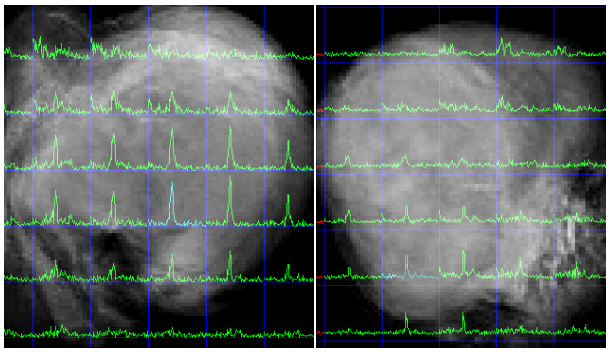

Figure 11. 2D chemical shift imaging lactate spectra from 5mm sagittal slice within MDA-435 tumor (tumor volume= 160 mm3) as a function of Avastin treatment- 0th day (left) and 2nd day (right). Reduction in the lactate levels are visible at the 2nd day of the treatment.

Treatment: We have treated the breast tumors with targeted drugs. From the control data it is visible that lactate concentrations are high within tumor volumes of 150-200 mm3. So we started treating the mice at this tumor volume. Representative data on MDA-435 tumors treatment with Avastin demonstrated that lactate levels were decreased at the 2nd day of treatment with no visible reduction in the tumor volume (Figure 11). Results demonstrate that lactate can be an early biomarker in treatment. Similar effect was observed in MDA-231 tumors with Avastin treatment (Figure 12). At 2nd day after the treatment, lactate levels were decreased with no visible reduction in the tumor volume. In MCF7 tumors, we did not observe any significant effect as a function of Herceptin or Avastin treatments.

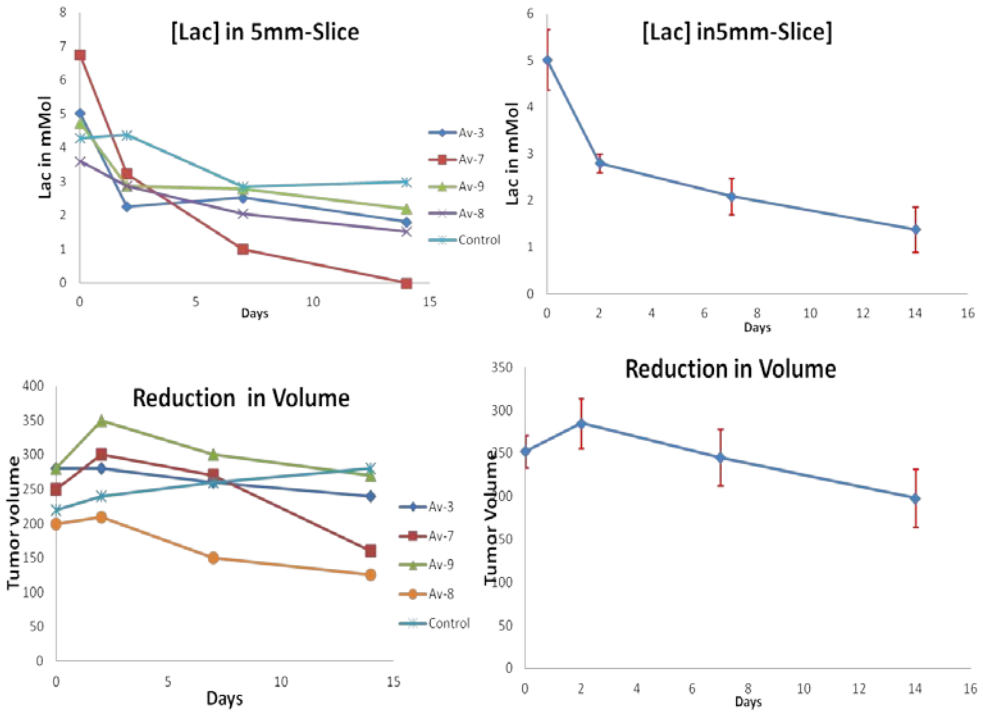

Figure 12. Lactate (Lac) concentrations (TOP PANEL) and tumor volumes (BOTTOM PANEL) in MDA-MB-231 tumors as a function of Avastin treatment at 0^{th}, 2^{nd}, 7th, and 14^{th} day (TOP PANEL).

We did the analysis for tumor tissue histology pre- and post treatments. We are in the process of presenting this work for NMR in biomedicine to describe the correlation of the 2D lactate voxel-by-voxel maps and texture features to explain tumor heterogeneity and treatment response.

KEY RESEARCH ACCOMPLISHMENTS:

1. SS-SelMQC with 1331 binomial pulses was developed for efficient Lac detection in the presence of frequency shifts. T1- and T2- versions were designed to derive the relaxation correction factors.

2. [Lac] can be used as a marker to differentiate slow growing from fast growing breast tumors. Lactate concentrations are low in slow growing tumors and high in fast growing tumors.

3. T2 may act as a marker for differentiation of these triple negative aggressive tumors. T2 relaxation constant was shorter in triple negative tumors compared with rest of tumors.

4. We have developed predictive models using novel image features and tested our predictive models with them extracted from MR, PET, and CT images. Texture features have added predictive power to classify these tumors (triple-negative versus non-triple negative).

5. [Lac] seems to be an early marker for studying treatment response. Treatment response was detected within 48 hours of treatment.

REPORTABLE OUTCOMES:

1. Serganova I, Rizwan A, Ni X, Thakur SB, Vider J, Russell J, Blasberg R, Koutcher JA. Metabolic Imaging: A link between Lactate Dehydrogenase A, Lactate and Tumor Phenotype. *Clin Cancer Res* 2011; 17:6250-6261. (APPENDIX 1)
2. Annarao S, Thomas K, Pillarsetty N, Koutcher JA and Thakur SB. In vivo lactate T1 and T2 relaxation measurements in ER-positive breast tumors using SS1-SelMQC editing sequence, ISMRM 20th Scientific Meeting & Exhibition, 2012, Melbourne, Australia. (APPENDIX 2)
3. Annarao S, and Thakur SB, 'Quantification of lactate concentrations in orthotopic breast tumors with different growth rates', ISMRM 20th Scientific Meeting & Exhibition, 2012, Melbourne, Australia. (APPENDIX 3)
4. Rizwan A , Serganova I , Khanin R , Karabeber H, Ni X, Thakur SB, Zakian KL , Blasberg RG, Koutcher JA. Relationships between LDH-A, Lactate and Metastases in 4T1 Breast Tumors. Clin Cancer Res 2013; 19:5158-5169. (APPENDIX 4)
5. Measurement of Lactate Concentrations in the Breast Mammary Tumors Using Selective Multiple Quantum Coherence Editing Sequence at 4.7T (In the process of submission)

CONCLUSION:

Lactate concentrations are high at low tumor volumes and decreases as increasing tumor volumes in all tumor models. The classification of two groups (triple-negative vs non-triple negative) showed great predictive power using LDA and logistic regression. When these tumors were treated with targeted drugs, [Lac] was shown to be an early marker and predicted the treatment response within 48 hours following the treatment. These results may help in understanding the tumor aggressiveness and its relation to LDH-A expression levels in these tumors. Additionally, monotherapy treatment results in our mammary tumors will help to explore the treatment response using combinational therapy in breast cancer patients.

References

1. Thakur SB, Yaligar J, Koutcher JA. In vivo lactate signal enhancement using binomial spectral-selective pulses in selective MQ coherence (SS_SelMQC) spectroscopy. Magn Reson Med 2009 Sept; 62(3):591-598.
2. He Q, Shungu DC, van Zijl PC, Bhujwalla ZM, Glickson JD. Single-scan in vivo lactate editing with complete lipid and water suppression by selective multiple-quantum-coherence transfer (Sel-MQC) with application to tumors. J Magn Reson B 1995 Mar; 1 06(3):203-11.
3. Annarao S, and Thakur SB, 'Quantification of lactate concentrations in orthotopic breast tumors with different growth rates ',International Society of Magnetic Resonance Medicine, 5-11 May 2012, Melbourne, Australia.
4. Annarao S, Ku T, Pillarseti NK, Koutcher JA, Thakur SB. In Vivo Lactate T1 and T2 Relaxation Measurements in Breast Tumors Using SS1-SelMQC Editing Sequence. ISMRM 20th Scientific Meeting & Exhibition, 2012, Melbourne, Australia.
5. Serganova I, Rizwan A, Ni X, Thakur SB, Vider J, Russell J, Blasberg R, Koutcher JA. Metabolic Imaging: A link between Lactate Dehydrogenase A, Lactate and Tumor Phenotype. *Clin Cancer Res* 17(19):6250-61. Epub 2011 Aug 15.
6. Annarao, K. Thomas, N. Pillarsetty, J. Koutcher and S. Thakur. In vivo lactate T1 and T2 relaxation measurements in ER-positive breast tumors using SS1-SelMQC editing sequence, International Society of Magnetic Resonance Medicine, 5-11 May 2012, Melbourne, Australia.

Appendices: The following were added in sequence.

APPENDIX 1
APPENDIX 2
APPENDIX 3
APPENDIX 4

Published OnlineFirst August 15, 2011; DOI:10.1158/1078-0432.CCR-11-0397

Clinical Cancer Research

Metabolic Imaging: A Link between Lactate Dehydrogenase A, Lactate, and Tumor Phenotype

Inna Serganova, Asif Rizwan, Xiaohui Ni, et al.

Clin Cancer Res 2011;17:6250-6261. Published OnlineFirst August 15, 2011.

Published OnlineFirst August 15, 2011; DOI:10.1158/1078-0432.CCR-11-0397

Imaging, Diagnosis, Prognosis

Clinical Cancer Research

Metabolic Imaging: A Link between Lactate Dehydrogenase A, Lactate, and Tumor Phenotype

Inna Serganova[1], Asif Rizwan[2], Xiaohui Ni[2], Sunitha B. Thakur[2,3], Jelena Vider[1], James Russell[2], Ronald Blasberg[1,3,5], and Jason A. Koutcher[2,3,4,5]

Abstract

Purpose: We compared the metabolic profiles and the association between LDH-A expression and lactate production in two isogenic murine breast cancer cell lines and tumors (67NR and 4T1). These cell lines were derived from a single mammary tumor and have different growth and metabolic phenotypes.

Experimental Design: LDH-A expression, lactate concentration, glucose utilization, and oxygen consumption were measured in cells, and the potential relationship between tumor lactate levels [measured by magnetic resonance spectroscopic imaging (MRSI)] and tumor glucose utilization [measured by [^{18}F]2-deoxy-2-fluoro-D-glucose positron emission tomography ([^{18}F]FDG-PET)] was assessed in orthotopic breast tumors derived from these cell lines.

Results: We show a substantial difference in LDH-A expression between 67NR and 4T1 cells under normoxia and hypoxia. We also show that small orthotopic 4T1 tumors generate 10-fold more lactate than corresponding 67NR tumors. The high lactate levels in small primary 4T1 tumors are associated with intense pimonidazole staining (a hypoxia indicator). Less-intense hypoxia staining was observed in the larger 67NR tumors and is consistent with the gradual increase and plateau of lactate concentration in enlarging 67NR tumors.

Conclusions: Lactate-MRSI has a greater dynamic range than [^{18}F]FDG-PET and may be a more sensitive measure with which to evaluate the aggressive and metastatic potential of primary breast tumors. *Clin Cancer Res; 17(19); 6250–61. ©2011 AACR.*

Introduction

Metabolic changes in primary tumors have a significant impact on tumor progression and on the development of the metastatic phenotype (1, 2). The accumulation of lactate in tumor cells was first described by Warburg and is associated with aerobic glycolysis (3). Clinical studies showed that high lactate levels (with median concentrations >8 mmol/L) are associated with the subsequent development of metastases (4) and include primary cervical, head and neck, and rectal cancers (5–7). The recent coupling between metabolic and genetic variations in cancer cells has stimulated renewed interest in the role of cellular metabolism (2, 8, 9). In cancer patients, serum total lactate dehydrogenase (LDH) levels are often increased, and the gene for *LDH-A* protein is often upregulated in tumors (10, 11). These features have been linked to poor prognosis (11–15), and a greater metastatic potential has been reported in patients with high LDH serum levels (11, 14). Because LDH-A protein is required for the maintenance and progression of many tumors (10, 16), it is also becoming a potential target for cancer therapy (16–18). Many cancers, particularly those originating in the breast and ovary, are highly heterogeneous, representing a large array of diseases with different etiologies (19) and with distinct genetic and phenotypic signatures (20). The metabolic response of individual tumor cells within a tumor is dependent on the environmental conditions (nutrient depletion, hypoxia, acidity, specific stromal cell components, etc.) encountered within the local tumor microenvironment, as well as specific oncogenic and/or tumor suppressor mutations of the tumor cell itself (9).

We investigated the relationship between LDH-A expression and lactate production in 2 isogenic breast cancer lines (67NR and 4T1). These 2 cell lines were derived from a single mammary tumor that developed spontaneously in a BALB/c mouse. Each subclone was shown to have different phenotypic properties (21–23). 67NR cells form primary tumors but do not metastasize. 4T1 cells are able to

Authors' Affiliations: Departments of [1]Neurology, [2]Medical Physics, [3]Radiology, and [4]Medicine, [5]Molecular Pharmacology and Chemistry Program, Memorial Sloan Kettering Cancer Center, New York, New York

Note: Supplementary data for this article are available at Clinical Cancer Research Online (http://clincancerres.aacrjournals.org/).

I. Serganova, A. Rizwan, and X. Ni contributed equally to this work.

Corresponding Author: Jason A. Koutcher, Imaging and Spectroscopic Physics, Department of Medical Physics, Genitourinary Oncology Medicine, Memorial Sloan Kettering Cancer Center, Room MRI 1125, 1275 York Avenue, New York, NY 10021. Phone: 212-639-8834; Fax: 212-717-3676; E-mail: koutchej@mskcc.org

doi: 10.1158/1078-0432.CCR-11-0397

Published OnlineFirst August 15, 2011; DOI:10.1158/1078-0432.CCR-11-0397

Translational Relevance

Using subclones derived from a single spontaneous murine breast tumor, we show that the more aggressive clone (4T1, with a high propensity to metastasize to lung and other organs) produces higher levels of lactate in small tumors that are associated with higher *LDH-A* expression and a higher intensity of pimonidazole staining, when compared with the nonmetastatic 67NR clone. Lactate-MRSI, but not [^{18}F]2-deoxy-2-fluoro-D-glucose positron emission tomography ([^{18}F]FDG-PET) imaging, was able to identify significant differences in the metabolic phenotype between these 2 orthotopic tumors. There was a 10-fold higher level of lactate in small 4T1 tumors than in 67NR tumors, at the time 4T1 lung metastases were developing. In contrast, there was only a 1.1-fold difference in [^{18}F]FDG accumulation in the same tumors. These studies show a much greater dynamic range for tumor lactate measurements than for measurements of [^{18}F]FDG accumulation in these tumor models.

complete all steps leading to distant metastases and efficiently form macroscopic nodules in the lung (21) and other organs (22, 24). We have shown a substantial variation in LDH-A expression between these 2 cell lines under normoxia and hypoxia that reflect LDH enzyme activity and lactate concentrations in tumors. Consistent with other reports (25, 26), only minor changes in LDH-B expression were observed. We also studied the potential correlation between glucose utilization, as measured by [^{18}F]2-deoxy-2-fluoro-D-glucose uptake and positron emission tomography ([^{18}F]FDG-PET), and lactate production, as measured by magnetic resonance spectroscopic imaging (MRSI), in growing orthotopic tumors.

We consider LDH to be a critical branch point in metabolism. It is involved in the metabolism of the 2 major nutrients, glucose and glutamine, as well as in determining tumor pH and the activity of the tricarboxylic acid (TCA) cycle (27). We hypothesized that tumor lactate levels monitored by MRSI will reflect LDH-A enzymatic activity and tumor phenotype. We show that lactate-MRSI measurements have a greater dynamic range than concurrent [^{18}F]FDG-PET measurements. We suggest that lactate-MRSI is a more sensitive measure than [^{18}F]FDG-PET and could be used in the clinic to evaluate the aggressive potential of primary breast tumors, as this imaging technology has been applied in human tumors.

Materials and Methods

Cell culture and growth

Two isogenic tumorigenic cell lines (67NR and 4T1), derived from a spontaneous breast tumor in a BALB/c mouse (provided by Fred Miller; Karmanos Cancer Institute, Detroit, MI), were studied. Cells were grown in complete Dulbecco's Modified Eagle's Media containing 10% fetal calf serum with 2 mmol/L L-glutamine and penicillin/streptomycin. Cells were plated at a density of 5×10^6 cells. Fourteen hours later, plates were placed under normal or hypoxic (1%) conditions to assess cell growth. During days 2 to 6, cells were trypsinized and resuspended in 1 mL of medium. Cells were counted using Countess Automated Cell Counter (Invitrogen).

Assessment of *LDH-A* mRNA expression

For all mRNA and proteins assays, we used cells growing for 48 hours (exponential growth phase). RNA was isolated using an "RNeasy" total RNA isolation kit (Qiagen), following the manufacturer's protocol. The presence of LDH-A and β-actin mRNAs was assessed using a QIAGEN One-Step RT-PCR kit. The mouse LDH-A cDNAs were amplified using the oligonucleotides 5′-CCTGTGGCTGGGCTCTTGGC-3′ and 5′-AGCCGGCTCTCCCCCTCTTG-3′. The level of β-actin transcript was used as an internal control and amplified using the oligonucleotides 5′-CCTAAGGCCAACCGTGAAAAGATG-3′ and 5′-GGGTGTAAACGCAGCTCAGTAAC-3′.

Western blotting

Breast cancer cell pellets underwent protein extraction using RIPA Buffer (25 mmol/L Tris HCl, pH = 7.6, 150 mmol/L NaCl, 1% NP-40, 1% sodium deoxycholate, 0.1% SDS; Thermo Scientific) and protease inhibitors cocktail (1:100; Thermo Scientific Halt Protease Inhibitor Cocktail). Protein concentrations were determined with bicinchoninic acid assay (BCA Protein Assay Kit; Pierce). In equivalent amounts (5–20 μg per well), the proteins were separated by electrophoresis using a NuPAGE 4-12% Bis-Tris gradient gel (Invitrogen) and transferred to an Immun-Blot PVDF membrane (BioRad). Membranes were blocked in 5% milk in TBS with Tween-20 buffer and were immunoblotted with anti-LDH-A antibody (#2012; Cell Signaling Technology) at a 1:1,000 dilution, anti-HXKII antibody (c-14, sc-6521; Santa Cruz Biotechnology) at a 1:200 dilution, anti-PKM2 antibody (#3198; Cell Signaling Technology) at a 1:1,000 dilution, and anti-LDH-B antibody (#1974-1; Epitomics) at a 1:1,000 dilution. Bound primary antibodies were visualized with appropriate horseradish peroxidase–conjugated secondary antibodies (1:2,000) using enhanced chemiluminescence reagent (Western Lightning-ECL). Immunoblots were stripped using Restore Western Blot Stripping Buffer (Thermo Scientific) and reprobed with anti-β-actin antibody (Abcam) at a 1:5,000 dilution.

LDH activity

Total LDH activity of 67NR and 4T1 cells was assessed using the Cytotoxicity Detection Kit PLUS (LDH; Roche Diagnostics). Different numbers of cells were plated in 96-well plates and incubated (37°C, 5%CO_2, 90% humidity) for 3 to 6 hours and lysed, and LDH activity was measured as described by the manufacturer.

Published OnlineFirst August 15, 2011; DOI:10.1158/1078-0432.CCR-11-0397

Glucose utilization

Glucose utilization of 67NR and 4T1 cells was assessed using the Glucose Assay Kit (MBL International). The glucose concentration in growth medium was measured and compared with a control medium at days 2 and 5.

L-Lactate

Lactate production by 67NR and 4T1 cells during growth was assessed by measuring the culture medium lactate using an L-lactate assay kit (Eton Bioscience).

Oxygen consumption assay

Oxygen consumption was measured using the OxyLite system (Oxford Optronics; ref. 28). Cells were cultured in 75 cm^2 flasks to approximately 90% confluence. Cells were trypsinized to prepare single cells in the growth media containing 25 mmol/L HEPES. Cells were suspended in 5 mL medium and incubated in sealed Reacti-vials (Pierce Scientific, now known as Thermo Fisher Scientific Inc.) at 37°C, with continuous stirring. The OxyLite probe was introduced into the cell mix using a 19-G needle to pierce the rubber septum. Measurements were recorded over 30 to 60 minutes. Medium pH was measured before and after the experiment. To show a maximal inhibition of the electron transfer chain, an inhibitor of the respiratory chain, rotenone was added to cells for 30 minutes at concentrations of 1 or 10 μmol/L. All experiments were repeated at least 3 times with cells from independent cultures.

Animal model

The animal protocol was approved by the Institutional Animal Care and Use Committee of Memorial Sloan Kettering Cancer Center. A total of 1×10^6 67NR and 4T1 cells were injected into the fourth right mammary fat pad of athymic *nu/nu* female mice (National Cancer Institute). Tumors were categorized into following 3 groups: small (<150 mm^3), medium (150–400 mm^3), and large (>400 mm^3). Tumor volume (V) was calculated from caliper measurements, where $V = (\pi/6) \times x \times y \times z$ where x, y, and z are 3 orthogonal diameters. A total of 20 mice [67NR ($n = 8$) and 4T1 ($n = 12$)] were used in the imaging experiments.

In vivo lactate detection

The lactate level in the tumor was detected using MRSI. Tumor-bearing mice were anesthetized with isoflurane (1.5%) combined with oxygen. MRSI experiments were carried out on a 7T Bruker Biospec Spectrometer using home-built 2-turn solenoid coils (7 and 12 mm in diameters). The coil was positioned in the center of the platform and matched with the isocenter of the magnet. Scout images acquired with the Bruker ParaVision TriPilot Sequence ensured that the tumor was in the center of the magnet. The body temperature of the mice was monitored and maintained at 35°C using a rectal temperature probe and warm air was directed on the animal (MR-compatible, small rodent Heater System; SA Instruments). The lactate signal was detected using the Selective Multiple Quantum Coherence (SelMQC) editing sequence (29, 30). Spectra of both the whole tumor and a 5-mm thick center slice in the coronal plane were acquired with repetition time (TR) = 2 seconds, number of excitations = 8,512 data points, and spectral width = 2,510 Hz. Two-dimensional chemical shift imaging (2D-CSI) of the localized, 5-mm thick coronal slice was conducted with the following parameters: matrix size = 16 × 16 and field of view = 24 mm (1.5 × 1.5 mm^2 in plane resolution). The voxel volume of the CSI was 11.25 mm^3, and total 2D-CSI acquisition time was 70 minutes. The 2D-CSI was coregistered with a T_2-weighted image using a multislice multiecho sequence (MSME). The parameters for the MSME included a slice thickness = 1 mm, field of view = 24 mm, 2,217-ms repetition time, 40-ms echo time, matrix size = 512 × 256, and number of average = 8. Multislice images of the tumor in the coronal plane were also acquired using rapid acquisition with relaxation enhancement (RARE) sequence with a slice thickness of 1 mm. The volumes of the tumor in the central slice for CSI were calculated by drawing regions of interest (ROI) in the T_2-weighted image to find the tumor area and then multiplying the area by the slice thickness.

Magnetic resonance data processing

The 1D lactate spectra from the 5-mm thick center slice were processed by a 1D Fourier transform, similar to our previous methodology (31). The absolute magnitude of the echo signal from the slice was fitted by a home-written program using Matlab (The MathWorks) and normalized to the slice volume. Lactate spectra quantitation was conducted by the phantom replacement technique (32), using a 10 mmol/L lactate/H_2O cylinder. The concentration of *in vivo* tumor lactate, C, can be calculated from the phantom solution of known lactate concentration C^{ref} as follows:

$$C = C^{ref} \times f_{T_1,T_2} \times \frac{A}{A^{ref}}$$

where A and A^{ref} are the measured areas under the fitted peaks in tumor and in the reference phantom, respectively. The relaxation times, T_1 and T_2, were measured using modified T_1-SelMQC and T_2-SelMQC sequences which have been described elsewhere (30). The correction factor for T_1 and T_2 differences between phantom and *in vivo* data is as follows:

$$f_{T_1,T_2} = \exp\left[TE\left(\frac{1}{T_{2\,vivo}} - \frac{1}{T_{2\,phantom}}\right)\right] \times \frac{\left[1 - \exp\left(-TR/T_{1\,phantom}\right)\right]}{\left[1 - \exp\left(-TR/T_{1\,vivo}\right)\right]}$$

The T_1 values for the 67NR and 4T1 are 1.61 and 1.86 seconds, respectively. The T_2 values for the 67NR and 4T1 tumors are 0.21 and 0.34 seconds, respectively. For the lactate phantom, the T_1 is 1.3 seconds and T_2 is 0.5 seconds. The 2D-CSI data from the tumor and the phantom were processed voxel by voxel by the 3DiCSI Software Package (courtesy of Truman Brown, PhD, Columbia University, New York, NY). The spectra from the 2D-CSI were superimposed on the corresponding T_2-weighted MSME image

Published OnlineFirst August 15, 2011; DOI:10.1158/1078-0432.CCR-11-0397

using the 3DiCSI software. The spectrum from each tumor voxel was extracted for further processing by software written using Matlab. Voxel volume was selected as 11.25 mm^3 for both tumor and phantom. Also, the maximum concentration of lactate in a voxel was identified (hot spot for lactate) and recorded.

MicroPET

[^{18}F]FDG-PET imaging was conducted after lactate-MRSI, as previously described (33). [^{18}F]FDG (specific activity > 11 Ci/mmol, average purity 99%) was provided by IBA Molecular. An experimentally determined system calibration factor was used to convert voxel count rate to radioactivity concentrations, expressed as percentage of injected dose/mL (%ID/mL). ROI analysis of the reconstructed images was conducted using ASIPro software (Siemens Medical Solutions) to determine the average and maximum tumor radioactivity values. A partial volume correction was applied to the ROI-measured radioactivity data (Supplementary Fig. S1).

Immunohistochemical staining

Selected animals were injected with pimonidazole hydrochloride (hypoxyprobe-1, HPI) and Hoechst 33342 (Sigma-Aldrich) at 60 and 40 mg/kg, respectively. These agents were dissolved in PBS and administered by way of the tail vein. Pimonidazole hydrochloride was administered 1 hour presacrifice, and Hoechst 33342 was administered 5 minutes presacrifice (34). Tumors were immediately frozen at −80°C for immunohistochemistry. Ten-micrometer thick, adjacent frozen sections from the estimated location of the MRS slice were obtained using a Microm HM500 cryostat microtome (Microm International GmbH). The sections were imaged for Hoechst (blood perfusion) and for pimonidazole (hypoxia) detection. The sections were then stained with CD31 antibody (endothelial cell marker), and adjacent tumor sections were processed for hematoxylin and eosin (H&E) staining. Images of the sections were processed using Matlab to estimate the fraction of tumor necrosis (31).

Statistical analyses

All values are expressed as mean ± SD. Statistical significance was determined by a 2-tailed Student's *t* test; a value of $P < 0.05$ was considered significant.

Results

Metabolic characterization of 67NR and 4T1 murine breast cancer cell lines

The metabolic features of 2 isogenic tumor cell lines, with different phenotypic growth and metastatic characteristics, were compared and related to LDH-A mRNA expression and protein levels. Semiquantitative reverse transcriptase (RT)-PCR and immunoblotting for LDH-A showed that nonmetastatic 67NR cells express lower levels of LDH-A in comparison with highly aggressive, metastases prone 4T1 cells during exponential growth under normal incubation conditions (Fig. 1A and B). To confirm that LDH-A expression levels correlate with the functional activity of LDH as an enzymatic complex, we conducted an enzymatic assay in viable 67NR and 4T1 cancer cells (Fig. 1C). LDH activity was approximately 5-fold higher in 4T1 cells than in 67NR cells.

We also assessed the expression levels of 2 other glycolytic enzymes, HXKII (hexokinase II) and PKM2 (pyruvate kinase muscle isozyme 2; Fig. 1B). HXKII and PKM2 are overexpressed in 4T1 cells compared with 67NR cells; the relative intensity of the immunoblot bands was measured and showed a 3- and 2-fold difference, respectively (data not shown).

A significant difference in acidification of the incubation medium and lactate production was also observed between the 2 cell lines (Fig. 1D and G). At day 5 of cell growth, the medium pH of 4T1 was 6.9 ± 0.1 whereas the medium pH of 67NR cells was 7.4 ± 0.1. Glucose utilization by 67NR and 4T1 cells was also significantly different (Fig. 1F); 4T1 cells exhausted the supply of glucose in the medium within 5 days of incubation whereas 67NR cells used only 50% of the available glucose during this period. These differences are significant at day 5 of cell growth and cannot be explained by differences in cell numbers.

Many advanced cancers that reflect the Warburg phenotype have high glucose uptake with conversion of glucose to lactate. Cells with this phenotype consume available oxygen at a rate dictated by their oxidative capacity, and this consumption rate can be measured. Interestingly, 4T1 cells had a 3-fold higher rate of oxygen consumption than 67NR cells. The inhibition of the mitochondrial respiratory chain complex I by 1 μmol/L rotenone was approximately 90% in 4T1 cells and 100% in 67NR cells (Fig. 1E). Rotenone at 10 μmol/L completely inhibited oxygen consumption in both cell lines.

In vivo lactate detection with ^{1}H-MRSI using a SelMQC sequence

Because 67NR and 4T1 cancer cells show significant differences in the expression of HXKII, PKM2, and LDH-A, as well as glycolytic flux and mitochondrial respiration, we decided to assess whether they exhibited a different metabolic phenotype *in vivo* as well. Lactate concentration in 67NR and 4T1 tumors was monitored by MRSI using the SelMQC sequence during tumor growth (the tumor growth profiles are shown in Supplementary Fig. S2). The 2D-CSI of nonmetastatic 67NR and metastatic-prone 4T1 tumors are compared at 3 different tumor volumes (Fig. 2A and B). Note that the distribution of lactate signal varies spatially across both 67NR and 4T1 tumors, reflecting the heterogeneity of tumor metabolism. A difference in total LDH-A expression is also present in 67NR and 4T1 tumors, as assessed by Western blotting (Fig. 2C).

Small (<150 mm^3) 67NR tumors showed very low levels of lactate (average lactate = 0.9 ± 1.9 mmol/L; Fig. 3A and C). Lactate levels in 67NR tumors larger than 150 mm^3 gradually increased and reached a plateau during tumor growth, with an average concentration of

Published OnlineFirst August 15, 2011; DOI:10.1158/1078-0432.CCR-11-0397

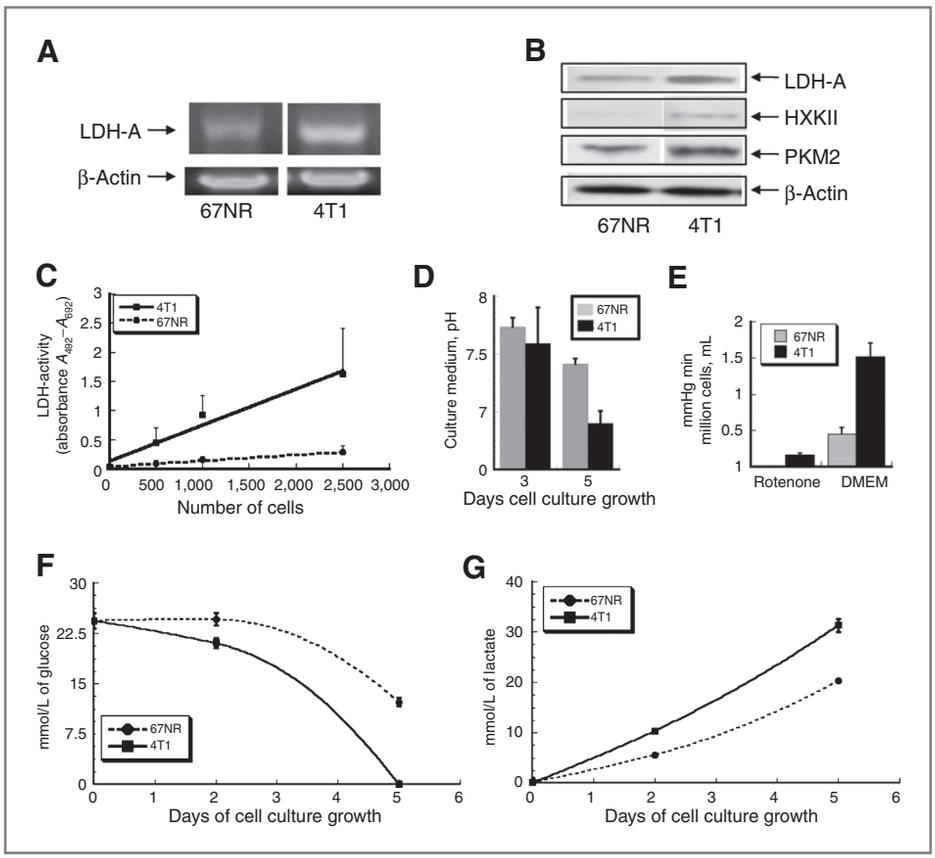

Figure 1. Metabolic features of isogenic 67NR and 4T1 breast cancer cells. A, LDH-A mRNA expression in 67NR and 4T1 cells by the semiquantitative RT-PCR. B, LDH-A, HXKII, and PKM2 proteins expression assessed by Western blotting. C, total LDH enzyme activity in 67NR cells and 4T1 cells. D, cell culture medium acidification; supernatant pH. E, oxygen consumption of 67NR and 4T1 cells in normal growth media [Dulbecco's Modified Eagle's Media (DMEM; high glucose) + 10% fetal calf serum + 2 mmol/L L-glutamine, 25 mmol/L HEPES] and upon treatment with 1 μmol/L of rotenone using the OxyLite system. F, glucose utilization; clearance of glucose from the culture medium. G, lactate production; appearance of lactate in the culture medium.

5.5 ± 1.8 mmol/L. Small (<150 mm^3) 4T1 tumors have significantly higher lactate concentrations (9.3 ± 2.7 mmol/L) than small 67NR tumors ($P = 0.0001$). In contrast to 67NR tumors, the lactate signal in 4T1 tumors decreased rapidly, as tumor size increased (Fig. 3B and C). Expressed differently, primary 4T1 tumors (6–8 days after orthotopic implantation when metastases are first detected; mean volume = 73 ± 14 mm^3) have very high lactate levels (11.0 ± 1.5 mmol/L). Plotting tumor lactate concentrations versus time after orthotopic implantation yielded lactate concentration profiles (Fig. 3D) similar to that obtained when plotted versus tumor volume (Fig. 3A and B).

An examination of the H&E sections of different size 67NR and 4T1 tumors showed that necrosis became visible in 4T1 tumors even at 100 mm^3 in size whereas necrotic areas were essentially absent in large (>400 mm^3) 67NR tumors (Supplementary Fig. S3). The decrease in lactate signal as 4T1 tumors increase in size (Fig. 3B) may be explained, in part, by the increase in tumor necrosis. We analyzed the H&E sections of 5 large 4T1 (450, 530, 670, 770, and 860 mm^3) tumors that had lactate-MRSI measurements just prior to sacrifice. The fraction of viable-appearing tissue in these large 4T1 tumors was calculated from the H&E images of these tumors using Matlab (described in Materials and Methods). When the lactate signal was corrected for the viable tissue volume, the average lactate concentration in those large 4T1 tumors was calculated to be 7.3 ± 1.4 mmol/L.

FDG microPET imaging

[^{18}F]FDG microPET scans were conducted following lactate ^{1}H-MRSI imaging on the same tumor-bearing animals. Small 67NR tumors (<150 mm^3) had an average partial volume-corrected [^{18}F]FDG uptake of 6.2 ± 1.5 %ID/mL, which slowly declined as the tumors increased in size (Fig. 4A and C). The partial volume-corrected [^{18}F]FDG uptake of small 4T1 tumors was 6.8 ± 2.2 %ID/mL, which decreased rapidly with tumor growth, approaching a plateau value of approximately 3%ID/mL as the tumors increased in size (Fig. 4B and C). All 4T1 tumors exhibited more-intense FDG accumulation along the periphery during the late stages of the growth (Fig. 4D), reflecting lower metabolism in central tumor areas with greater necrosis. MRSI also showed heterogeneity of lactate levels in medium and large 4T1 tumors, but there was not a strong segregation between the periphery and central core.

Comparison of growth profiles and LDH-A and LDH-B expression under normoxic and hypoxic conditions

4T1 cells grow more rapidly than 67NR cells during first 4 days of culture and then plateau whereas 67NR cells

Published OnlineFirst August 15, 2011; DOI:10.1158/1078-0432.CCR-11-0397

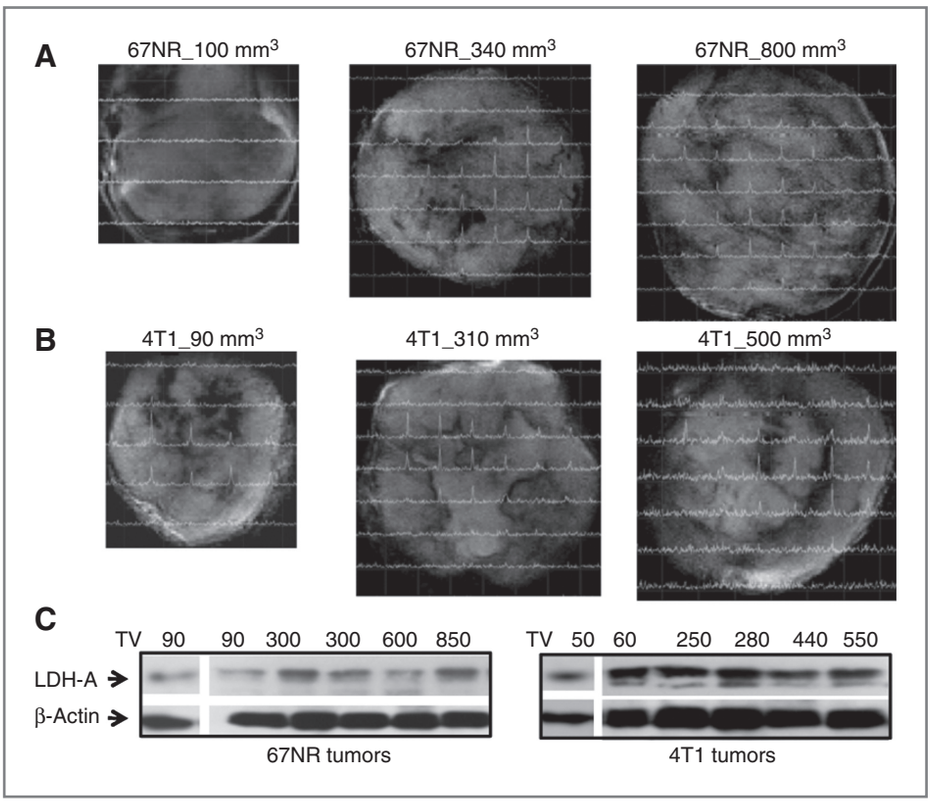

Figure 2. Lactate CSI spectra. A, different sizes of 67NR nonmetastatic tumors are shown. B, 4T1 metastasis-prone tumors are shown. Lactate signal was detected using CSI and a SelMQC editing sequence. C, LDH-A protein expression was assessed by Western blotting in different sizes of 67NR and 4T1 tumors. TV, tumor volume.

continue exponential cell growth through day 7 (Fig. 5A). Because we determined that 4T1 cells have a higher rate of oxygen consumption than 67NR cells (Fig. 1E), we conducted experiments to study the effect of hypoxia (1% oxygen) on cell growth. We found that the growth of 4T1 cells under hypoxic conditions declined after day 3 (Fig. 5A), suggesting that 4T1 cells are very sensitive to hypoxia. In contrast, 67NR cells were less affected by hypoxia and continued to grow slowly after day 3 (Fig. 5A).

We also assessed the impact of hypoxia (1% of oxygen) on LDH-A and LDH-B expression levels by immunoblotting. Hypoxia had little effect on LDH-B levels in the 2 cell lines, consistent with previous published studies (25, 26); the major change was found in LDH-A expression (Fig. 5). Importantly, 4T1 cells had a higher expression of more than 10-fold of LDH-A than 67NR cells under normoxic culture conditions, and both cell lines increase LDH-A expression in response to hypoxia (based on the β-actin–normalized intensity of the bands; Fig. 5B and C). 67NR cells have very low levels of LDH-A under normoxia, but an 18-fold upregulation was observed under hypoxia (Fig. 5B and C). Note that the LDH-A protein levels were similar in both cell lines under hypoxia.

The differential expression of LDH-A protein in 4T1 and 67NR cells under normoxic and hypoxic conditions in cell culture is consistent with the variation and difference in lactate levels measured by MRSI in small 4T1 and medium-to-large 67NR orthotopically growing tumors (Fig. 3). In support of this explanation, tumor samples were collected and processed after administration of pimonidazole hydrochloride and Hoechst 33342 (hypoxia and the blood perfusion probes, respectively; Fig. 6). Consistent with the *in vitro* results, small (100 mm^3) 4T1 tumors show small zones of necrosis (or impending necrosis) associated with pimonidazole (hypoxia) and attenuated perfusion staining. The intensity of pimonidazole staining was significantly higher in all 4T1 samples than in 67NR tumors. The visible, but less intense, hypoxia staining was observed only in the larger 67NR tumor samples. These results could partially explain the gradual increase and plateau level (5.5 ± 1.8 mmol/L) of lactate in medium and large sizes 67NR tumors as a result of increasing hypoxia that develops in the enlarging tumors (>150 mm^3; Fig. 3A). Moreover, the development of significant necrosis observed in all enlarging 4T1 tumors (Supplementary Fig. S3) may explain the lower lactate accumulation in comparison with small 4T1 tumors.

Discussion

Glucose and glutamine are the major carbon sources for rapidly proliferating tumors, providing precursors for nucleic acids, proteins, and lipids, as well as metabolic-reducing capability (NADPH). Pyruvate is largely derived from both glucose and glutamine metabolism; it can be converted to lactate by the LDH complex and/or enter the TCA cycle for conversion to CO_2 and ATP. The conversion of pyruvate to lactate is also catalyzed by LDH which is a

Published OnlineFirst August 15, 2011; DOI:10.1158/1078-0432.CCR-11-0397

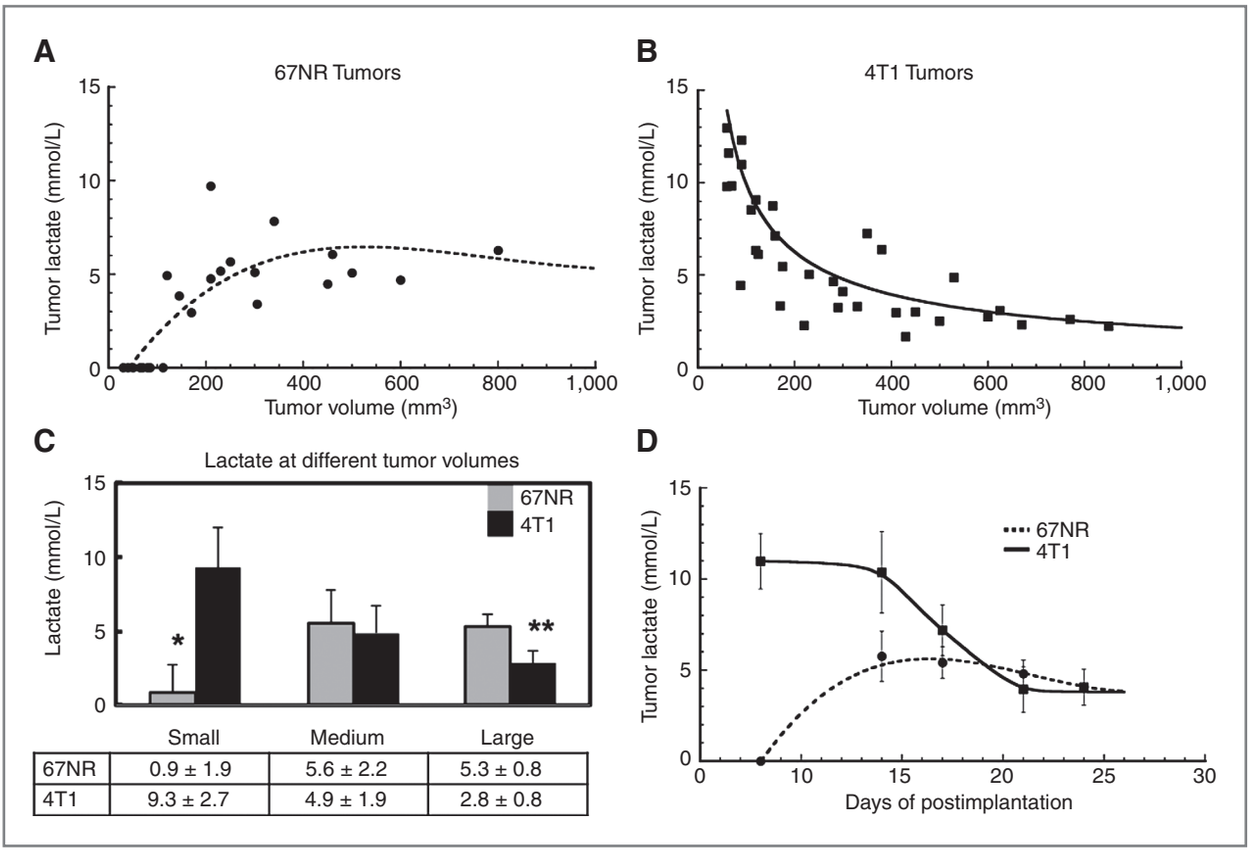

	Small	Medium	Large
67NR	0.9 ± 1.9	5.6 ± 2.2	5.3 ± 0.8
4T1	9.3 ± 2.7	4.9 ± 1.9	2.8 ± 0.8

Figure 3. MRSI measurements of lactate concentration in orthotopic 67NR and 4T1 breast tumors during tumor growth. Lactate concentration in (A) 67NR tumors (solid circles, dashed line) and in (B) 4T1 tumors (solid squares, solid line) plotted versus tumor volume. C, average lactate concentration at 3 different tumor volumes (small, <150 mm^3; medium, 150–400 mm^3; and large, >400 mm^3). Values are the mean ± SD. *, $P < 0.05$; **, $P < 0.01$. D, tumor lactate concentration plotted versus days postorthotopic implantation.

reversible reaction that results in the formation of NAD^+, which is necessary for further glycolysis. LDH isoenzymes are found in almost all eukaryotic cells and tissues, reflecting the importance of this metabolic step. As a consequence of increased glucose and glutamine metabolism, tumors secrete lactate, alanine, and NH_4^+. When oxygen is available, the accumulated and exogenous lactate can be reutilized and converted back to pyruvate, where it is further oxidized to CO_2 and H_2O in the TCA cycle, generating ATP and NAD^+ (35). Recently, it was shown that LDH-A is required for the maintenance and progression of many tumors (10, 16, 17), but the mechanisms by which LDH-A facilitates tumor progression are poorly understood.

We studied 2 isogenic cell lines (67NR and 4T1) originating from the same mammary tumor (21). Both cell lines generate orthotopic breast tumors with different growth and metastatic profiles (21): 67NR cells form primary tumors but no metastases, whereas 4T1 cells generate tumors that rapidly complete all steps leading to macroscopic nodules in lungs within 6 to 8 days of orthotopic implantation. In this study, we show that these cell lines and their corresponding orthotopic tumors have different metabolic profiles as well.

Significant differences in the gene expression pattern of 4T1 and 67NR cells have been described (22, 24, 36), and these differences contribute to the distinct metabolic and phenotypic behaviors of 4T1 and 67NR cells and tumors. A substantial number of highly expressed genes in 4T1 cells/tumors are associated with cell adhesion, migration, angiogenesis, extracellular matrix modification, cytoskeleton function, cell proliferation, apoptosis, survival, inflammation, immune response, and cellular metabolism. 4T1 cells also displayed elevated levels of *Gadd45*, *Pfkfb3*, *Vegfc*, *Flt1*; some of these genes are known to be regulated by hypoxia and glucose deprivation. This gene expression profile suggests that 4T1 cells are in a stress-related state, with high metabolic requirements that are inadequately supplied by the vasculature leading to hypoxia and glucose deprivation.

Our additional analysis of published data (22, 36) identified several other important modulators of tumor metabolism. Carbonic anhydrase isoform-12 (CA12) in 4T1 cells is expressed 6.7-fold above that in 67NR cells. CA12 is a transmembrane enzyme that maintains normal intracellular pH and is known to be upregulated by hypoxia-inducible factor 1. Furthermore, a 2.3-fold elevation of MYC expression was observed in 4T1 cells compared

Published OnlineFirst August 15, 2011; DOI:10.1158/1078-0432.CCR-11-0397

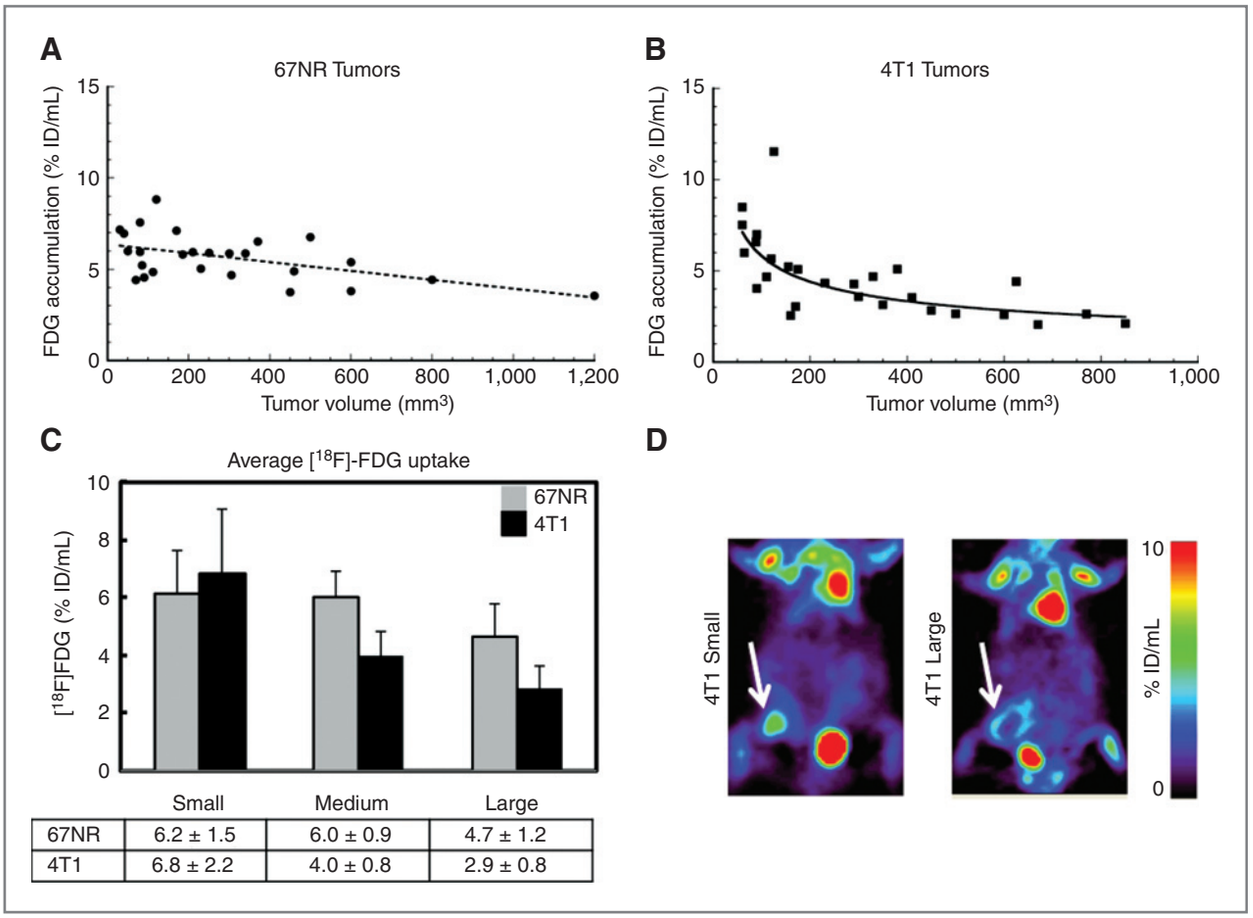

	Small	Medium	Large
67NR	6.2 ± 1.5	6.0 ± 0.9	4.7 ± 1.2
4T1	6.8 ± 2.2	4.0 ± 0.8	2.9 ± 0.8

Figure 4. FDG-PET measurements of [^{18}F]FDG accumulation in orthotopic 67NR and 4T1 breast tumors during tumor growth. [^{18}F]FDG accumulation in (A) 67NR tumors (solid circles, dashed line) and in (B) 4T1 tumors (solid squares, solid line) plotted versus tumor volume. C, average [^{18}F]FDG accumulation at 3 different tumor volumes (small, <150 mm^3; medium, 150–400 mm^3; and large, >400 mm^3). Values are the mean ± SD. D, representative [^{18}F]FDG microPET images of tumor-bearing mice; small and large 4T1 orthotopic tumors are visualized (white arrows). High radioactivity is seen in the cervical brown fat, heart, and bladder. Values are color coded to a range of values (%ID/mL).

with nonmetastatic 67NR cells (22). This raises the interesting possibility of a link between glucose and glutamine metabolism in these cells because Myc induces mitochondrial biogenesis in proliferating cells (37), stimulates mitochondrial glutamine metabolism (38), and upregulates *LDH-A* (39). In addition to data from gene expression analyses, comprehensive proteomics profiling across these cell lines has been conducted (40). The majority of the detected changes in protein expression are associated with metabolism-related proteins (>40%) including the expression of LDH-A (40).

A recently completed metabolomic analysis of the same cells using liquid chromatography/tandem mass spectroscopy confirmed the above observations (41). The metastatic capacity of 4T1 cells was shown to be associated with altered glycolysis, pentose phosphate pathway, and fatty acid synthesis, as well as decreased reduced glutathione/oxidized glutathione redox pool. In addition, 4T1 cells have shown enrichment of TCA cycle intermediates (citrate, isocitrate, and malate; ref. 41), which correlates with a 3.2-fold higher expression of malic enzyme in 4T1 cells (36). These data coincide with a recent study (42) showing that breast cancer cells with the potential to form brain metastases may use aerobic glycolysis coupled to the TCA cycle and oxidative phosphorylation to generate energy for cell growth. However, it is unclear whether the increase in TCA cycle activity is driven primarily by glucose or by glutamine metabolism, and additional studies will be required to answer this question.

The metabolism of both glucose and glutamine involves LDH. LDH is a tetrameric enzyme, containing 2 major subunits (A and B) coded by 2 different genes (*LDH-A* and *LDH-B*), which may form 5 isozymes (43). All 5 isozymes can catalyze the forward and backward conversion of pyruvate and lactate. LDH-A (LDH-5, M-LDH, or A4) kinetically favors the conversion of pyruvate to lactate whereas LDH-B (LDH-1, H-LDH, or B4) predominantly converts lactate to pyruvate, which will be further oxidized through the TCA cycle (44). The LDH-A and LDH-B subunits and their ratio are very important in the formation

Published OnlineFirst August 15, 2011; DOI:10.1158/1078-0432.CCR-11-0397

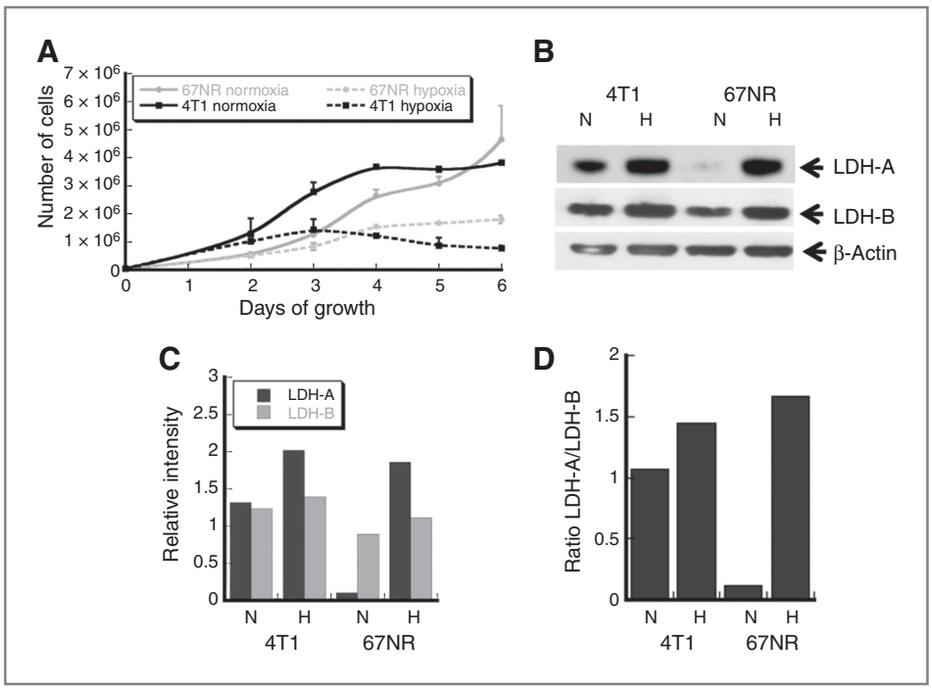

Figure 5. The effect of hypoxia on the cell growth and LDH-A expression. A, growth profiles of 67NR cells and 4T1 cells under normoxic (N, 21%) and hypoxic (H, 1%) conditions. B, immunoblot analysis of LDH-A and LDH-B subunits from 67NR and 4T1 cells exposed to normoxia and hypoxia for 24 hours. C, the β-actin–normalized intensity of LDH-A and LDH-B levels in cells under normoxic and hypoxic conditions. D, the ratio of β-actin–normalized LDH-A and LDH-B expression under normoxic and hypoxic conditions.

and function of the tetrameric enzyme, and the subunit composition impacts on the kinetics and the direction of the LDH-regulated reaction.

We found nearly equal levels of LDH-A and LDH-B expression in 4T1 cells using immunoblot analysis. The LDH-A/LDH-B ratio was 1.0 and 1.4 in 4T1 cells under normoxia and hypoxia, respectively. In 67NR cells the corresponding LDH-A/LDH-B ratio variation was much greater under normoxia and hypoxia, ranging from 0.11 to 1.66, respectively. The LDH isozymes of 4T1 and 67NR cells have the capacity to catalyze pyruvate–lactate reactions in both directions, with a tendency toward lactate formation under hypoxic conditions. Moreover, these results (reflecting a change in the LDH-A/LDH-B tetrameric enzyme ratio) are consistent with the oxygen consumption experiments, where high mitochondrial TCA cycle activity was observed in 4T1 cells and with the *in vivo* MRSI experiments showing high lactate and early development of necrosis in small 4T1 tumors. The hypoxia-induced change in the LDH-A/LDH-B tetrameric enzyme ratio of 67NR cells was more dramatic and consistent with the appearance of lactate in medium- and large-size 67NR tumors. Under hypoxia, 67NR cells significantly upregulate LDH-A and change the composition of the LDH enzymatic complex with the preference toward lactate formation (44).

The higher LDH-A expression in 4T1 cells than in 67NR cells under normal oxygen conditions is reflected in higher LDH enzymatic activity, higher lactate production, greater generation of hydrogen ions, and a greater consumption of glucose by 4T1 cells. In contrast with a traditional Warburg phenotype, 4T1 cells consume oxygen significantly faster than 67NR cells, showing high mitochondrial respiration in these metastatic-prone cancer cells. In the last several years, a number of publications have shown that oncogenes, such as *c-Myc* (37) and mutant *H-Ras* (45), increase mitochondrial metabolism which correlated with metastatic potential. Importantly, active oxidative phosphorylation could be very essential for the *in vivo* growth of highly glycolytic tumors, which could be a step to recycle secreted lactate to fuel mitochondrial activity (46) or be an adaptation to other metabolic stress (47, 48). In addition, the anchorage-independent growth phenotype, which is an important signature of metastatic tumors, is also associated with the activated mitochondrial biogenesis (49).

Several noninvasive imaging techniques can be used for the assessment of tumor metabolism. MRI/MRS provides a unique ability to noninvasively obtain structural as well as metabolic information from soft tissues. [^{18}F]FDG-PET is primarily used in tumor diagnosis to stage the extent of disease and to monitor the response to therapy (50); the magnitude of FDG uptake has also been shown to reflect, in part, the rate of glycolysis (50). The capability of MRSI to noninvasively obtain metabolic information is a valuable asset in the metabolic profiling of tumors and can provide molecular signatures of specific biological processes in discreet anatomic structures using natural metabolites and stable (nonradioactive) isotopes (^{13}C, ^{15}N, etc.). Using SelMQC transfer in combination with CSI for *in vivo* lactate detection, we have shown striking differences and changes in tumor lactate levels during orthotopic 67NR and 4T1 breast tumors growth. A 10-fold higher level of lactate was measured in small (<150 mm^3) 4T1 tumors than in small 67NR tumors (Fig. 3). Lung metastases are known to develop early (~6–8 days after orthotopic implantation

Published OnlineFirst August 15, 2011; DOI:10.1158/1078-0432.CCR-11-0397

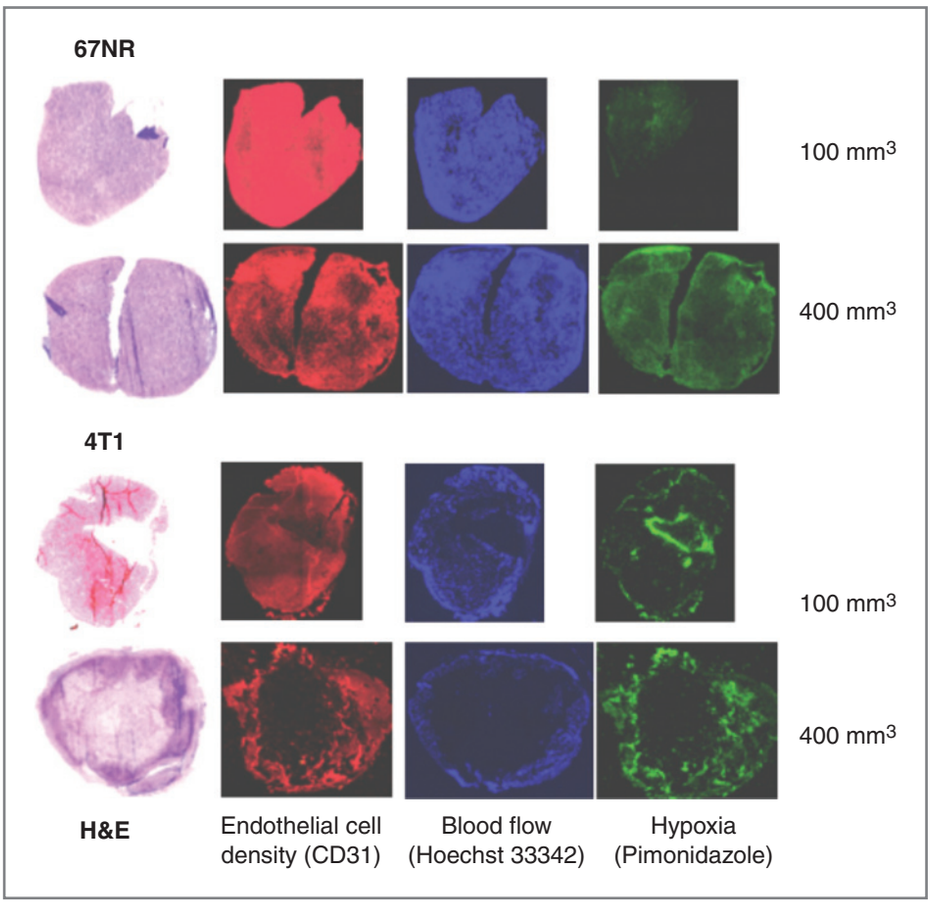

Figure 6. Immunohistochemical staining of 67NR and 4T1 tumors. Histology (H&E), endothelial cell density (CD31, red), blood flow (Hoechst 33342, blue), and hypoxia (Pimonidazole, green) are compared. Small 67NR tumors showed no necrosis, a uniform endothelial cell density and blood flow, and no hypoxia. Medium-size 67NR tumors showed some pimonidazole staining. This small 4T1 tumor shows some central necrosis, a decrease in endothelial cell density, and blood flow, with a corresponding zone of hypoxia surrounding the necrotic zone. These observations were amplified in medium-size 4T1 tumors.

of 4T1 cells; Supplementary Fig. S4; ref. 21) and at approximately the same time that 4T1 tumor lactate levels are very high (11.0 ± 1.5 mmol/L, 8 days after implantation; Fig. 3D). The correspondence of high lactate levels in small 4T1 tumors and concurrent development of lung metastases is of particular interest and suggests that high levels of lactate may be associated with the initiation of metastases.

Differences in lactate production and microenvironment acidity have been previously shown to differentiate metastatic and nonmetastatic human xenografts (51, 52). The high lactate concentration (~10 mmol/L; Fig. 3D) measured in small 4T1 tumors, concurrent with the development of lung metastases (days 6–8; Supplementary Fig. S4), is consistent with clinical studies (4, 6) where high lactate levels (with median concentrations >8 mmol/L) were associated with the subsequent development of metastases (4).

In comparison to tumor lactate levels, there were only small changes in [^{18}F]FDG accumulation during 4T1 and 67NR tumor growth. At the time metastases were developing from small orthotopic 4T1 tumors, there was only a 1.1-fold difference in [^{18}F]FDG accumulation between 4T1 and 67NR tumors. In contrast, there was a 10-fold difference in lactate levels in the same tumors at the time when there was little or no tumor necrosis. The subsequent decline in lactate concentration and [^{18}F]FDG accumulation during 4T1 tumor growth may reflect the effects of tumor necrosis. Because tumor lactate concentration and [^{18}F]FDG accumulation are likely to be related in a glycolytic phenotype, we compared the ratio of tumor lactate concentration and tumor [^{18}F]FDG accumulation, sequentially during tumor growth. Despite a fair amount of scatter, 67NR and 4T1 tumors showed marked differences in their lactate/FDG ratio profiles when the tumors were small (Supplementary Fig. S5) whereas both tumors approached a similar plateau ratio (1.0–1.1 mmol/L/%ID/mL) as they increased in size.

Cellular oxygen consumption is one of the determinants of intracellular oxygen levels (53). Under conditions of high oxygen demand, cells can become hypoxic due to high oxygen consumption (54). This is reflected in the metabolic profiles observed for small 4T1 and 67NR tumors and is very similar to those observed in the cell culture experiments. It suggests that the *in vitro* cell culture environment may better reflect the *in vivo* environment of small tumors. Thus, *in vitro* cell cultures may be better models for small well-perfused tumors prior to the development of significant ischemia, hypoxia, and necrosis. In culture, 4T1 cells produce lactate and consume significantly more glucose and oxygen than 67NR cells. The appearance of necrotic

Published OnlineFirst August 15, 2011; DOI:10.1158/1078-0432.CCR-11-0397

zones, even in small 4T1 tumors at the time early metastases are developing, is likely to reflect an oxygen requirement for efficient 4T1 cell metabolism and may contribute to hypoxia-induced cell death in these tumors. Moreover, the significant necrosis observed in all enlarging 4T1 tumors (Supplementary Fig. S3) is associated with lower levels of lactate production in medium- and large-size 4T1 tumors. The intensity of the pimonidazole staining was also significantly higher in all 4T1 samples than in 67NR tumors. Less-intense hypoxia staining was observed only in the larger 67NR tumors and is consistent with the gradual increase and plateau of lactate concentration in medium and large sizes 67NR tumors.

This study presents several important findings: (i) The expression of LDH-A and production of lactate in 4T1 breast cancer cells and small orthotopic tumors are higher than in isogenic 67NR cells and tumors; (ii) Changes in LDH-A level under hypoxic conditions could explain the formation of lactate in larger 67NR tumors; (iii) MRSI was considerably better than [^{18}F]FDG-PET in identifying significant differences in the metabolic phenotype of small 4T1 tumors (high lactate production and high glucose utilization) than in 67NR tumors, and these differences were most prominent during early tumor growth when 4T1 metastases were developing; and (iv) Lactate-MRSI has a greater dynamic range than [^{18}F]FDG-PET and may be a more sensitive measure with which to evaluate the aggressive potential of primary breast tumors.

Disclosure of Potential Conflicts of Interest

No potential conflicts of interest were disclosed.

Acknowledgments

We thank Mihaela Lupu for excellent technical assistance, Dr. Sean Carlin for providing some material and valuable discussions, Drs. Pat Zanzonico and Peter Smith-Jones for providing data for partial volume corrections, and Dr. Steven Larson for help and generous support.

Grant Support

This work was supported in part by funds: BC060114, CA098505, CA115675, CA86438, CA94060, U24CA83084, and DOD W81XWH-09-1-0042 (S.B. Thakur).

The costs of publication of this article were defrayed in part by the payment of page charges. This article must therefore be hereby marked *advertisement* in accordance with 18 U.S.C. Section 1734 solely to indicate this fact.

Received February 11, 2011; revised July 21, 2011; accepted July 27, 2011; published OnlineFirst August 15, 2011.

References

1. Gatenby RA, Gillies RJ. A microenvironmental model of carcinogenesis. Nat Rev Cancer 2008;8:56–61.
2. Gatenby RA, Gillies RJ. Why do cancers have high aerobic glycolysis? Nat Rev Cancer 2004;4:891–9.
3. Warburg O. On respiratory impairment in cancer cells. Science 1956;124:269–70.
4. Walenta S, Mueller-Klieser WF. Lactate: mirror and motor of tumor malignancy. Semin Radiat Oncol 2004;14:267–74.
5. Walenta S, Wetterling M, Lehrke M, Schwickert G, Sundfor K, Rofstad EK, et al. High lactate levels predict likelihood of metastases, tumor recurrence, and restricted patient survival in human cervical cancers. Cancer Res 2000;60:916–21.
6. Brizel DM, Schroeder T, Scher RL, Walenta S, Clough RW, Dewhirst MW, et al. Elevated tumor lactate concentrations predict for an increased risk of metastases in head-and-neck cancer. Int J Radiat Oncol Biol Phys 2001;51:349–53.
7. Walenta S, Chau TV, Schroeder T, Lehr HA, Kunz-Schughart LA, Fuerst A, et al. Metabolic classification of human rectal adenocarcinomas: a novel guideline for clinical oncologists? J Cancer Res Clin Oncol 2003;129:321–6.
8. Wise DR, Thompson CB. Glutamine addiction: a new therapeutic target in cancer. Trends Biochem Sci 2010;35:427–33.
9. Vander Heiden MG, Cantley LC, Thompson CB. Understanding the Warburg effect: the metabolic requirements of cell proliferation. Science 2009;324:1029–33.
10. Fantin VR, St-Pierre J, Leder P. Attenuation of LDH-A expression uncovers a link between glycolysis, mitochondrial physiology, and tumor maintenance. Cancer Cell 2006;9:425–34.
11. Koukourakis MI, Giatromanolaki A, Sivridis E, Bougioukas G, Didilis V, Gatter KC, et al. Lactate dehydrogenase-5 (LDH-5) overexpression in non-small-cell lung cancer tissues is linked to tumour hypoxia, angiogenic factor production and poor prognosis. Br J Cancer 2003;89:877–85.
12. Koukourakis MI, Giatromanolaki A, Simopoulos C, Polychronidis A, Sivridis E. Lactate dehydrogenase 5 (LDH5) relates to up-regulated hypoxia inducible factor pathway and metastasis in colorectal cancer. Clin Exp Metastasis 2005;22:25–30.
13. Koukourakis MI, Giatromanolaki A, Sivridis E, Gatter KC, Harris AL; Tumour Angiogenesis Research Group. Lactate dehydrogenase 5 expression in operable colorectal cancer: strong association with survival and activated vascular endothelial growth factor pathway–a report of the Tumour Angiogenesis Research Group. J Clin Oncol 2006;24:4301–8.
14. Ryberg M, Nielsen D, Osterlind K, Andersen PK, Skovsgaard T, Dombernowsky P. Predictors of central nervous system metastasis in patients with metastatic breast cancer. A competing risk analysis of 579 patients treated with epirubicin-based chemotherapy. Breast Cancer Res Treat 2005;91:217–25.
15. Koukourakis MI, Giatromanolaki A, Sivridis E, Gatter KC, Trarbach T, Folprecht G, et al. Prognostic and predictive role of lactate dehydrogenase 5 (LDH5) expression in colorectal cancer patients treated with PTK787/ZK 222584 (Vatalanib) anti-angiogenic therapy. Clin Cancer Res 2011;17:4892–900.
16. Le A, Cooper CR, Gouw AM, Dinavahi R, Maitra A, Deck LM, et al. Inhibition of lactate dehydrogenase A induces oxidative stress and inhibits tumor progression. Proc Natl Acad Sci U S A 2010;107:2037–42.
17. Seth P, Grant A, Tang J, Vinogradov E, Wang X, Lenkinski R, et al. On-target inhibition of tumor fermentative glycolysis as visualized by hyperpolarized pyruvate. Neoplasia 2011;13:60–71.
18. Xie H, Valera VA, Merino MJ, Amato AM, Signoretti S, Linehan WM, et al. LDH-A inhibition, a therapeutic strategy for treatment of hereditary leiomyomatosis and renal cell cancer. Mol Cancer Ther 2009;8:626–35.
19. Nevins JR, Potti A. Mining gene expression profiles: expression signatures as cancer phenotypes. Nat Rev Genet 2007;8:601–9.
20. Gupta GP, Massague J. Cancer metastasis: building a framework. Cell 2006;127:679–95.
21. Aslakson CJ, Miller FR. Selective events in the metastatic process defined by analysis of the sequential dissemination of subpopulations of a mouse mammary tumor. Cancer Res 1992;52:1399–405.
22. Tao K, Fang M, Alroy J, Sahagian GG. Imagable 4T1 model for the study of late stage breast cancer. BMC Cancer 2008;8:228.

Published OnlineFirst August 15, 2011; DOI:10.1158/1078-0432.CCR-11-0397

23. Heppner GH, Miller FR, Shekhar PM. Nontransgenic models of breast cancer. Breast Cancer Res 2000;2:331–4.
24. Eckhardt BL, Parker BS, van Laar RK, Restall CM, Natoli AL, Tavaria MD, et al. Genomic analysis of a spontaneous model of breast cancer metastasis to bone reveals a role for the extracellular matrix. Mol Cancer Res 2005;3:1–13.
25. Firth JD, Ebert BL, Ratcliffe PJ. Hypoxic regulation of lactate dehydrogenase A. Interaction between hypoxia-inducible factor 1 and cAMP response elements. J Biol Chem 1995;270:21021–7.
26. Ebert BL, Gleadle JM, O'Rourke JF, Bartlett SM, Poulton J, Ratcliffe PJ. Isoenzyme-specific regulation of genes involved in energy metabolism by hypoxia: similarities with the regulation of erythropoietin. Biochem J 1996;313:809–14.
27. Kroemer G, Pouyssegur J. Tumor cell metabolism: cancer's Achilles' heel. Cancer Cell 2008;13:472–82.
28. Urano M, Chen Y, Humm J, Koutcher JA, Zanzonico P, Ling C. Measurements of tumor tissue oxygen tension using a time-resolved luminescence-based optical oxylite probe: comparison with a paired survival assay. Radiat Res 2002;158:167–73.
29. He Q, Shungu DC, van Zijl PC, Bhujwalla ZM, Glickson JD. Single-scan *in vivo* lactate editing with complete lipid and water suppression by selective multiple-quantum-coherence transfer (Sel-MQC) with application to tumors. J Magn Reson B 1995;106:203–11.
30. Muruganandham M, Koutcher JA, Pizzorno G, He Q. *In vivo* tumor lactate relaxation measurements by selective multiple-quantum-coherence (Sel-MQC) transfer. Magn Reson Med 2004;52:902–6.
31. Yaligar J, Thakur SB, Bokacheva L, Carlin S, Thaler HT, Rizwan A, et al. Lactate MRSI and DCE MRI as surrogate markers of prostate tumor aggressiveness. NMR Biomed 2011. Epub 2011 May 25.
32. Danielsen ER, Michaelis T, Ross BD. Three methods of calibration in quantitative proton MR spectroscopy. J Magn Reson B 1995;106:287–91.
33. Moroz M, Kochetkov T, Cai S, Wu J, Shamis M, Nair J, et al. Imaging colon cancer response following treatment with AZD1152: a preclinical analysis of [18F]fluoro-2-deoxyglucose and 3′-deoxy-3′-[18F]fluorothymidine imaging. Clin Cancer Res 2011;17:1099–110.
34. Carlin S, Khan N, Ku T, Longo VA, Larson SM, Smith-Jones PM. Molecular targeting of carbonic anhydrase IX in mice with hypoxic HT29 colorectal tumor xenografts. PLoS One 2010;5:e10857.
35. Granchi C, Bertini S, Macchia M, Minutolo F. Inhibitors of lactate dehydrogenase isoforms and their therapeutic potentials. Curr Med Chem 2010;17:672–97.
36. Yang J, Mani SA, Donaher JL, Ramaswamy S, Itzykson RA, Come C, et al. Twist, a master regulator of morphogenesis, plays an essential role in tumor metastasis. Cell 2004;117:927–39.
37. Li F, Wang Y, Zeller KI, Potter JJ, Wonsey DR, O'Donnell KA, et al. Myc stimulates nuclearly encoded mitochondrial genes and mitochondrial biogenesis. Mol Cell Biol 2005;25:6225–34.
38. Wise DR, DeBerardinis RJ, Mancuso A, Sayed N, Zhang XY, Pfeiffer HK, et al. Myc regulates a transcriptional program that stimulates mitochondrial glutaminolysis and leads to glutamine addiction. Proc Natl Acad Sci U S A 2008;105:18782–7.
39. Shim H, Dolde C, Lewis BC, Wu CS, Dang G, Jungmann RA, et al. c-Myc transactivation of LDH-A: implications for tumor metabolism and growth. Proc Natl Acad Sci U S A 1997;94:6658–63.
40. Ho J, Kong JW, Choong LY, Loh MC, Toy W, Chong PK, et al. Novel breast cancer metastasis-associated proteins. J Proteome Res 2009;8:583–94.
41. Lu X, Bennet B, Mu E, Rabinowitz J, Kang Y. Metabolomic changes accompanying transformation and acquisition of metastatic potential in a syngeneic mouse mammary tumor model. J Biol Chem 2010;285:9317–21.
42. Chen EI, Hewel J, Krueger JS, Tiraby C, Weber MR, Kralli A, et al. Adaptation of energy metabolism in breast cancer brain metastases. Cancer Res 2007;67:1472–86.
43. Everse J, Kaplan NO. Lactate dehydrogenases: structure and function. Adv Enzymol Relat Areas Mol Biol 1973;37:61–133.
44. Stambaugh R, Post D. Substrate and product inhibition of rabbit muscle lactic dehydrogenase heart (H4) and muscle (M4) isozymes. J Biol Chem 1966;241:1462–7.
45. Telang S, Lane AN, Nelson KK, Arumugam S, Chesney J. The oncoprotein H-RasV12 increases mitochondrial metabolism. Mol Cancer 2007;6:77.
46. Sonveaux P, Vegran F, Schroeder T, Wergin MC, Verrax J, Rabbani ZN, et al. Targeting lactate-fueled respiration selectively kills hypoxic tumor cells in mice. J Clin Invest 2008;118:3930–42.
47. Chen V, Shtivelman E. CC3/TIP30 regulates metabolic adaptation of tumor cells to glucose limitation. Cell Cycle 2010;9:4941–53.
48. Wellen KE, Thompson CB. Cellular metabolic stress: considering how cells respond to nutrient excess. Mol Cell 2010;40:323–32.
49. Mori S, Chang JT, Andrechek ER, Matsumura N, Baba T, Yao G, et al. Anchorage-independent cell growth signature identifies tumors with metastatic potential. Oncogene 2009;28:2796–805.
50. Mankoff DA, Eary JF, Link JM, Muzi M, Rajendran JG, Spence AM, et al. Tumor-specific positron emission tomography imaging in patients: [18F] fluorodeoxyglucose and beyond. Clin Cancer Res 2007;13:3460–9.
51. Schornack PA, Gillies RJ. Contributions of cell metabolism and H+ diffusion to the acidic pH of tumors. Neoplasia 2003;5:135–45.
52. Jordan BF, Black K, Robey IF, Runquist M, Powis G, Gillies RJ. Metabolite changes in HT-29 xenograft tumors following HIF-1alpha inhibition with PX-478 as studied by MR spectroscopy *in vivo* and *ex vivo*. NMR Biomed 2005;18:430–9.
53. Hagen T, Taylor CT, Lam F, Moncada S. Redistribution of intracellular oxygen in hypoxia by nitric oxide: effect on HIF1alpha. Science 2003;302:1975–8.
54. Aragones J, Schneider M, Van Geyte K, Fraisl P, Dresselaers T, Mazzone M, et al. Deficiency or inhibition of oxygen sensor Phd1 induces hypoxia tolerance by reprogramming basal metabolism. Nat Genet 2008;40:170–80.

In vivo lactate T1 and T2 relaxation measurements in breast tumors using SS1-SelMQC editing sequence

Sanjay Annarao[1], Thomas Ku[2], Kishore Nagavara[3], Jason Koutcher[1,4], and Sunitha Thakur[1,3]

[1]Department of Medical Physics, Memorial Sloan-Kettering Cancer Center, New York, NY, United States, [2]Department of Molecular Pharmacology & Chemistry, Memorial Sloan-Kettering Cancer Center, New York, NY, United States, [3]Department of Radiology, Memorial Sloan-Kettering Cancer Center, New York, NY, United States, [4]Department of Medicine, Memorial Sloan-Kettering Cancer Center, New York, NY, United States

Introduction: Multiple quantum (MQ) editing techniques have been developed for lactate (Lac) detection with complete suppression of water and lipid resonances in a single scan (1). Recent studies on prostate cancer and breast tumor have shown changes in Lac level in tumor tissues (2-3). The presence of fat and water in high concentration makes it difficult in observing and quantifying Lac. The measurement of T_1 and T_2 is essential for absolute quantification of Lac to differentiate benign and malignant tumor. We measured Lac with improved lipid and water suppression using 1331 binomial composite Spectral-Selective Pulses in Selective MQ Coherence (SS1-SelMQC) compared to the original SS-SelMQC(1) sequence and T_1 and T_2 of Lac been determined by incorporating T_1 and T_2 variables in SS1-SelMQC (T_1-SS1-SelMQC and T_2-SS1-SelMQC). Here we report T_1-SS1-SelMQC and T_2-SS1-SelMQC sequence to measure in-vivo Lac T_1 and T_2. We have standardized our pulse sequences with phantom studies and demonstrated in nude mice implanted with MCF-7, BT-474, MDA-MB-231 and MDA-MB-435 breast tumors. Invivo T_2 of Lac was found to be significantly different in prognostic molecular markers.

Materials and Methods: All MR imaging and spectroscopy experiments were performed on a 4.7 Tesla Bruker Biospin spectrometer. Animal studies were conducted in compliance with protocols approved by the Institutional Animal Care and Use Committee. MCF-7, BT-474, MDA-MB-231and MDA-MB-435 cancer cells were purchased from ATCC. Cells were grown in DME F12, DME HG for MCF-7, BT-474 respectively and RPMI for MDA-MB-231 and MDA-MB-435, and media were supplemented with 10% FBS, 1% penicillin and 1% streptomycin. The cells were incubated in 5% CO_2 atmosphere at temperature 37 °C. Once cells reach 80-90% confluence, cells were washed with PBS followed by trypsinization. The cells were then re-suspended in media (5×10^7 cells/mL). To this equal volume of Matrigel was mixed and mixture is ready for inoculation in mice body. 4-6 week old Athymic nu/nu female mice were used for the study . Two days before estrogen pellet was inserted in MCF-7 and BT-474 group mice. $5 * 10^6$ cells inoculated on the mammary fat pad of the mice. Tumor volumes were calculated using a hemi ellipsoid formula $V = (\pi/6) * x * y * z$; where *x, y* and *z* are the length, breadth and depth of the tumor respectively. Phantom studies were performed with three Lac concentrations viz., 5, 15 and 30 mM.

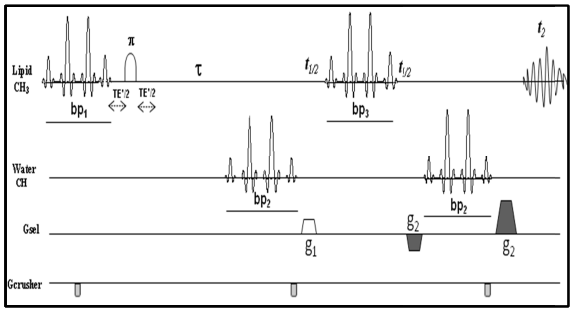

Fig1: T_2-SS1-SelMQC pulse sequence to measure T2 of Lactate

NMR Experiments Mice were anesthetized using a mixture of isoflurane (1.5 - 2.5%) air (10%) and placed inside a custom-designed MR probe. The magnet was shimmed to a half height line width of less than 50 Hz for the ^{1}H water signal. The non-localized spectra were acquired using T_1-SS1-SelMQC to measure T_1 of Lac and T_2-SS1-SelMQC to measure T_2 of Lac**.** The SS1-SelMQC sequence combines selective radio frequency pulses with gradient filtering to achieve Lac editing and efficient lipid and water suppression in a 'single-shot'. Frequency-selective pulses were employed to prepare MQ coherences for the Lac methyl signal. Single-quantum lipid and water resonances were then eliminated by multiple-quantum selection gradients. To ensure complete lipid suppression and a high signal-to-noise ratio for the Lac methyl signal, a two-step phase cycling (0°/180°) was applied for the selective 90° pulse at the Lac CH resonance frequency. In the T_1-SS1-SelMQC, T_1 measurement of Lac was performed with insertion of inversion 'mao4' shaped pulse with 2ms pulse width, similar to (4) and varied the inversion time before applying the SS1-SelMQC. In T_2-SS1-SelMQC, Lac T_2 relaxation was measured by Incorporating CH_3 selective 15ms single lobe 'sinc' pulse, during the MQ-preparation period of SS1-SelMQC (Fig1). This allows inserting a variable delay time TE' to measure Lac T_2 decay. The T_1 measurement was done by subtraction method (5). 1D-spectra were processed using Xwin-NMR, Bruker software. Statistical analysis was performed using SPSS software. Differences in T_1 and T_2 in molecular prognostic markers were analyzed using non-parametric Mann-Whitney U test.

Results and Discussion: T_1-SS1-SelMQC and T_2-SS1-SelMQC pulse sequences were used to measure T_1 and T_2 of Lac in phantom and *in-vivo* tumors. Representative spectra of MCF-7 of tumor volume 300mm^3 as a function of inversion time (T1) and its curve fit and echo time TE and its curve fit is shown in **Fig 2(A&B)**. The in-vitro Lac T_1 for 5, 15 and 30mM was found to be 1.34s± 0.05, 1.21s±0.002 and 1.13s±0.03 respectively. The T_2 of 5, 15 and 30 mM was 0.6s±0.02, 0.51±0.03 and 0.50±0.03 respectively. The measured T_1 and T_2 relaxation times of Lac in breast tumors are shown in Table 1. The T_2 of Lac was significantly different in ER PR+ vs – , Her2+ Vs – and TN+Vs – (Table 1). The T_1 was not significantly different in these three prognostic markers. Our experimental measured T_1 and T_2 are in the range of reported T_1 and T_2 (4).

Conclusion: The reported T_1-SS1-SelMQC and T_2-SS1-SelMQC pulse sequences are effective to measure T_1 and T_2 of Lac in various tumor types. Measurement of T_2 could be used to differentiate different tumor types.

Reference: 1) Thakur SB, et al., Magn Reson Med., 62: p 591-598 (2009). 2) Inna Serganova et al, August 15, 2011; doi: 10.1158/1078-0432.CCR-11-039. 3) J.Yaligar et al, 25 May, 2011, DOI: 10.1002/nbm.1723. 4) Muruganandham M, et al., Magn Reson.Med ,52:p 902-906 (2004). 5) Kim S, et al., Magn Reson Med. 31: p 445-449 (1994).

Acknowledgement: We want to thank Dr. Mihaela Lupu and Ms.Natalia Kruchevsky for their help.

This work is supported by DOD BCRP award W81XWH-09-1-0042.

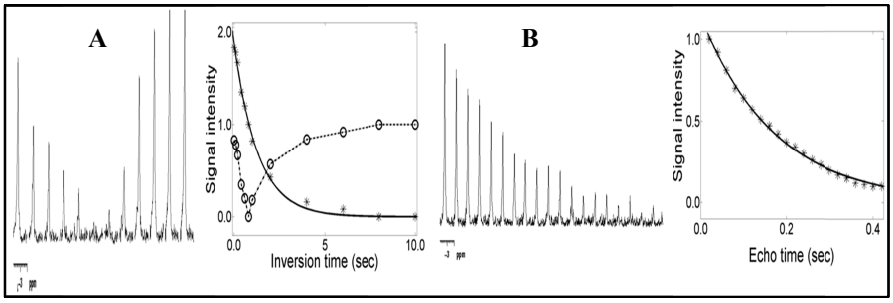

Fig 2: In vivo (MCF-7 tumor) Lac signal recovery of (A) T_1-SS1-SelMQC with variable recovery delay 0.1 to 10s. Lac signal decay (B) T_2-SS1-SelMQC with 2*TE ′(0.08 to 0.42s) with 0.02 s increments. And their respective curve fits.

Table1: T1 and T2 of Lac in different tumors and differences in molecular prognostic factors.

Tumor	No of Mice	T_1(mean±SD) (sec)	T_2(mean±SD) (sec)
MCF-7	6	1.80±0.23	0.16±0.02
BT-474	6	1.66±0.26	0.17±0.02
MDA-MB-231	5	1.49±0.18	0.12±0.004
MDA-MB-435	4	1.87±0.23	0.12±0.009
Factor		p-Value(T_1)	p-Value(T_2)
ER,PR+/ER,PR-	9/12	0.28	0.0001
Her2+/Her2-	6/15	0.32	0.004
TP+/TP-	6/9	0.49	0.0002

2083

Quantification of lactate concentrations in orthotopic breast tumors with different growth rates

Sanjay Annarao[1], and Sunitha Thakur[1,2]

[1]*Department of Medical Physics, Memorial Sloan-Kettering Cancer Center, New York, NY, United States,* [2]*Radiology, Memorial Sloan Kettering Cancer Centre, New York, NY, United States*

Introduction: Detection and quantification of metabolic markers using magnetic resonance spectroscopy (MRS) is a non-invasive powerful tool for early cancer diagnosis and treatment monitoring (1-2). Lactate (Lac) a metabolic product of glycolysis plays a vital role in energy metabolism,Recent studies have shown that high level of lactate concentration [Lac] is associated with breast cancer and prostate cancer (3-4). The predominant use of glycolysis for energy demand due to poor tissue oxygenation has been observed in cancerous tissues. We used the modified Spectral-Selective Pulses in Selective MQ coherences (SS-SelMQC) method (5) to detect Lac by effectively suppressing water and fat with signal enhancement. Lac signal enhancement was achieved by using short binomial frequency selective pulses, which reduces signal loss in the evolution period due to the effects of scalar coupling and molecular diffusion. In the present work, we measured Lac with improved lipid and water suppression using 1331 binomial composite pulses (SS1-SelMQC). This sequence was used to detect and quantify Lac levels in orthotopic breast tumors with different growth rates. MCF-7(n=6) and BT-474 (n=6) breast tumors were used to represent fast growing tumors compared with slow growing MDA-MB-231(n=6) and MDA-MB-435 (n=6) tumors. We discreminated the molecular prognostic markers with respect to [Lac] viz., ER(Estrogen) PR(Progesterone) +/-, Her2(Human Epidermal growth factor Receptor 2)+/- and TN(Triple)+/TN-.

Materials and Methods: Animal studies were conducted in compliance with protocols approved by MSKCC's IACUC committee. 4 to 6 weeks old Athymic nu/nu nude mice were used for the study. Animals were randomly classified into four groups for four different cell lines viz.**,** MCF-7 and BT-474, MDA-MB-231 and MDA-MB-435. Two days before estrogen pellet was inserted in MCF-7 and BT-474 group mice. 5 * 10^6 cells were inoculated on the mammary fat pad of the all the four group mice and tumor growth was started after one week of cell inoculation and tumor growth was monitored every week **(Fig.1A).** Tumors were categorized into three groups: small (<**150** mm^3), medium (**200-350** mm^3), and large (>**450**mm^3). The tumor volume was calculated by measuring the length (l) breadth (b) and height (h) of the tumor using the formula π*(l*b*h)/6. All MR imaging and spectroscopy experiments were performed on a 4.7 Tesla Bruker Biospin spectrometer (40 cm horizontal bore). The mice were anesthetized using a mixture of isoflurane and oxygen (10% O_2) and placed in the animal holder. The tumor was placed inside a 2 turn home built 15 mm diameter tuned coil. A rectal fiberoptic probe was used to monitor the mouse body temperature. Warm air was blown to maintain the animal body temperature at 37 °C. The magnet was shimmed to a half height line width of less than 50 Hz for the ^{1}H water signal. Spectra were obtained for localized (5mm thick) to detect Lac signal from the tumor. The SS1-SelMQC, spectral editing technique to measure [Lac] by efficiently suppressing lipid (1.3 ppm) and water (4.7 ppm) signal in a single shot was used to measure Lac in tumor. One-dimensional slice spectra in the sagittal plane were acquired with TR = 3 sec, echo time of 72 ms, number of excitations 16, 1024 data points and spectral width of 2510 Hz. The One-dimensional spectra were processed by a 1D Fourier transform, similar to our previous report (5). The absolute magnitude of the echo signal from the slice was fitted in in-house matlab (Matworks 7.6.0) program and normalized to the slice volume. Quantification of Lac was performed by the phantom replacement technique using a 15 mM Lac (4). Statistical analysis was performed using SPSS software. Non-Parametric Mann-Whitney U test(2 sample) were used to differentiate molecular prognostic markers. Correlation coefficient b/n slice [Lac] with tumor volume was performed by Pearson two tailed test.

Results and Discussion: The [Lac] in MCF-7, BT-474 (Fig 1B) MDA-MB-231and MDA-MB-435 (Fig 1C) tumors were measured using MRSI with respect to tumor volume. In all four tumor types, the [Lac] was found to be higher in small tumor volume (100-150mm^3), as tumor reaches 400mm^3, [Lac] level tend to decrease, at higher tumor volume (> 400mm^3) [Lac] level declined (Fig 1D&E). [Lac] found to be significantly higher (p=0.00 for all three prognostic markers) in ER PR +, Her2+ and TN+ compared to ER PR -, Her2- and TN- markers respectively (Fig 1F).

Conclusion: Our results, inferred the decrease in Lac level as tumor volume increases. At smaller tumor volumes, in fast growing tumors (low metastatic potential), [Lac] was higher, whereas in slow growing tumors (high metastatic potential) has lower [Lac]. In all these tumors [Lac] is negatively correlated with tumor volume. Significant correlation was found in MDA-MB-231 (r=-0.84), MCF-7 (r=-0.76) and moderate correlation was found in BT-474 (r=-0.51) and in MDA-MB-435 (r=-0.69). [Lac] is significantly differentiate the molecular prognostic marker.

Reference: 1) Kristine Glunde et al, NMR Biomed 24(6): p 673-690 (2011). 2)Yanping Luo et al, Magn Reson.Med.,41(4): p 676-685(1999). 3) Inna Serganova et al, August 15, 2011; doi: 10.1158/1078-0432.CCR-11-039. 4) J.Yaligar et al, 25 May, 2011, DOI: 10.1002/nbm.1723. 5) Thakur SB, et al., Magn Reson Med. 62: 591-598 (2009).

Acknowledgement: We want to thank Dr. Mihaela Lupu and Ms.Natalia Kruchevsky for their help. This work is supported by DOD BCRP award W81XWH-09-1-0042.

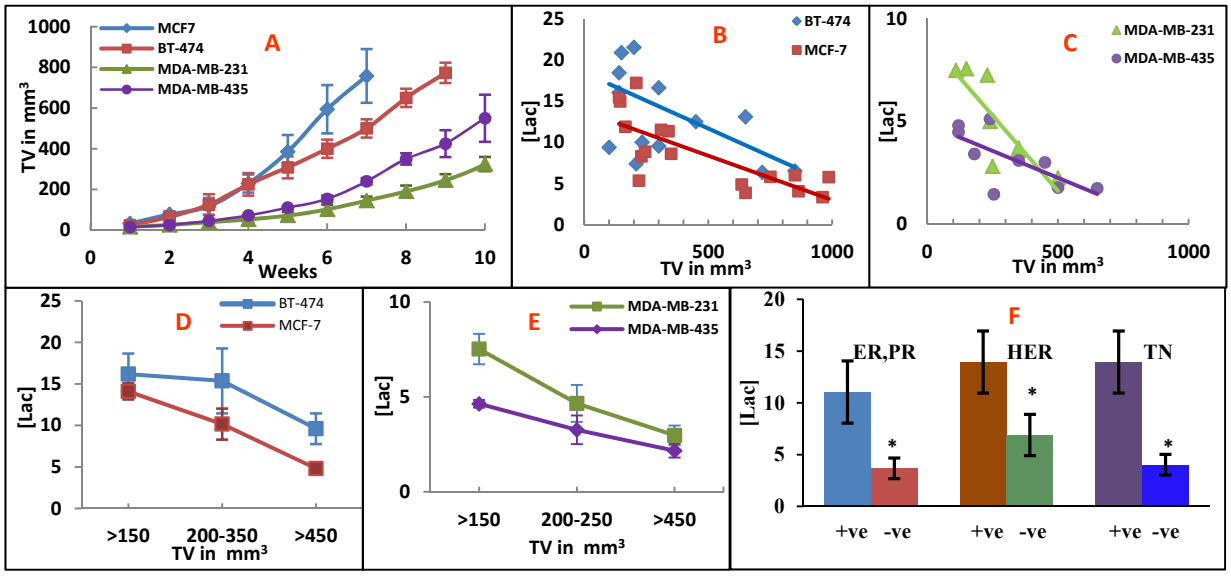

Fig 1: Tumor volume (TV) growth curve (A) , [Lac] level with respect to TV in fast [B] and slow growing [C] tumors, mean [Lac] level in small , medium and bigger TV in slow [D] and fast [E] growing tumors and [Lac] level with respect to protein prognostic factor with statistical analysis p=0.00 * (F).

Published OnlineFirst July 5, 2013; DOI: 10.1158/1078-0432.CCR-12-3300

Clinical Cancer Research

Relationships between LDH-A, Lactate, and Metastases in 4T1 Breast Tumors

Asif Rizwan, Inna Serganova, Raya Khanin, et al.

Clin Cancer Res Published OnlineFirst July 5, 2013.

Published OnlineFirst July 5, 2013; DOI: 10.1158/1078-0432.CCR-12-3300

Imaging, Diagnosis, Prognosis

Clinical Cancer Research

Relationships between LDH-A, Lactate, and Metastases in 4T1 Breast Tumors

Asif Rizwan[1,7], Inna Serganova[2], Raya Khanin[5], Hazem Karabeber[3], Xiaohui Ni[1], Sunitha Thakur[1], Kristen L. Zakian[1,3], Ronald Blasberg[2,3,6], and Jason A. Koutcher[1,3,4,6,7]

Abstract

Purpose: To investigate the relationship between lactate dehydrogenase A (LDH-A) expression, lactate concentration, cell metabolism, and metastases in murine 4T1 breast tumors.

Experimental Design: Inhibition of LDH-A expression and protein levels were achieved in a metastatic breast cancer cell line (4T1) using short hairpin RNA (shRNA) technology. The relationship between tumor LDH-A protein levels and lactate concentration (measured by magnetic resonance spectroscopic imaging, MRSI) and metastases was assessed.

Results: LDH-A knockdown cells (KD9) showed a significant reduction in LDH-A protein and LDH activity, less acid production, decreased transwell migration and invasion, lower proliferation, reduced glucose consumption and glycolysis, and increase in oxygen consumption, reactive oxygen species (ROS), and cellular ATP levels, compared with control (NC) cells cultured in 25 mmol/L glucose. *In vivo* studies showed lower lactate levels in KD9, KD5, and KD317 tumors than in NC or 4T1 wild-type tumors ($P < 0.01$), and a linear relationship between tumor LDH-A protein expression and lactate concentration. Metastases were delayed and primary tumor growth rate decreased.

Conclusions: We show for the first time that LDH-A knockdown inhibited the formation of metastases, and was accompanied by *in vivo* changes in tumor cell metabolism. Lactate MRSI can be used as a surrogate to monitor targeted inhibition of LDH-A in a preclinical setting and provides a noninvasive imaging strategy to monitor LDH-A–targeted therapy. This imaging strategy can be translated to the clinic to identify and monitor patients who are at high risk of developing metastatic disease. *Clin Cancer Res; 1–12. ©2013 AACR.*

Introduction

Metabolic alterations in tumors impact their evolution, progression, and development of metastases (1–7). Cancer cells modify their energy metabolism as they proliferate and adjust to a changing microenvironment to meet their energy and macromolecular synthetic demands. Many cancer cells have high glucose and glutamine usage and high rates of aerobic glycolysis (1), which impact the development of the metastatic phenotype (2, 8).

This article focuses on lactate dehydrogenase A (LDH-A). LDH-A provides a link between several metabolic pathways. The product of LDH-A activity (lactate) can be assessed noninvasively and quantitatively using magnetic resonance spectroscopic imaging (MRSI). The low sensitivity and overlapping peaks of the lactate and lipid magnetic resonance spectra present technical difficulties during magnetic resonance spectroscopy, but can be overcome by the use of spectral editing methods, such as SELective Multiple Quantum Coherence (SEL-MQC) techniques (9). We previously showed that tumor lactate concentration can be measured in murine breast tumor models by *in vivo* ^{1}H MRSI (10).

The inhibition of LDH-A has an antiproliferative effect on primary breast tumors (5). However, there have been no studies investigating the effect of LDH-A inhibition on the development and progression of metastases, or to evaluate methods to noninvasively monitor LDH-A inhibition. We focused on the role of lactate and LDH-A in the development of metastases, as the cause of death in breast cancer is almost always due to metastases. We hypothesized that there is a relationship between LDH-A expression, tumor lactate concentration, and the growth and metastatic potential of murine breast tumor models. We use short hairpin RNA (shRNA) knockdown (KD) technology to inhibit

Authors' Affiliations: Departments of [1]Medical Physics, [2]Neurology, [3]Radiology, and [4]Medicine, [5]Bioinformatics Core, [6]Molecular Pharmacology and Chemistry Program, Memorial Sloan-Kettering Cancer Center; and [7]Department of Physiology and Biophysics, Weill Cornell Graduate School of Medical Sciences, New York, New York

Note: Supplementary data for this article are available at Clinical Cancer Research Online (http://clincancerres.aacrjournals.org/).

A. Rizwan and I. Serganova contributed equally to this work.

Corresponding Author: Jason A. Koutcher, Department of Medical Physics, Memorial Sloan-Kettering Cancer Center, Z-492, 1275 York Avenue, New York, NY 10065. Phone: 212-639-8834; Fax: 212-717-3676; E-mail: koutchej@mskcc.org

doi: 10.1158/1078-0432.CCR-12-3300

Published OnlineFirst July 5, 2013; DOI: 10.1158/1078-0432.CCR-12-3300

Translational Relevance

Elevated lactate dehydrogenase A (LDH-A) expression is characteristic of many aggressive tumors and is associated with development of metastases. We show that decreased lactate concentration alters tumor cell metabolism, delays metastases, and reduces tumor growth rate, and that LDH-A breakthrough is associated with disease progression. Our focus on tumor LDH-A and noninvasive monitoring of LDH-A–targeted therapy using lactate magnetic resonance spectroscopic imaging (MRSI), where lactate concentration is a potential surrogate marker for LDH-A expression, is novel and extends our prior studies. We suggest that this imaging, treatment, and monitoring strategy can be translated to the clinic, where lactate MRSI can be used to identify and monitor women at high risk of developing metastatic disease, and to monitor LDH-A–targeted drug treatment.

LDH-A expression, and to study the effects of LDH-A inhibition on tumor cell metabolism, growth, and the development of metastases. We address several new questions: (i) will shRNA-mediated reduction of LDH-A expression in 4T1 breast cancer cells alter orthotopic 4T1 tumor lactate concentrations?; (ii) does shRNA-mediated reduction of LDH-A expression in 4T1 breast cancer cells alter metabolism and sensitivity to metabolic stress (reactive oxygen species, ROS)?; (iii) does shRNA-mediated reduction of LDH-A expression in 4T1 breast cancer cells alter the development of metastases and tumor growth?; (iv) is there a relationship between tumor LDH-A protein levels and MRSI-measured tumor lactate concentration?

Materials and Methods

Cell culture

4T1 cells were derived from a spontaneous breast tumor in a BALB/c mouse and were provided by Fred Miller (Karmanos Cancer Institute, Detroit, MI; ref. 11). The cell line was not authenticated by the authors as cell authentication testing can be conducted only on human cell lines. *LDH-A* knockdown and NC (control) cells, derived from 4T1 murine breast cancer cells, were grown in standard Dulbecco's modified Eagle medium (DMEM) containing 10% fetal calf serum (FCS) supplemented with either 25 or 5 mmol/L glucose and 6 mmol/L L-glutamine, penicillin/streptomycin, and 4 mg/L of puromycin.

Generation of LDH-A knockdown and control cell lines

4T1 cells were transfected with SureSilencing shRNA plasmids (SABiosciences) to specifically knockdown expression of the mouse *LDH-A* gene. The vectors contained shRNA under the control of the U1 promoter and included a puromycin resistance gene. Stably transduced clones (knockdown cell lines) were developed along with a control (NC) cell line bearing a scrambled shRNA. LDH-A quantitative real-time PCR (qRT-PCR) RNA and immunoblotting protein assays confirmed successful transduction (see Supplementary Methods).

In vitro assays

Cell proliferation and metabolic assays (glucose use, glycolysis, LDH activity, lactate production, oxygen consumption rate (OCR), oxidative phosphorylation, ROS, cellular mitochondria) and cell migration and invasion assays were conducted (see Supplementary Data).

Experimental animal model

Cells were orthotopically implanted as described previously (10). Primary tumor volume was determined by caliper measurements and tumor-doubling times were calculated from the tumor volume versus time profiles (12).

In vivo lactate detection

MRSI experiments were carried out on a 7T Bruker Biospec Spectrometer. The lactate signal was acquired using a SEL-MQC editing sequence in combination with chemical shift imaging (CSI; refs. 9, 10, 13) as detailed in the Supplementary Data.

Magnetic resonance images

Lung metastases were imaged using the Bruker gradient echo fast imaging (GEFI) sequence with TR = 300 milliseconds, TE = 2.5 milliseconds, NA = 4, and matrix = 512 × 256. Gated respiration was used to reduce respiratory artifacts.

Analysis of breast cancer microarray datasets

A compendium of four breast cancer microarray datasets was analyzed using the Bioconductor set of tools (www.bioconductor.org) in R statistical language (www.r-project.org). Data were downloaded from Gene Expression Omnibus (GEO). The four breast cancer datasets that were analyzed included: (i) MSKCC-82 GSE-2603 (14), (ii) EMC-286 GSE-2034 (15), (iii) ECM 192 GSE12276: 204 samples (16), and (iv) EMC-344 [EMC 286 and 58 cases of estrogen receptor–negative (ER^-) tumors, GSE 5327; ref. 17]. Data were normalized using the standard gcrma procedure (18). Survival analysis was conducted using R package survival. Details are provided in Supplementary Methods.

Statistical analysis

Results are presented as mean ± SD. Statistical significance was determined by a two-tailed Student *t* test. A *P* value of less than 0.05 was considered significant.

Results

Selection/characterization of KD9 and NC 4T1 cells

To assess the link between LDH-A expression and the metabolic and metastatic characteristics of an established murine breast cancer model, we transfected 4T1 breast tumor cells with four different SureSilencing shRNAs plasmids specifically targeting mouse LDH-A mRNA (knockdown), and a nonspecific scrambled shRNA (NC), respectively. Several knockdown clones with different levels of

Published OnlineFirst July 5, 2013; DOI: 10.1158/1078-0432.CCR-12-3300

LDH-A protein expression were isolated for further experiments. The shRNA knockdown efficiency was evaluated by analyzing LDH-A mRNA expression using qRT-PCR and protein expression by immunoblotting. Knockdown cells have significantly lower levels of LDH-A mRNA (Fig. 1A) and decreased LDH-A protein expression (Fig. 1B) compared with NC cells. Clone #9 (KD9) transduced with shRNA #2 had the lowest LDH-A mRNA and protein levels, and an unchanged LDH-B level (Fig. 1A and B). Another clone, KD317, was developed from cells bearing the plasmid with shRNA#3 (Fig. 1E).

To validate the correlation between LDH-A expression levels and functional activity of the LDH enzyme complex, we conducted an enzymatic assay on viable KD9 and NC tumor cells in growth medium containing 25 or 5 mmol/L glucose. KD9 cells have 3-fold lower LDH activity than NC cells when cultured in 25 mmol/L glucose-containing media and more than a 4-fold difference in 5 mmol/L glucose ($P < 0.01$; Fig. 1C). KD9 cells also produce significantly less lactate ($P < 0.01$; Fig 1D) than NC cells. We also found that LDH-A expression (Western blot analysis) remains high in the control group (NC) and low in the knockdown group (KD9 and KD317) in both high-glucose and low-glucose culture medium (Fig. 1E and F).

Metabolic properties of KD9 and NC cells

Glucose usage was significantly less in KD9 cells compared with NC cells, growing in either 25 or 5 mmol/L glucose-containing medium ($P < 0.01$; Fig. 2A). We used a Seahorse Bioscience XF96 Extracellular Flux Analyzer to measure the extracellular acidification rate (ECAR) and the OCR of these cells. We obtained a baseline measure of ECAR using basic glucose-free XF assay medium, then added glucose to assess glycolysis, and then inhibited the process by adding 2-deoxyglucose (2-DG) to the incubation medium. The injection of glucose (final concentration of 25 mmol/L) caused a significant increase in ECAR in both cell lines, with a higher increase in NC cells compared with KD9 cells (Fig. 2B). The subsequent injection of 2-DG (final concentration of 50 mmol/L) decreased ECAR to basal levels. The effects of these treatments are reflected in the integrated areas under the profile measurements (Fig. 2C); the differences between KD9 and NC cells were significant ($P < 0.01$) for cells growing under 25 mmol/L of glucose; a similar trend was noted for cells growing in 5 mmol/L glucose, but the difference was not significant ($P = 0.147$). These results showed a lower glycolytic rate for KD9 cells compared with NC cells (Fig. 2B and C) growing under a high concentration of glucose, and a corresponding lower rate of acidification of the incubation medium over 48 hours (Fig. 2D).

Oxygen consumption is an indicator of mitochondrial respiration. A Seahorse Bioscience XF96 Analyzer was used to measure the real-time OCR (pmol/min) in serum-free DMEM with 25 and 5 mmol/L glucose and 6 mmol/L of glutamine (Fig. 2E and F). FCCP (carbonyl cyanide

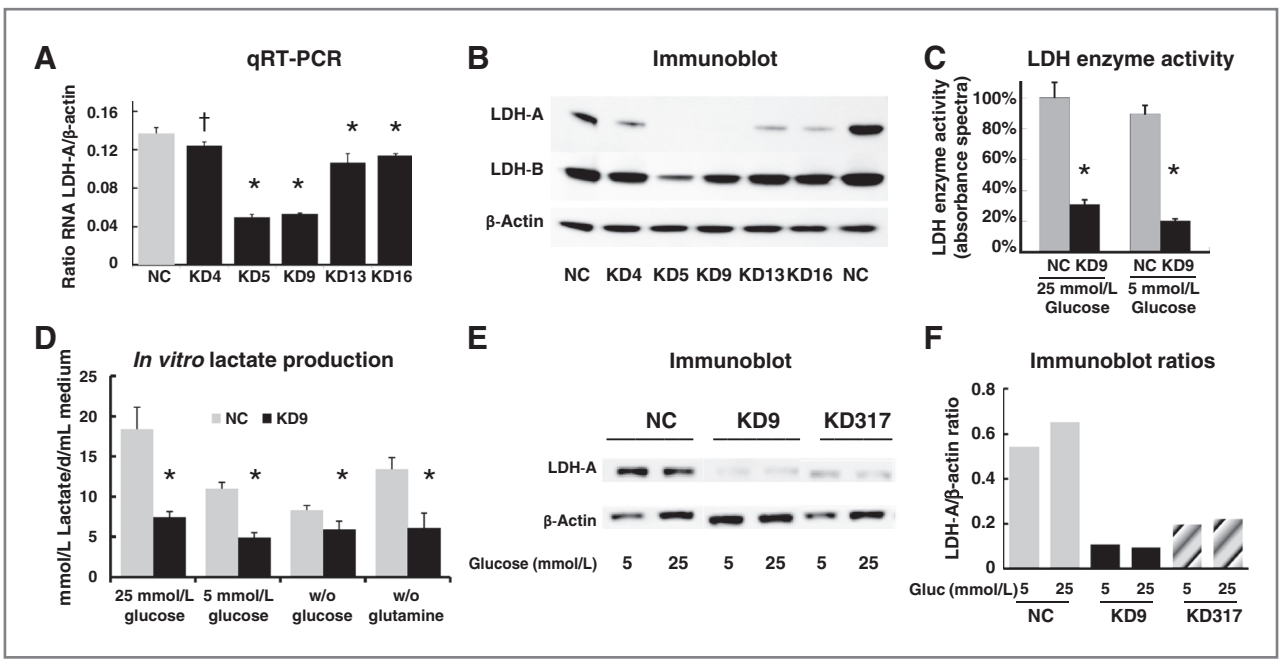

Figure 1. Selection and characterization of LDH-A knockdown cells. A, qRT-PCR analysis of LDH-A mRNA expression in the 4T1 cell lines transfected with scrambled shRNA (NC, control) and shRNA to mouse LDH-A mRNA (knockdown) $n = 3$. P values for KD4, KD5, KD9, KD13, and KD16 cells were $P = 0.03$; $P < 0.0001$; $P < 0.0001$; $P < 0.01$; and $P < 0.01$, respectively (*, $P < 0.01$; †, $P < 0.05$). B, Western blot analyses on whole-cell lysates prepared from NC and knockdown clones. C, total LDH enzyme activity in NC and KD9 cells cultured in DMEM with 25 or 5 mmol/L glucose, 6 mmol/L L-glutamine, and 10% FCS (*, $P < 0.01$). D, lactate production: appearance of lactate in different culture medium between NC and KD9 cells (*, $P < 0.01$ comparing NC and KD9 cells). E, Western blot analysis of LDH-A expression: cells were grown in DMEM with 5 or 25 mmol/L glucose, and whole-cell lysates were analyzed for LDH-A, and β-actin expression. F, LDH-A/β-actin proteins bands ratio were assessed by ImageJ software.

Published OnlineFirst July 5, 2013; DOI: 10.1158/1078-0432.CCR-12-3300

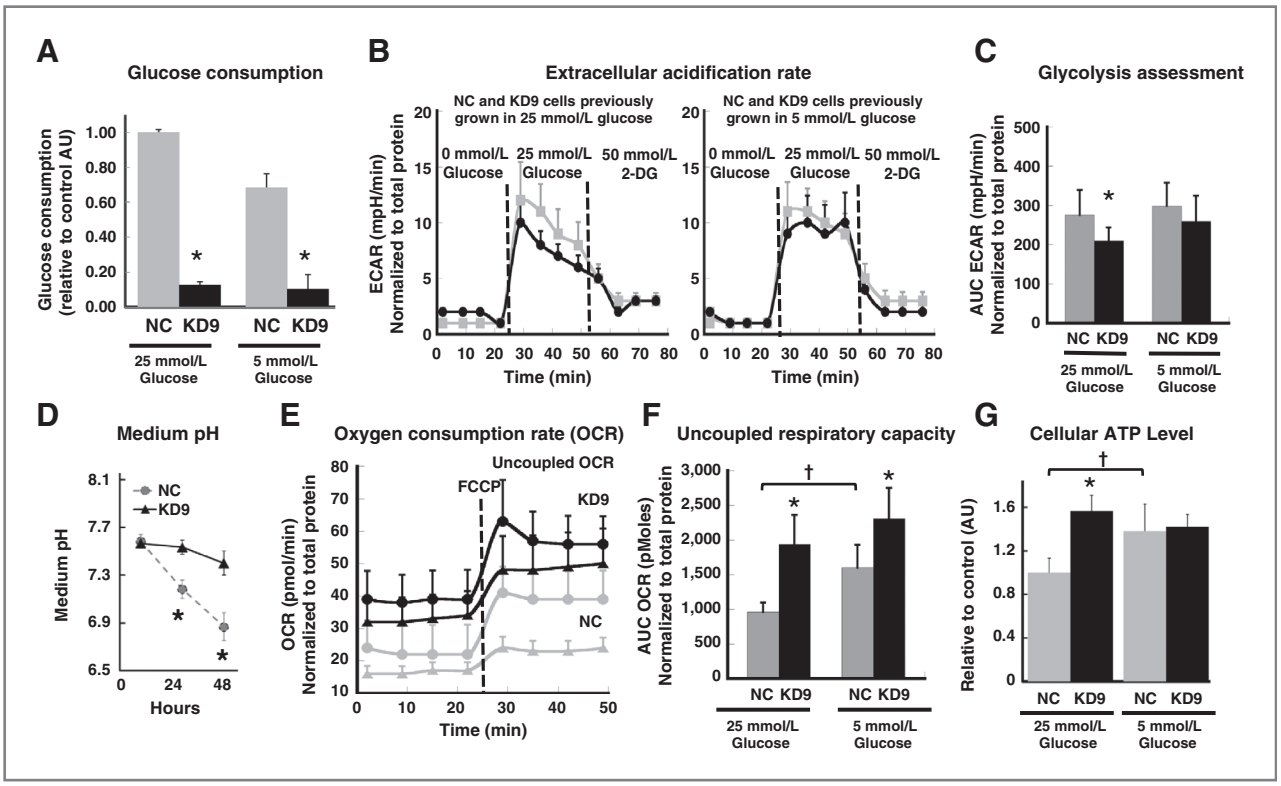

Figure 2. Metabolic properties of NC and KD9 cells *in vitro*. A, glucose consumption: cell culture media (standard DMEM with 5 or 25 mmol/L glucose) were assayed for glucose following 48 hours of incubation. Fluorescence intensity was normalized to the number of viable cells and background fluorescence (*, $P < 0.01$). B, ECAR: measurements were obtained before and after injection of glucose (initiate glycolysis) and 2-DG (block glycolysis), sequentially. A typical experiment is shown. C, glycolysis assessment calculated from ECAR results (B) for cells previously growing in 25 and 5 mmol/L glucose-containing media; the mean ECAR area under the curve (AUC; mpH/min; *, $P < 0.01$ comparing NC and KD9 cells) normalized to total protein (μg). D, cell culture medium acidification during NC and KD9 cell growth in standard DMEM with 25 mmol/L glucose (*, $P < 0.01$). E, OCR and the maximal mitochondrial capacity of cells cultured in 25 mmol/L (triangles) and 5 mmol/L (circles) glucose-containing media. FCCP was used as a potent uncoupler of oxidative phosphorylation in mitochondria. F, the uncoupled respiratory capacity was calculated from (E) results: AUC OCR (pmol; *, $P < 0.01$ comparing NC and KD9 cells; †, $P < 0.01$ comparing NC cells in 25 vs. 5 mmol/L glucose-containing media). G, ATP levels were measured in cells growing in standard DMEM containing 25 or 5 mmol/L glucose; results were normalized to the number of viable cells, and corrected for background luminescence (* and †, $P < 0.01$).

p-trifluoromethoxy phenylhydrazone) was added to uncouple oxidative phosphorylation from the electron transport chain to measure the maximum respiratory capacity (19). The respiratory rate (OCR) of KD9 cells was significantly higher (2- and 1.5-fold) than that of NC cells cultured in 25 and 5 mmol/L glucose, respectively ($P < 0.01$). OCR increased by a similar level for KD9 and NC cells after FCCP was added (Fig. 2F). Similar results were obtained in separate experiments using trypsinized cells growing in the media with 25 mmol/L of glucose using an Oxylite fiber optic probe; KD9 cells had a 60% higher OCR ($P < 0.01$) than NC cells (Supplementary Fig. S1A).

The high basal level of OCR is consistent with the 40% higher ATP levels observed in KD9 cells compared with NC cells ($P < 0.01$; Fig. 2G), and suggests that ATP production in KD9 cells may be associated with greater proton leak and ROS production than in NC cells. However, this trend occurs only in cells growing in 25 mmol/L glucose. The ATP level was notably higher in NC cells cultured in 5 mmol/L of glucose (compared with 25 mmol/L glucose), whereas the difference in ATP levels for KD9 cells growing under 25 and 5 mmol/L of glucose was not significant (Fig. 2G). These differences in ATP levels between NC and KD9 cells at 25 mmol/L glucose can be explained by the higher mitochondrial oxidative phosphorylation of KD9 cells in high glucose-containing media. It is interesting to note the higher OCR and ATP results in NC cells growing in 5 mmol/L glucose compared with 25 mmol/L glucose media (Fig. 2F and G). These data support the concept that some cancer cells, which use aerobic glycolysis, can also switch from glycolysis to oxidative phosphorylation under glucose-limiting conditions (20). This plasticity reflects the interplay between glycolysis and oxidative phosphorylation and the ability to adapt metabolism and energy production to changes in the microenvironment, and to adapt to differences in tumor energy needs or biosynthetic activity (21).

We measured mitochondrial ROS in cells growing under 25 mmol/L of glucose (Supplementary Fig. S1B). Intracellular ROS was significantly higher in KD9 cells compared with NC cells ($P < 0.01$), consistent with prior findings (4). However, the level of mitochondrial mass was similar in these two cell lines (Supplementary Fig. S1C). These

Published OnlineFirst July 5, 2013; DOI: 10.1158/1078-0432.CCR-12-3300

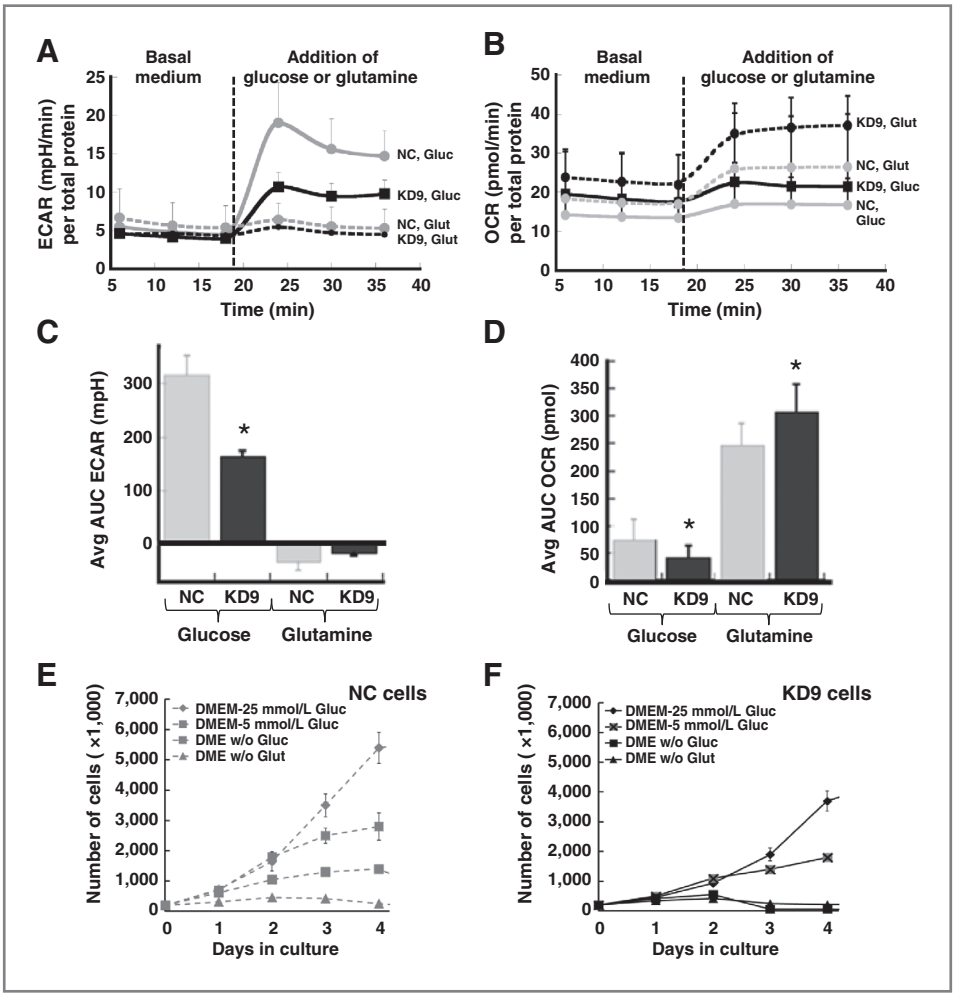

Figure 3. Effect of LDH-A knockdown on *in vitro* growth and metabolic properties. Changes in ECAR (A) and OCR (B) following the separate addition of glucose (Gluc; final concentration 25 mmol/L) or glutamine (Glut; final concentration 6 mmol/L) to a nonbuffered glucose-free DMEM culture medium without FCS (the standard medium for the XF assays). The mean AUC ECAR (mpH; C) and OCR (pmol; D) results are compared, respectively. The mean of 12 independent measurements normalized to total amount of protein (μg) was calculated. Significant differences between NC and KD9 cells are indicated (*, $P < 0.01$). Growth profiles of NC (E) and KD9 (F) cells in standard DMEM (25 mmol/L glucose, 6 mmol/L glutamine) compared with growth profiles with 5 mmol/L glucose or with the absence of glucose or glutamine.

findings are consistent with a higher proton leak and consequent increase in ROS formation in the LDH-A knockdown cells. These results show that LDH-A shRNA knockdown in 4T1 cells leads to an increase in TCA activity and mitochondrial respiration (in KD9 cells compared with NC cells), by switching from aerobic glycolysis (NC cells) to enhanced mitochondrial respiration. However, these cell-response properties are more evident when cells are grown under high concentrations of glucose, and this may reflect their "addiction" to high glucose levels.

In summary, the magnitude of glucose consumption, ECAR and pH changes (Fig. 2A–D) indicate higher aerobic glycolysis in NC compared with KD9 cells under high concentrations of glucose. In contrast, O_2 consumption (Fig. 2E and F and Supplementary Fig. S1A) and ROS (Supplementary Fig. S1B) were greater for KD9 than NC cells, and O_2 consumption was higher at 5 mmol/L glucose than at 25 mmol/L glucose for both cell lines (Fig. 2E and F).

We also studied the effect of excluding either glucose or glutamine from the incubation medium on the two major energy producing pathways of the cell–mitochondrial respiration and glycolysis–using the XF96 Extracellular Flux Analyzer. ECAR in basic glucose-free XF assay medium was low in both cell lines (Figs. 2B and 3A). ECAR (reflecting glycolysis) markedly increased on the addition of 25 mmol/L glucose alone, whereas there was little or no change in glycolysis following the addition of 6 mmol/L glutamine alone (Fig. 3A and C). We intentionally used 25 mmol/L of glucose to saturate the glycolytic pathway and measure the maximal upregulation of ECAR. In contrast, OCR increased markedly in both cell lines following the addition of 6 mmol/L glutamine alone, whereas a smaller increase in OCR was observed following the addition of 25 mmol/L glucose alone (Fig. 3B and D). The ECAR and OCR responses of KD9 and NC cells to the addition of glucose and glutamine indicate that glucose metabolism (not glutamine metabolism) is the primary source of extracellular acidification and aerobic glycolysis in both cell lines and that glutamine metabolism is the significant source of oxidative phosphorylation. The results also suggest that inhibition of LDH-A in 4T1 breast cancer cells leads to enhanced mitochondrial respiration through the glutamine pathway, and is associated with an increase in mitochondrial activity (Supplementary Fig. S1A) and ROS (Supplementary Fig. S1B), but not in mitochondrial number (Supplementary Figs. S1C and S2).

Published OnlineFirst July 5, 2013; DOI: 10.1158/1078-0432.CCR-12-3300

Growth profiles of KD9 and NC cells

The proliferation of KD9 and NC cells was studied in DMEM medium with different D-glucose (0, 5, and 25 mmol/L) and L-glutamine (0 and 6 mmol/L) concentrations. KD9 cells have a considerably slower growth rate compared with NC cells (Fig. 3E and F; Table 1). The doubling times were calculated and showed no differences between cells growing under high (25 mmol/L) and a more physiologic concentration of glucose (5 mmol/L) in the media (Table 1). The growth of the cells in 5 mmol/L glucose are similar to their growth in 25 mmol/L glucose medium for the first 48 hours, but slows after day 2, compared with their growth in 25 mmol/L glucose ($P < 0.01$), as glucose is consumed from the medium. Both cell lines have markedly reduced growth in the absence of glucose or glutamine, and the effect was greater in KD9 cells (Fig. 3E and F).

Growth and metabolic profiles of KD9 and NC tumors

Downregulation of LDH-A expression leads to slower growth, reduced glycolytic flux, and increased mitochondrial respiration *in vitro*. We asked whether enhanced mitochondrial respiration and dependence on glutamine could affect *in vivo* tumor growth, lactate production, and the potential for developing distant metastases. We injected cells into the mammary fat pad and evaluated the effect of LDH-A suppression on the tumorigenicity of the 4T1 breast cancer cell clones. We compared the growth profiles of KD9, KD5, and KD317 with NC and wild-type 4T1 tumors (Fig. 4A). By 2 weeks after injection, a significant tumor volume differences had developed, and LDH-A knockdown KD9, KD5, and KD317 tumors had significantly longer doubling times compared with NC and 4T1 wild-type tumors (Table 2). However, there was no difference in the doubling time of tumors derived from cells cultured in 5 mmol/L compared with 25 mmol/L glucose.

4T1 tumors are known to undergo necrosis at volumes greater than approximately 100 mm^3 (10), and necrosis increases significantly as tumors grow beyond 200 to 300 mm^3 (10). Therefore, we measured *in vivo* lactate levels using MRSI (Fig. 4B and C) in tumors that were approximately 100 mm^3 in size, to avoid the complicating effects of tumor necrosis. We found a significant reduction of lactate in KD9, KD5, and KD317 tumors compared with NC and 4T1 wild-type tumors (Fig. 4C), and the mean lactate levels measured in small (100 mm^3) KD9 and NC tumors ($n = 13$) were significantly different: 6.1 ± 1.5 and 9.6 ± 1.8 mmol/L ($P < 0.01$), respectively.

Table 1. *In vitro* cell doubling time

Medium glucose concentration	Cell line doubling time, h[a]		
	KD9	NC	4T1 WT
5 mmol/L	19.6 ± 0.5	15.3 ± 0.3	14.7 ± 0.3
25 mmol/L	20.5 ± 0.6	15.4 ± 0.3	14.5 ± 0.2

[a]Estimated over 2 days following cell plating and media change.

In some animals, tumors were removed and underwent histologic examination. Tumor histology showed similar features for both the KD9 and NC tumors at small volumes (Supplementary Fig. S2). Hematoxylin and eosin (H&E) staining of small NC and KD9 tumors showed only minimal necrosis, predominantly in the tumor core. Hoechst perfusion staining showed a heterogeneity of perfusion across the tumor sections. LDH-A enzyme expression levels in small ($\sim$100 mm^3) KD9 tumors were compared with small NC tumors by immunoblot analyses of whole tumor lysates. Ten representative immunoblots (5 from each group) and their band intensity ratios are shown in Fig. 4D and E. The mean Western blot analysis band intensity for LDH-A from 18 mice, 9 from each group, showed that LDH-A expression was approximately 4-fold lower in KD9 tumors compared with NC tumors ($P < 0.01$; Fig. 4F). We also noted that there was a linear relationship between tumor lactate concentration and the corresponding tumor LDH-A/β-actin protein band ratio ($R^2 = 0.64$; $P < 0.01$; Fig. 4G), indicating the potential of lactate MRS to monitor the expression of LDH-A and the extent of LDH-A knockdown or inhibition.

Migration potential of KD9 and NC cells

Migration and invasiveness of tumor cells are important aspects of metastasis formation. In transwell migration assays at 25 and 5 mmol/L glucose, fewer KD9 cells migrate through the 8-μm pores of a transwell chamber compared with NC cells (Fig. 5A). Invasion through a Matrigel environment (3-mm thick) also showed a significantly smaller number of invading KD9 cells compared with NC cells. These differences were more profound in 5 mmol/L glucose ($P < 0.001$; Fig. 5A), but were significant in both glucose environments. In the *in vitro* scratch assay (Fig. 5B), KD9 cell migration (wound closure) was significantly slower compared with NC cell migration over 6 hours in both 25 and 5 mmol/L glucose ($P < 0.01$). In the absence of glucose or glutamine, wound closure was similar for both cell lines and the reduction in closure was marked in the absence of glutamine (Fig. 5B).

Metastatic potential of KD9 and NC tumors

We tested the effects of LDH-A knockdown on the development of metastases by comparing orthotopic KD9 and NC primary tumors. All animals bearing orthotopic NC tumors developed lung metastases 1 to 3 weeks after tumor inoculation, whereas no animals bearing orthotopic KD9 tumors developed visible metastases over the first 3 weeks. This MRI observation was confirmed by India ink injection and histology in one set (5 animals/group) of animals that were sacrificed and examined after 21 days of primary tumor growth (Fig. 5C). The mean lung weight for animals bearing primary KD9 tumors was 0.16 ± 0.03 g, whereas the corresponding lung weight of NC tumor-bearing animals was 0.27 ± 0.03 g ($P < 0.01$; Supplementary Fig. S3). In another cohort of animals, MRI-identified lung metastases and survival were monitored. A 2- to 3-week delay in the

Published OnlineFirst July 5, 2013; DOI: 10.1158/1078-0432.CCR-12-3300

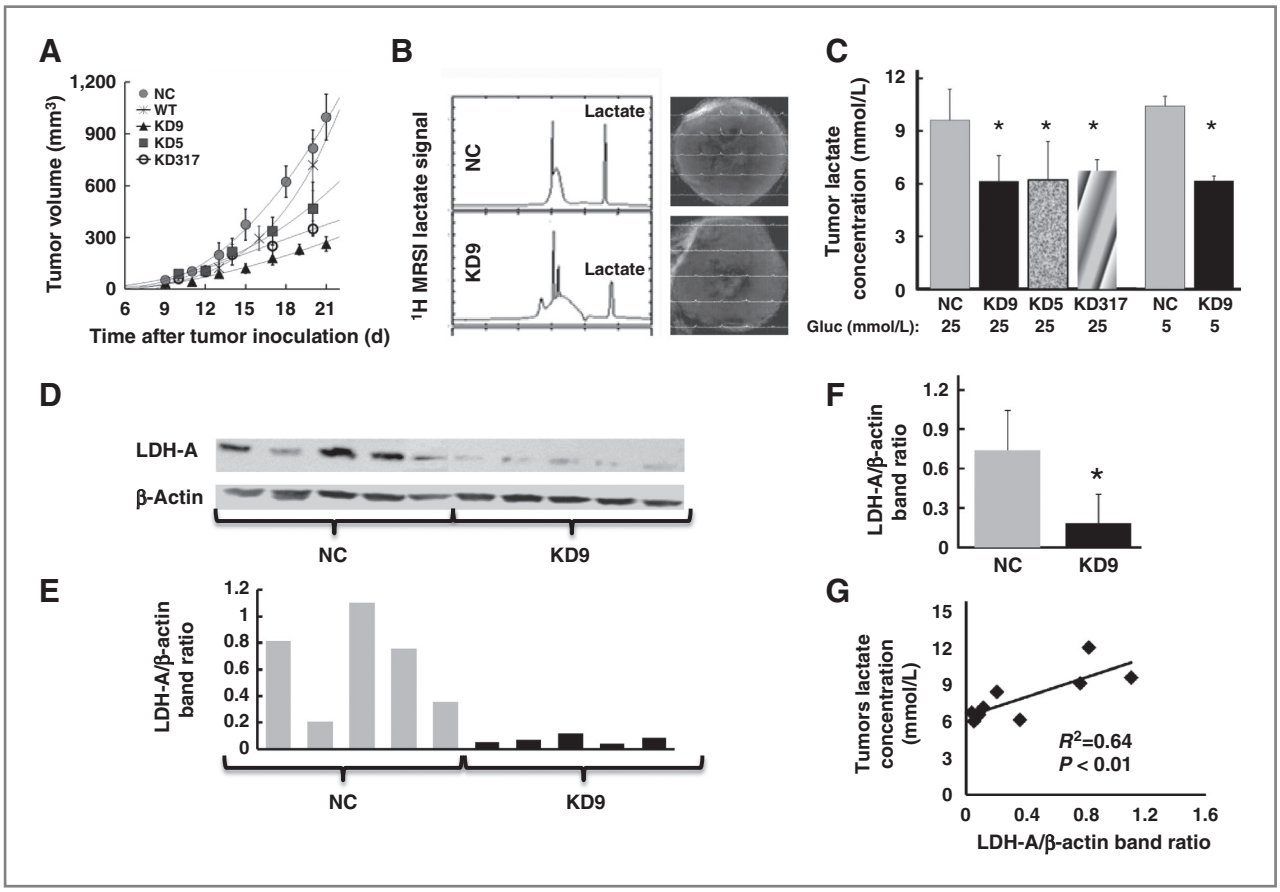

Figure 4. Effect of LDH-A knockdown on tumor growth, lactate, and LDH-A protein expression. A, growth profiles of KD9, KD5, and KD317 orthotopic breast tumors compared with NC and wild-type 4T1 tumors [$n = 13$ (NC), $n = 18$ (KD9), $n = 6$ (KD5), $n = 4$ (KD317)]. B, representative MRSI lactate spectra from NC and KD9 tumors are shown. C, mean lactate concentration of small (~100 mm^3) KD9, KD5, and KD31 orthotopic breast tumors, measured by MRSI, are compared with NC (*, $P < 0.01$). D, LDH-A expression assessed by Western blotting from 10 small (100 mm^3) NC and KD9 tumors. E, LDH-A/β-actin protein band ratios of Western blot analyses shown in (D) were analyzed by ImageJ software. F, the mean LDH-A/β-actin ratio assessed in small (100 mm^3) orthotopic tumors (9 NC and 9 KD9; *, $P < 0.01$). G, tumor lactate concentration assessed by MRS was plotted versus LDH-A protein level of the corresponding tumor assessed by Western blotting.

development of lung metastases and survival were observed between KD9 and NC tumor-bearing mice (Fig. 5D).

The growth of primary NC and 4T1 tumors were significantly more rapid than that of primary KD9, KD5, and KD317 tumors (Fig. 4A and Table 2). NC and KD9 cells cultured for 2 weeks in DMEM with 5 mmol/L glucose were also injected orthotopically into the mammary fat pad. These tumor growth profiles and calculated tumor-doubling times were similar to that obtained when the glucose concentration in the culture medium was 25 mmol/L (Table 2).

Table 2. Tumor volume doubling time

	Doubling time, d[a] Glucose concentration[b]	
Tumor cell line	**25 mmol/L**	**5 mmol/L**
KD9	3.9 ± 0.5	3.5 ± 0.2
KD5	3.6 ± 0.3	—
KD317	3.4 ± 0.4	—
NC	2.3 ± 0.2	2.0 ± 0.2
4T1	2.2 ± 0.4	—

[a]Estimated over first 2 weeks following implantation.
[b]Glucose concentration in preimplantation culture medium.

To control for the effect of differing tumor volumes and growth rates, and to more closely simulate the clinical situation where the primary tumor is removed, we studied a separate group of animals (10 per group) and surgically removed the primary mammary tumor (tumor volume, ~100 mm^3). The NC tumor-resected animals began to die 4 weeks after tumor inoculation, whereas the KD9 tumor-resected animals began to die 6 weeks after tumor inoculation (Fig. 5E). A 2-week increase was observed in the survival of the KD9 tumor-resected animals, compared with NC tumor-resected animals (Fig. 5E). The mean survival time for tumor-resected animals was 33.5 ± 6 days for NC and 44 ± 7 days for the KD9 ($P < 0.01$).

Published OnlineFirst July 5, 2013; DOI: 10.1158/1078-0432.CCR-12-3300

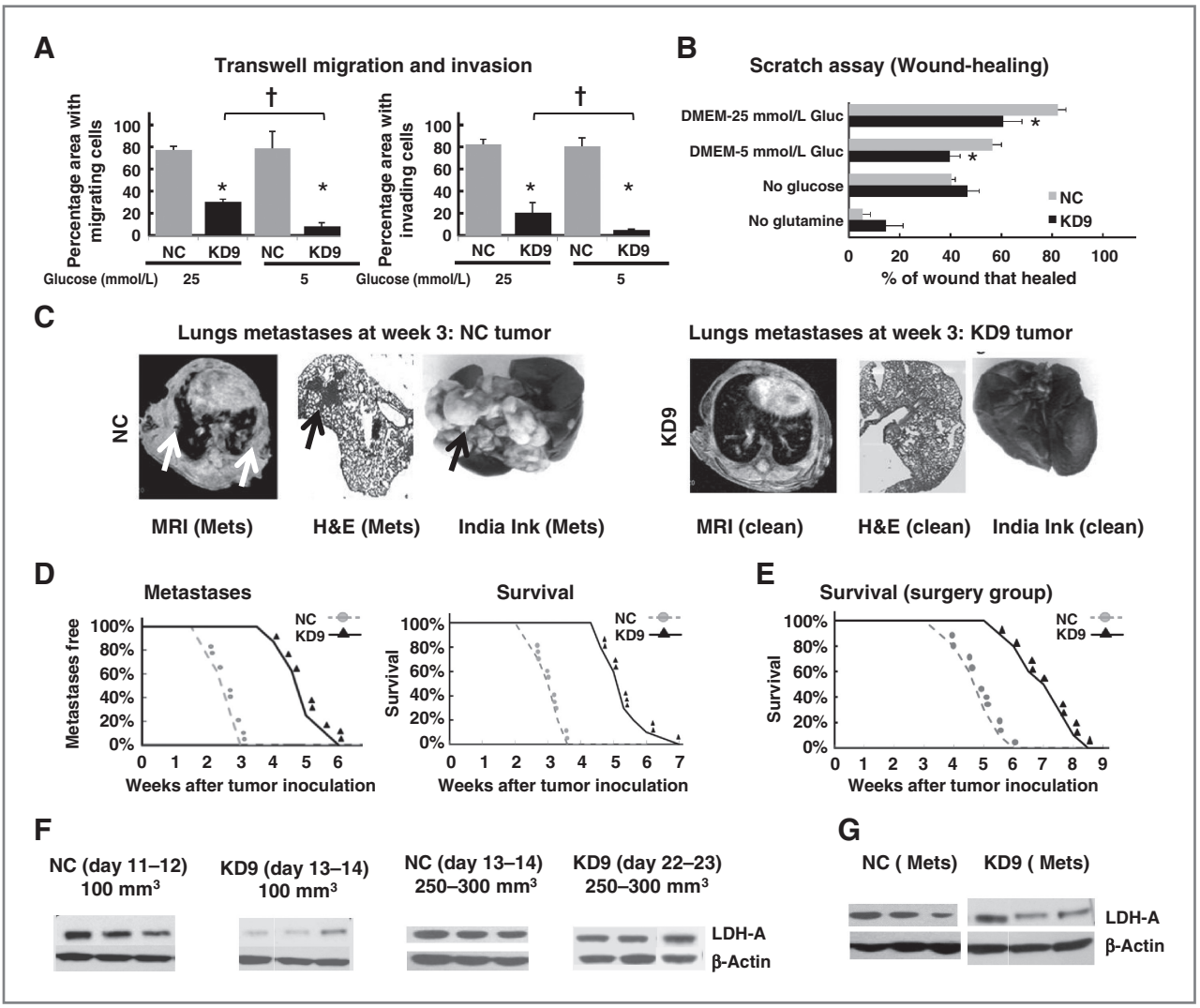

Figure 5. Metastatic profile of LDH-A knockdown (KD9) and control (NC) cells and tumors. A, inhibition of LDH-A in KD9 tumor cells decreases their migration and invasiveness compared with NC tumor cells (*, $P < 0.01$ comparing NC and KD9; †, $P < 0.01$ comparing 5 and 25 mmol/L glucose). B, the effect of nutrient absence on wound-healing is plotted (*, $P < 0.01$). C, magnetic resonance, H&E, and India Ink imaging of lungs show extensive metastases in the control group (NC) compared with no visible metastases in the LDH-A knockdown group (KD9) at week 3. D, Percentage of metastatic-free lungs and survival of animals bearing NC and KD9 tumors is plotted versus time (weeks after orthotopic inoculation). Survival was determined from the day of orthotopic tumor cell implantation until the day of death or day of euthanasia (primary tumor volume reached 1 cm^3, or severe stress, weight loss, or immobility were noted). E, survival following surgical removal of the primary orthotopic tumor (100 mm^3; ~1–2 weeks after orthotopic inoculation). Animal survival is plotted versus time (weeks after inoculation). F, Western blot analyses of LDH-A protein from primary tumors harvested at various times after orthotopic inoculation. All NC tumors had high expression of LDH-A. In contrast, small (~100 mm^3) knockdown tumors had low LDH-A, whereas larger knockdown tumors (~250–1,000 mm^3) had high LDH-A expression, similar to NC tumors. G, Western blot analyses of LDH-A protein from distant metastases are shown. The primary tumor was removed surgically (at ~100 mm^3), and distant NC and KD9 lymph node and lung metastases were assayed; all metastases (both NC and KD9) were found to have high LDH-A expression.

LDH-A expression in NC and KD9 tumors and metastases

LDH-A protein (immunoblotting) levels in small (~100 mm^3) KD9 tumors were approximately 4-fold less than in comparable, small-size NC tumors ($P < 0.01$; Figs. 4D and F and 5F). However, there was a reappearance of LDH-A protein expression in KD9 tumors as they enlarged (from ~100 to 250–300 mm^3), and LDH-A protein levels in the larger KD9 and NC tumors were similar (Fig. 5F). Metastases to lymph nodes and lungs, as well as recurrent tumor at the primary site (KD9 and NC) had similar high expression of LDH-A (Fig. 5F and G). Thus, the larger KD9 and NC tumors, and metastatic nodules from both tumors, had similar LDH-A protein expression levels.

Discussion

Tumors with high tissue lactate concentrations and high LDH-A expression have been linked to poor prognosis (22–25), and are associated with greater metastatic potential (24, 25). Shifts in metabolism have been shown to have a

Published OnlineFirst July 5, 2013; DOI: 10.1158/1078-0432.CCR-12-3300

significant impact on the tumor microenvironment, disease evolution, progression, and development of metastases (1, 3–6, 26–28). In our analysis of 4 clinical datasets (622 patients with breast cancer; refs. 14–17), we show that patients with high levels of LDH-A expression have a significantly higher probability ($P < 10^{-16}$) of developing metastases compared with women with low levels of LDH-A (Fig. 6).

We also focused on LDH-A, because it is a bridge between several metabolic pathways, and because the product of LDH-A activity (lactate) can be assessed noninvasively and quantitatively using MRSI. Although it has been shown that the inhibition of LDH-A has an antiproliferative effect on primary breast tumors (5), in human alveolar adenocarcinoma A549 xenografts (29), and human hepatocellular carcinoma HCCLM3 xenografts (30), there have been no studies investigating the effect of LDH-A inhibition on the development and growth of metastases. This is an important clinical issue, as the cause of death in patients with breast cancer is almost always due to metastases.

The inhibition of LDH-A by a small-molecule inhibitor, FX-11, reduces progression of human lymphoma P493 xenografts (4). The inhibition of pyruvate conversion to lactate by oxamate (pyruvate analog) also resensitizes taxol-resistant human MDA-MB-435 breast tumor xenografts (31). The inhibition of LDH-A may enhance oxidative stress, and is linked to tumor cell death (4, 5, 29, 30). We previously measured greater amounts of LDH-A protein and lactate production in 4T1 cells and tumors (metastatic phenotype) compared with isogenic 67NR cells and tumors (nonmetastatic phenotype; ref. 10). We selected the murine 4T1 breast cancer metastatic model to test whether LDH-A

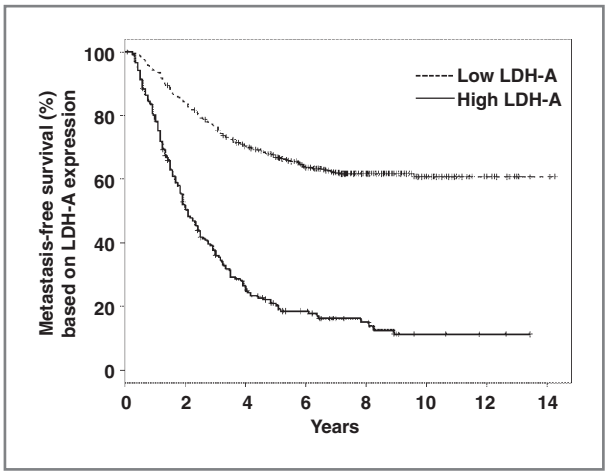

Figure 6. Metastatic-free breast cancer survival: *LDH-A* gene expression. Kaplan–Meier estimators for metastasis-free survival from a compendium of four breast cancer patient datasets (14–17). Survival data were separated into low-medium and high groups according to the expression level of LDHA: 2 of 3 of data points are in the low group (dashed line) and 1 of 3 are in the high group (solid line). Patients with high levels of LDH-A expression have a significantly higher ($P < 10^{-16}$) probability of developing metastases compared with women with low levels of LDH-A.

silencing, using shRNA-knockdown technology, has a significant effect on the development of metastases, as well as on cell/tumor metabolism and cell/tumor growth, and can we measure these changes noninvasively by MRSI using lactate as a surrogate marker of LDH-A.

We show a close association between *LDH-A* gene and protein expression, LDH enzyme activity, cell proliferation, and transwell migration assays between KD9 and NC cells. *In vitro* experiments also show a reduction in the rate of glucose usage and glycolysis (ECAR), and a compensatory increase in OCR, maximum respiratory capacity, ROS, and cellular ATP levels (reflecting increased oxidative phosphorylation) following stable LDH-A shRNA knockdown in 4T1 cells. Glucose and glutamine dependence studies were also conducted, and they showed that glucose metabolism (not glutamine metabolism) is the primary source of extracellular acidification and aerobic glycolysis. Glutamine is essential for cell proliferation and wound-healing (scratch) assay, and may have a significant impact on mitochondrial activity of LDH-A knockdown cells.

4T1 cells and variants reported here (NC, KD9, etc.) were grown in DMEM with high and normal concentrations of glucose (25 and 5 mmol/L, respectively) and glutamine (6 mmol/L). Many tumor cell lines are routinely cultured in media containing high amounts of glucose and glutamine (32–34), ensuring the survival of most cells over longer periods of cell culture, without the need to monitor glucose or glutamine concentration. However, most healthy, nondiabetic adults maintain fasting glucose levels at about 5 mmol/L and glutamine levels at 1 mmol/L (35–38), considerably less than that in most cell culture media. Therefore, we conducted comparison studies of cells growing in 25 and 5 mmol/L glucose, as it is known that "hyperglycemic" conditions may lead to changes in cellular functions, such as carbohydrate and fatty acid metabolism, proliferation, and cell motility (39). In addition, glucose concentrations in tumors can vary considerably in different tumor regions during tumor progression, and can be significantly lower than that in normal tissues (40). Thus, the tumor microenvironment can be variable and characterized as being "glucose starved" to "glucose addicted" in comparison with other tissues, reflecting an imbalance between poor supply and high consumption rate. Despite the differences in glucose and glutamine concentrations between our *in vitro* and *in vivo* experiments, we found no significant differences in the tumor growth and metastatic ability when we used cells that had been adapted to 5 mmol/L glucose over 2 weeks. These 5 mmol/L glucose-adapted NC and KD9 cells had similar *in vitro* and *in vivo* growth (doubling times) and similar metastatic patterns compared with cells grown in 25 mmol/L glucose.

A close relationship between *LDH-A* gene and protein expression, tissue lactate levels, and tumor metastatic potential was shown. Significant *in vivo* biologic effects of LDH-A silencing were shown, which included, decreased lactate production *in vivo*, the slowing of tumor growth and a reduction and delay in the development of metastases of several knockdown clones (KD9, KD5, and KD317).

Published OnlineFirst July 5, 2013; DOI: 10.1158/1078-0432.CCR-12-3300

Therefore, we explored the evolution of LDH-A protein expression in primary orthotopic KD9 and NC tumors, and conducted immunoblots on enlarging tumors (from ~100 to 250–300 mm^3), and on metastases in the same animals. Most notable were the similar high LDH-A protein levels that were measured in the larger primary KD9 and NC tumors, and in the metastatic lesions as well. These data, along with our previous studies (10), suggest that small (~100 mm^3) wild-type 4T1 and NC tumors (with high LDH-A expression and high lactate levels) are already seeding metastatic cells into the circulation. Nevertheless, small KD9 tumors (with lower LDH-A expression and only moderate lactate levels) are capable of forming metastases, but at a delayed rate.

The eventual appearance of delayed metastases in knockdown tumor-bearing mice may be explained in several ways, including the fact that LDH-A silencing was incomplete. We have seen reexpression of LDH-A protein in knockdown cells, when cells were cultured without antibiotic selection (Supplementary Fig. S4). We show an outgrowth of non-LDH-A–silenced KD9 cells in enlarging primary KD9 tumors (250–300 mm^3) that lead to higher lactate levels, and the presence of high LDH-A protein levels in distant KD9 metastases, similar to that measured in distant NC metastases.

Reappearance of LDH-A *in vivo* could also explain the moderate levels of lactate in small (100 mm^3) primary KD9 tumors, resulting in failure to more effectively suppress tumor growth and development of metastases. Other explanations for the growth and metastatic profile of KD9 tumors include the fact that the KD9 cells use oxidative metabolism more than NC or wild-type 4T1 cells to produce metabolic intermediates, and they are less dependent on glycolysis (greater use of the TCA cycle and oxidative phosphorylation). In addition, enhanced mitochondrial oxidative activity and elevated ROS can induce a more aggressive tumor phenotype through hypoxia-inducible factor 1 (HIF-1; refs. 41, 42), as well as increased oxidative stress and cell death (41).

Other possible factors include the use of other metabolic fuels, such as glutamine, which could feed in through the TCA cycle and provide metabolic intermediates (43). Stromal tissue surrounding the tumor cells can also play an important role in tumor progression and metastasis (44). This mechanism could account for KD9 tumor growth and metastases, where the production of either lactate or pyruvate by the tumor stroma could be used to "feed" the malignant tumor cells and to alter the microenvironment (45). The production of lactate by tumor stromal cells (requiring LDH-A) would not be affected by LDH-A silencing in tumor KD9 cells, as the stromal cells originate from the host animal. Thus, several possible explanations exist that could account for the modest and increasing levels of LDH-A expression and lactate concentration in small and larger KD9 tumors. Such changes would be consistent with the slower growth profile of primary orthotopic KD9 breast tumors and their delayed ability to form metastases.

Imaging paradigms developed in this study can be translated to the clinic for selecting patients at high risk for developing subsequent metastases and who need closer surveillance, or patients appropriate for treatment with metabolic inhibitors. The noninvasive monitoring of LDH-A–targeted therapy using lactate MRSI is novel, even though lactate ^{1}H MRSI has been conducted in a limited number of oncology studies previously (9, 10, 13, 46, 47). In contrast to hyperpolarized ^{13}C NMR studies, lactate ^{1}H MRSI measurements do not require special instrumentation and injection of hyperpolarized molecules. Pulse sequences for lactate detection have been implemented on clinical scanners (46–49). Therefore, the barrier to translation is modest and these studies can be implemented with currently available technology. These preclinical studies support the wider clinical application of lactate ^{1}H MRSI, including the identification and monitoring of women with breast cancer who are at high risk of developing metastatic disease, and to specifically monitor LDH-A–targeted drug treatment.

Conclusions

Because elevated LDH-A is a component of many aggressive tumors (4–6, 22, 28), it is a potential drug target for cancer therapy (4, 31). Our results show for the first time that LDH-A inhibition reduces and delays the development of metastases, effects tumor cell metabolism, and confirms the reduction of primary tumor growth in an established murine model of breast cancer (4T1). Our LDH-A shRNA silencing experiments show a strong association between *LDH-A* gene and protein expression, tumor lactate levels, and development of metastases. LDH-A–targeted drug therapy may avoid the loss of shRNA-based LDH-A silencing, that we observed, and it will also affect both tumor and stromal components.

These results suggest that LDH-A drug-targeted therapy is likely to be effective in aggressive breast cancer, and that lactate MRSI could serve as a surrogate for measuring LDH-A expression and target inhibition in the development of LDH-A–targeted therapies. Inhibition of LDH-A in patients is expected to be tolerable and associated with low toxicity. LDH-A deficiency is a rare, but well-characterized human disease that can lead to exercise intolerance, cramps, myoglobinuria, but is not associated with severe dysfunction of major organs (50, 51).

Disclosure of Potential Conflicts of Interest

No potential conflicts of interest were disclosed.

Authors' Contributions

Conception and design: A. Rizwan, I. Serganova, R. Blasberg, J.A. Koutcher
Development of methodology: A. Rizwan, I. Serganova, H. Karabeber, S. Thakur
Acquisition of data (provided animals, acquired and managed patients, provided facilities, etc.): A. Rizwan, I. Serganova, H. Karabeber, X. Ni, S. Thakur
Analysis and interpretation of data (e.g., statistical analysis, biostatistics, computational analysis): A. Rizwan, I. Serganova, R. Khanin, H. Karabeber, X. Ni, R. Blasberg, J.A. Koutcher
Writing, review, and/or revision of the manuscript: A. Rizwan, I. Serganova, H. Karabeber, S. Thakur, K.L. Zakian, R. Blasberg, J.A. Koutcher

Published OnlineFirst July 5, 2013; DOI: 10.1158/1078-0432.CCR-12-3300

Administrative, technical, or material support (i.e., reporting or organizing data, constructing databases): A. Rizwan, K.L. Zakian, R. Blasberg, J.A. Koutcher
Study supervision: R. Blasberg, J.A. Koutcher

Grant Support

This work was supported in part by grants entitled Breast Cancer Molecular Imaging Fund (to J.A. Koutcher), P01-CA94060 (to J.A. Koutcher), P30 CA08748 (to J.A. Koutcher), Department of Defense - Breast Cancer Research Program (DOD-BCRP) W81XWH-09-1-0042 (S. Thakur) and Memorial Sloan-Kettering Cancer Center for Molecular Imaging in Cancer 2P50CA086438 (R.G. Blasberg).

The costs of publication of this article were defrayed in part by the payment of page charges. This article must therefore be hereby marked *advertisement* in accordance with 18 U.S.C. Section 1734 solely to indicate this fact.

Received October 24, 2012; revised May 31, 2013; accepted June 27, 2013; published OnlineFirst July 5, 2013.

References

1. Gatenby RA, Gillies RJ. Why do cancers have high aerobic glycolysis? Nat Rev Cancer 2004;4:891–9.
2. Gatenby RA, Gillies RJ. A microenvironmental model of carcinogenesis. Nat Rev Cancer 2008;8:56–61.
3. Gillies RJ, Robey I, Gatenby RA. Causes and consequences of increased glucose metabolism of cancers. J Nuclear Med 2008;49 (Suppl 2):24S–42S.
4. Le A, Cooper CR, Gouw AM, Dinavahi R, Maitra A, Deck LM, et al. Inhibition of lactate dehydrogenase A induces oxidative stress and inhibits tumor progression. Proc Natl Acad Sci U S A 2010;107: 2037–42.
5. Fantin VR, St-Pierre J, Leder P. Attenuation of LDH-A expression uncovers a link between glycolysis, mitochondrial physiology, and tumor maintenance. Cancer Cell 2006;9:425–34.
6. Vander Heiden MG, Cantley LC, Thompson CB. Understanding the Warburg effect: the metabolic requirements of cell proliferation. Science 2009;324:1029–33.
7. DeBerardinis RJ, Thompson CB. Cellular metabolism and disease: what do metabolic outliers teach us? Cell. 2012;148:1132–44.
8. Hanahan D, Weinberg RA. Hallmarks of cancer: the next generation. Cell 2011;144:646–74.
9. He Q, Shungu DC, van Zijl PC, Bhujwalla ZM, Glickson JD. Single-scan *in vivo* lactate editing with complete lipid and water suppression by selective multiple-quantum-coherence transfer (Sel-MQC) with application to tumors. J Magn Reson B 1995;106:203–11.
10. Serganova I, Rizwan A, Ni X, Thakur SB, Vider J, Russell J, et al. Metabolic imaging: a link between lactate dehydrogenase A, lactate, and tumor phenotype. Clin Cancer Res 2011;17:6250–61.
11. Aslakson CJ, Miller FR. Selective events in the metastatic process defined by analysis of the sequential dissemination of subpopulations of a mouse mammary tumor. Cancer Res 1992;52:1399–405.
12. Mehrara E, Forssell-Aronsson E, Ahlman H, Bernhardt P. Specific growth rate versus doubling time for quantitative characterization of tumor growth rate. Cancer Res 2007;67:3970–5.
13. Yaligar J, Thakur SB, Bokacheva L, Carlin S, Thaler HT, Rizwan A, et al. Lactate MRSI and DCE MRI as surrogate markers of prostate tumor aggressiveness. NMR Biomed 2012;25:113–22.
14. Minn AJ, Gupta GP, Siegel PM, Bos PD, Shu W, Giri DD, et al. Genes that mediate breast cancer metastasis to lung. Nature 2005;436: 518–24.
15. Wang Y, Klijn JG, Zhang Y, Sieuwerts AM, Look MP, Yang F, et al. Gene-expression profiles to predict distant metastasis of lymph-node-negative primary breast cancer. Lancet 2005;365:671–9.
16. Bos PD, Zhang XH, Nadal C, Shu W, Gomis RR, Nguyen DX, et al. Genes that mediate breast cancer metastasis to the brain. Nature 2009;459:1005–9.
17. Minn AJ, Gupta GP, Padua D, Bos P, Nguyen DX, Nuyten D, et al. Lung metastasis genes couple breast tumor size and metastatic spread. Proc Natl Acad Sci U S A 2007;104:6740–5.
18. Wu ZJ, Irizarry RA, Gentleman R, Martinez-Murillo F, Spencer F. A model-based background adjustment for oligonucleotide expression arrays. J Am Stat Assoc 2004;99:909–17.
19. Moran M, Rivera H, Sanchez-Arago M, Blazquez A, Merinero B, Ugalde C, et al. Mitochondrial bioenergetics and dynamics interplay in complex I-deficient fibroblasts. Biochim Biophys Acta 2010;1802:443–53.
20. Griguer CE, Oliva CR, Gillespie GY. Glucose metabolism heterogeneity in human and mouse malignant glioma cell lines. J Neurooncol 2005; 74:123–33.
21. Jose C, Bellance N, Rossignol R. Choosing between glycolysis and oxidative phosphorylation: a tumor's dilemma? Biochim Biophys Acta 2011;1807:552–61.
22. Koukourakis MI, Giatromanolaki A, Simopoulos C, Polychronidis A, Sivridis E. Lactate dehydrogenase 5 (LDH5) relates to up-regulated hypoxia inducible factor pathway and metastasis in colorectal cancer. Clin Exp Metastasis 2005;22:25–30.
23. Koukourakis MI, Giatromanolaki A, Harris AL, Sivridis E. Comparison of metabolic pathways between cancer cells and stromal cells in colorectal carcinomas: a metabolic survival role for tumor-associated stroma. Cancer Res 2006;66:632–7.
24. Ryberg M, Nielsen D, Osterlind K, Andersen PK, Skovsgaard T, Dombernowsky P. Predictors of central nervous system metastasis in patients with metastatic breast cancer. A competing risk analysis of 579 patients treated with epirubicin-based chemotherapy. Breast Cancer Res Treat 2005;91:217–25.
25. Koukourakis MI, Giatromanolaki A, Sivridis E, Bougioukas G, Didilis V, Gatter KC, et al. Lactate dehydrogenase-5 (LDH-5) overexpression in non–small-cell lung cancer tissues is linked to tumour hypoxia, angiogenic factor production and poor prognosis. Br J Cancer 2003;89: 877–85.
26. Brizel DM, Schroeder T, Scher RL, Walenta S, Clough RW, Dewhirst MW, et al. Elevated tumor lactate concentrations predict for an increased risk of metastases in head-and-neck cancer. Int J Radiat Oncol Biol Phys 2001;51:349–53.
27. Walenta S, Chau TV, Schroeder T, Lehr HA, Kunz-Schughart LA, Fuerst A, et al. Metabolic classification of human rectal adenocarcinomas: a novel guideline for clinical oncologists? J Cancer Res Clin Oncol 2003;129:321–6.
28. Walenta S, Wetterling M, Lehrke M, Schwickert G, Sundfor K, Rofstad EK, et al. High lactate levels predict likelihood of metastases, tumor recurrence, and restricted patient survival in human cervical cancers. Cancer Res 2000;60:916–21.
29. Seth P, Grant A, Tang J, Vinogradov E, Wang X, Lenkinski R, et al. On-target inhibition of tumor fermentative glycolysis as visualized by hyperpolarized pyruvate. Neoplasia 2011;13:60–71.
30. Sheng SL, Liu JJ, Dai YH, Sun XG, Xiong XP, Huang G. Knockdown of lactate dehydrogenase A suppresses tumor growth and metastasis of human hepatocellular carcinoma. FEBS J 2012;279: 3898–910.
31. Zhou M, Zhao Y, Ding Y, Liu H, Liu Z, Fodstad O, et al. Warburg effect in chemosensitivity: targeting lactate dehydrogenase-A re-sensitizes taxol-resistant cancer cells to taxol. Mol Cancer 2010;9:33.
32. Chaneton B, Hillmann P, Zheng L, Martin AC, Maddocks OD, Chokkathukalam A, et al. Serine is a natural ligand and allosteric activator of pyruvate kinase M2. Nature 2012;491:458–62.
33. Yang W, Zheng Y, Xia Y, Ji H, Chen X, Guo F, et al. ERK1/2-dependent phosphorylation and nuclear translocation of PKM2 promotes the Warburg effect. Nat Cell Biol 2012;14:1295–304.
34. Xiang X, Zhuang X, Ju S, Zhang S, Jiang H, Mu J, et al. miR-155 promotes macroscopic tumor formation yet inhibits tumor dissemination from mammary fat pads to the lung by preventing EMT. Oncogene 2011;30:3440–53.
35. Tannock IF, Steele D, Roberts J. Influence of reduced concentration of L-glutamine on growth and viability of cells in monolayer, in spheroids, and in experimental tumours. Br J Cancer 1986;54:733–41.
36. Coutinho M, Gerstein HC, Wang Y, Yusuf S. The relationship between glucose and incident cardiovascular events. A metaregression

Published OnlineFirst July 5, 2013; DOI: 10.1158/1078-0432.CCR-12-3300

analysis of published data from 20 studies of 95,783 individuals followed for 12.4 years. Diabetes Care 1999;22:233–40.

37. Elia M, Neale G, Livesey G. Alanine and glutamine release from the human forearm: effects of glucose administration. Clin Sci 1985;69: 123–33.
38. Minokoshi Y, Alquier T, Furukawa N, Kim YB, Lee A, Xue B, et al. AMP-kinase regulates food intake by responding to hormonal and nutrient signals in the hypothalamus. Nature 2004;428:569–74.
39. Sedoris KC, Thomas SD, Miller DM. c-myc promoter binding protein regulates the cellular response to an altered glucose concentration. Biochemistry 2007;46:8659–68.
40. Hirayama A, Kami K, Sugimoto M, Sugawara M, Toki N, Onozuka H, et al. Quantitative metabolome profiling of colon and stomach cancer microenvironment by capillary electrophoresis time-of-flight mass spectrometry. Cancer Res 2009;69:4918–25.
41. Klimova T, Chandel NS. Mitochondrial complex III regulates hypoxic activation of HIF. Cell Death Differ 2008;15:660–6.
42. Patten DA, Lafleur VN, Robitaille GA, Chan DA, Giaccia AJ, Richard DE. Hypoxia-inducible factor-1 activation in nonhypoxic conditions: the essential role of mitochondrial-derived reactive oxygen species. Mol Biol Cell 2010;21:3247–57.
43. DeBerardinis RJ, Cheng T. Q's next: the diverse functions of glutamine in metabolism, cell biology and cancer. Oncogene 2010;29: 313–24.
44. de Kruijf EM, van Nes JG, van de Velde CJ, Putter H, Smit VT, Liefers GJ, et al. Tumor–stroma ratio in the primary tumor is a prognostic factor in early breast cancer patients, especially in triple-negative carcinoma patients. Breast Cancer Res Treat 2011;125:687–96.
45. Rattigan YI, Patel BB, Ackerstaff E, Sukenick G, Koutcher JA, Glod JW, et al. Lactate is a mediator of metabolic cooperation between stromal carcinoma associated fibroblasts and glycolytic tumor cells in the tumor microenvironment. Exp Cell Res 2012;318:326–35.
46. Mellon EA, Lee SC, Pickup S, Kim S, Goldstein SC, Floyd TF, et al. Detection of lactate with a hadamard slice selected, selective multiple quantum coherence, chemical shift imaging sequence (HDMD-SelMQC-CSI) on a clinical MRI scanner: application to tumors and muscle ischemia. Magn Reson Med 2009;62:1404–13.
47. Adalsteinsson E, Spielman DM, Pauly JM, Terris DJ, Sommer G, Macovski A. Feasibility study of lactate imaging of head and neck tumors. NMR Biomed 1998;11:360–9.
48. Pan JW, Hamm JR, Hetherington HP, Rothman DL, Shulman RG. Correlation of lactate and pH in human skeletal muscle after exercise by ^{1}H NMR. Magn Reson Med 1991;20:57–65.
49. Smith MA, Koutcher JA, Zakian KL. J-difference lactate editing at 3.0 Tesla in the presence of strong lipids. J Magn Reson Imaging 2008;28:1492–8.
50. Spriet LL, Howlett RA, Heigenhauser GJ. An enzymatic approach to lactate production in human skeletal muscle during exercise. Med Sci Sports Exerc 2000;32:756–63.
51. Maekawa M, Sudo K, Li SS, Kanno T. Genotypic analysis of families with lactate dehydrogenase A (M) deficiency by selective DNA amplification. Hum Genet 1991;88:34–8.